Università degli Studi di Padova
Facoltà di Ingegneria

Finito di scrivere il giorno January 27, 2011 utilizzando LaTeX 2ε

UNIVERSITÀ DEGLI STUDI DI PADOVA

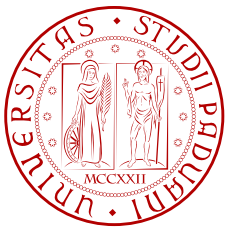

DIPARTIMENTO DI INGEGNERIA
DELL'INFORMAZIONE
Dottorato di Ricerca in Ingegneria dell'Informazione
Indirizzo in Scienza e Tecnologia dell'Informazione
XXIII Ciclo

—

This thesis is presented for the degree of Doctor of Philosophy of the University of Padova

—

A Neuromuscular Human-Machine Interface for Applications in Rehabilitation Robotics

PhD Advisor: Professor Enrico Pagello
PhD Reviewer: Professor Yoshihiko Nakamura

PhD Candidate: MASSIMO SARTORI

Padova, January, 2011

Abstract

This research work presents a novel *neuromusculoskeletal* (NMS) model of the human lower limb that is physiologically accurate and computationally fast. The NMS model uses electromyography (EMG) signals recorded from 16 muscles to predict the force developed by 34 musculotendon actuators (MTAs). The operation of each MTA is constrained to simultaneously satisfy the joint moments generated with respect to 4 degrees of freedom (DOF) including: hip adduction-abduction, hip flexion-extension, knee flexion-extesion and ankle dorsi-plantar flexion. Advanced methods are developed to capture the human movement and produce realistic motion simulations. These are used to provide dynamic consistency to the NMS model operation. Pattern recognition and machine learning technology is used to predict the human motor intention from the analysis of EMG signals and integrate context knowledge into the EMG-driven NMS model.

This research develops the technology needed to establish an EMG-driven human-machine interface (HMI) for the simultaneous actuation of multiple joints in a lower limb powered orthosis. This work, indeed, shows for the first time it is possible to use EMG signals to estimate the joint moments simultaneously produced about multiple DOFs and this is crucial to provide better estimates of muscle force with respect to the state of the art. This thesis also suggests the NMS model can be exploited to address the challenge of autonomous locomotion in musculoskeletal humanoids.

The objective of this work therefore, is to provide effective solutions and readily available software tools to improve the human interaction with robotic assistive devices. This is achieved by advancing research in neuromusculoskeletal modeling to better understand the mechanisms of actuation provided by human muscles. Understanding these mechanisms is the key to realize human interaction with wearable assistive devices. This work designs and develops the technology for achieving this.

Sommario

Questo lavoro di ricerca presenta un innovativo modello *neuromuscoloscheletrico* (NMS) dell'arto inferiore umano. Il modello è fisiologicamente accurato e computazionalmente efficiente. Utilizza segnali elettromiografici (EMG) acquisiti da 16 muscoli per predire la forza sviluppata da 34 attuatori muscolo-tendinei (MTAs). Ogni MTA è vincolato a soddisfare i momenti articolari generati rispetto a 4 gradi di libertà: adduzione-abduzione e flessione-estensione dell'anca, flessione-estensione del ginocchio e flessione plantare-dorsale della caviglia. Sono stati sviluppati metodi avanzati per digitalizzare il movimento umano e creare simulazioni motorie realistiche. Queste vengono utilizzate per assicurare consistenza dinamica durante l'esecuzione del modello NMS. Tecniche di *pattern recognition* e *machine learning* vengono poi utilizzate per predire il tipo di movimento che il soggetto umano vuole compiere attraverso l'analisi dei segnali EMG. Questa ricerca sviluppa gli strumenti necessari per realizzare un interfaccia uomo macchina (HMI) comandata da segnali EMG che consenta l'attuazione simultanea dei giunti articolari in un esoscheletro dell'arto inferiore.

Viene mostrato, infatti, per la prima volta, che è possibile usare segnali EMG per stimare i momenti articolari prodotti rispetto a più gradi di libertà e che questo è fondamentale per ottenere stime corrette della forza muscolare. Questa tesi illustra anche la possibilità di implementare strategie di locomozione per robot umanoidi dotati di una struttura muscoloscheletrica.

L'obiettivo di questo lavoro è quindi quello di fornire soluzioni efficaci e strumenti software avanzati per migliorare l'interazione umana con dispositivi robotici di assistenza. Questo è ottenuto attraverso una ricerca nel campo della modellazzione neuromuscoloscheletrica per comprendere i meccanismi di attuazione propri dei muscoli uniarticolari e biarticolari umani. La comprensione di tali meccanismi rappresenta il punto chiave per lo sviluppo di soluzioni efficaci per il controllo di sistemi assistivi indossabili. Questo lavoro mette a disposizione la tecnologia necessaria per ottenere tali risultati.

Contents

List of Figures

List of Tables

Chapter 1

Introduction

The skeletal muscles are the natural actuators responsible for human movement [1–4]. Understanding how muscles activate and generate force about multiple joints and propel the human body towards a specific motion will significantly impact several research areas ranging from physical therapy to neuro-rehabilitation, from computer animation to robotics [5]. Research in rehabilitation robotics strongly relies on understanding the mechanisms underlying human muscle activation for the purpose of improving the interaction between the human and the machine [5–7]. The design of intelligent assistive devices such as powered orthoses or exoskeletons requires indeed a deep understanding of the force the patient's muscles are able to produce. Such knowledge will better define the dynamics and the magnitude of support the machine will have to provide the user with [7–11]. Research in humanoid robots is also moving toward human-inspired methodologies. The new-generation of humanoid robots will have highly complex skeletal structures and artificial muscle actuators that increasingly resemble the human musculoskeletal system [12, 13]. Understanding how muscles are activated to actuate the human body will directly allow designing motion and balance controller to move humanoid robots in a more sophisticated way.

1.1 The Problem

Research on assistive devices to support disabled people's mobility or to augment healthy subjects' capabilities has always been an important topic in the robotics community. In 1970's the pioneer group around Vukobratovic proposed one of the first wearable exoskeletons to help patients with defects in their locomotion system regain their motor capabilities [14]. However, lack of computer processor power, heavy actuators (both pneumatic and electrical), and heavy power supplies limited the realization of interesting theoretical results. Since then, the mechanics and electronics design has significantly improved. This led to light-weight and reduced-size devices that the operator can easily wear and carry [7–10, 15–17]. The fast advancement of mechatronics design (i.e. mechanics and electronics), was not followed however by an equally fast advancement in the design of effective interfaces between the operator and the device [18]. Whatever the application of the assistive device is, there is the need for a human-machine interface (HMI) to realize the online device control. The HMI needs to be intuitive, i.e. it has to allow the operator to concentrate on fulfilling a task in cooperation with the assistive device rather than on the control.

A HMI essentially has to estimate the subject's *motor intention* and provide an adequate device control command. The motor intention can be evaluated in different ways. A common solution is that of evaluating the dynamics of the operator together with that of the assistive device and use them to calculate the support moment for the joints. In other words, the HMI evaluates the current contribution of both subject and assistive device to the movement and defines how much extra support has to be given. In case of the BLEEX exoskeleton for example, the evaluation of the inverse dynamics model of the exoskeleton results in the joint moments that are currently applied [19]. By contributing a certain share of these moments through the actuation of the exoskeleton, the operator is relieved of some of the load. In other projects the exoskeletons add fixed shares of the moment that is required to maintain a static pose with the current joint configuration [16, 20]. The drawback of these HMIs is that to perform a movement, the operator has to be able to initiate the movement *before* they can receive

support from the system. As a result, the assistive device operation is not directly coupled to that of the operator. Furthermore, the utilized dynamic models are very sensitive to kinematic measurements and to changes in the mass of operators, exoskeletons, payloads, and to external contact forces that have not been modeled or have not been accurately measured [9].

In recent years a body of research has been conducted on connecting the control system to biological signals generated by the operator that are directly linked to the desire of motion [7–9, 15, 17]. The process of generation of movement is dealt by the central and peripheral nervous systems. That is, movements are generated in the brain, some in the brain stem, and some in the spinal cord. As a result, muscles are activated to actuate the human joints. HMIs have been proposed in which EEG[1] signals recorded from the brain motor cortex are evaluated [21–23]. EEG signals are described using a series of parameters in both the frequency and time domain. These are used to generate a set of features that can be used to identify EEG patterns as members of specific classes associated to a type of movement. This approach uses *pattern recognition* and *machine learning* technology and does not need biologically relevant models of the human neuromusculoskeletal system. Once the specific movement is recognized, predefined trajectories are used to actuate the assistive device and passively move the patient limb. This technique is mostly used for the control of prosthetic upper limbs. Indeed, rhythmic and cyclic movements such as walking are generated in the spinal cord rather than in the brain and EEG classification cannot be exploited effectively [24, 25].

An alternative solution is that of recording the *final output* of the process of generation of movement, that is the muscle activity. This can be done by using *electromyography* (EMG). According to [26], electromyography is *the study of muscle function through the inquiry of the electrical signals the muscles emanate.* EMG signals are emitted prior to muscle contraction and can be detected by superficial non-invasive electrodes. EMG signals appear in lower limb muscles approximately $10ms$ before the muscle actually contracts [27]. In the upper limb muscles, delays are between 20 and $80ms$. This is called electromechanical delay (EMD). If the EMD can be exploited in the assistive device control system, the

[1] Abbreviation for Electroencephalography

evaluation of the signal can be done by the time muscles contract and a robust coupling between human and machine can be achieved [9, 10]. Furthermore, even if the muscles are too weak to perform any movement, a support can still be given as long as a proper evaluation can be done within the EMD. Furthermore, EMG signals are generated unconsciously and no additional mental load is needed by the operator. This makes EMG signals good candidates for establishing an intuitive and effective HMI. A lot of interest was therefore paid in the development of EMG-driven HMIs.

Pattern recognition and machine learning methods have also been used to classify EMG activation patterns for the detection of different lomotion modes [7, 28–30]. Likewise the EEG-based approach, this one does not need biologically relevant models of the human musculoskeletal system and predefined trajectories are used to actuate the assistive device and passively move the patient limb.

Neuromusculoskeletal (NMS) models of the human joints can alternatively be used in which EMG signals are continuously evaluated and used as input to the NMS model to estimate somatosensory information including: length, contraction velocity and force of the muscles crossing a joint. These are then used to estimate the moments produced at the subject's joints during movement which are used to subsequently control the actuation of the powered orthosis joints as in [9, 10]. EMG-driven NMS models allow designing HMIs that allow the user to actively control the assistive device at all times as opposed to pattern-recognition-based techniques that use predefined trajectories to actuate the device. The idea is that of exploiting the natural actuation provided by muscles to create human-machine interaction.

The most important problem in the study of human movement is the development of accurate, non-invasive methods of calculating individual muscle and ligament forces [31]. Furthermore, the use of EMG-driven NMS models to estimate somatosensory informations has also been regarded as a key-point for the design of assistive device control systems that can robustly embody humans ability of moving. Citing Nakamura et al.: *when the man-machine interface obtains access to the somatosensory information, machines would make the first step to understand humans* [6].

1.2 Statement of the Problem

The role of technology in the health sector has been growing increasingly in the past years as well as the capability and the power of the systems involved. People suffering from a debilitating disease can now benefit from the recent progresses in healthcare technologies but many issues are still open. Current motor rehabilitation therapies still cannot give back to patients their lost motor capabilities within a short time frame or at affordable cost. The possibility of integrating robot-assisted treatments in the physiotherapy could help decrease the length of the recovery process as well as the costs involved. Researchers are currently developing models of the human body that can simulate the motion of the human limbs and help design better assistive robotic devices for people with disabilities. Indeed, the availability of accurate and comprehensive human limbs models is required for the development of effective human-machine interfaces (HMIs) and control systems for rehabilitation robotic devices such as powered orthoses.

Mobility represents a basic need that has to be guaranteed to ensure independence and to boost the integration of disabled people in the society. This is one motivation that led this study to focus on lower limbs. A significant lack of research on lower limbs compared to upper limbs was another reason.

This work presents the design and development of a novel NeuroMusculoSkeletal (NMS) model of the human lower extremity. This model aims to be used as an innovative HMI for the continuous active control of wearable assistive devices such as powered orthoses to support disabled people's lower limbs.

Because the intended HMI has to be able to recognize the motor intention of disabled people, the use of methods that evaluate the subject's dynamics (i.e. as in the BLEEX example [19]) were regarded as unsuitable. The operator would have to be able to move autonomously *before* receiving support from the system.

Because the intended HMI has to be able to recognize the motor intention associated to lower limbs, EEG-based HMIs were regarded as unsuitable as rhythmic movements such as walking are generated at the spinal cord level [24, 25].

In this research work, EMG signals were therefore chosen to establish the HMI.

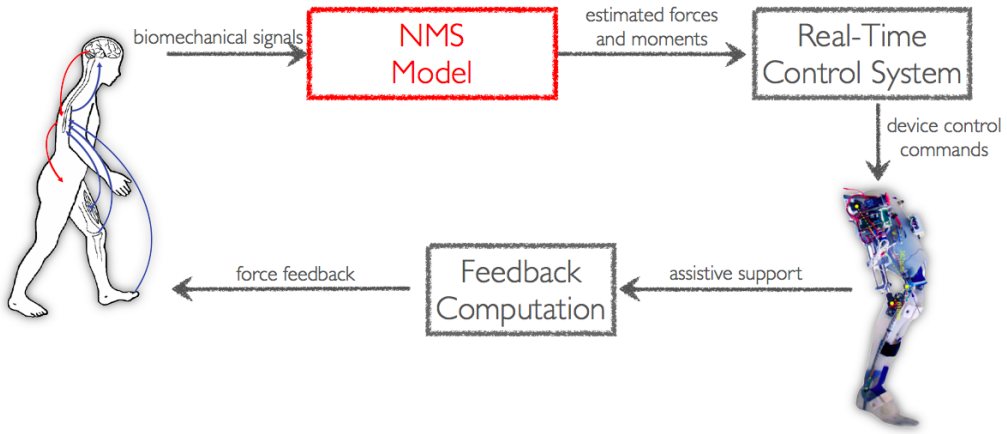

Figure 1.1: Man-in-the-Loop approach using an EMG-driven NMS model to control a powered orthosis.

Because the HMI has to provide active and continuous control, the use of pattern recognition and machine learning techniques were regarded as unsuitable because they use predefined joint trajectories to control the device. In this context the operator plays a passive role. This fact leads to poor rehabilitation processes as the user passively adapts to the imparted movements [7].

To ensure the user can continuously control the assistive device, EMG signals were used in this work to drive a novel biologically relevant neuromusculoskeletal model of the lower limb for the estimation of somatosensory information including: length, contraction velocity, activation and force of the muscles crossing a joint. The model is designed so that it can provide accurate estimates of forces produced by the lower limb muscles during the human movement as well as the moments simultaneously produced at the hip, knee and ankle joints. Pattern recognition and machine learning methods were still investigated in this work with the plan to combine this technology to that based on NMS models.

1.2.1 Man in the Loop

The general idea behind the use of the NMS model to control assistive devices is depicted in Fig. 1.1. The human subject is placed in a loop within which the NMS model evaluates motion data and biological signals generated by the subject as they move. Evaluations are used by the NMS model to predict the force the subject's muscles are able to generate. These are then further evaluated to calculate the amount of support the assistive device will have to provide the user with, in order to allow for the proper execution of the desired movement. The assistive device will then actively support the subject by providing a force feedback. For this to work, by the time the human muscles contract, the entire loop has to be completed. This will allow actuating the orthosis as soon as the human muscles activate. The real-time constraint for our proposed NMS model is therefore the EMD. That is, the NMS model has to be able to produce estimates of muscle forces and joint moments in less than $10ms$.

1.3 EMG-driven NMS Modeling: An Overview

A great body of research has been previously conducted in the field of neuromusculoskeletal modeling. In the literature there have been adopted either simplified neuromusculoskeletal models that are suitable for applications with real-time constraints or very detailed and physiologically accurate models that are not efficients from a computational point of view.

Biomechanists have developed complex NMS models that combine together kinematic and kinetic data with EMG signals to study human muscle behavior in vivo. This technique has been separately applied to various joints in the human body such as the elbow [32], lower back [33], shoulder [34] and the knee [1–3, 35–37]. These models are extremely accurate in the way they represent physiological properties of the musculoskeletal system but are not suitable for robotics applications with stringent real-time constraints. Only recently, robotics researchers have developed models that are suitable for real-time applications [8–10, 15, 38]. In [10], the authors present a model of the elbow joint that is able to predict flexion-extension moments as a function of the joint kinematics and

muscle neural activation level. The controlled device is an arm exoskeleton in which the user straps into and performs exercises imparted by the machine. In [9] EMG signals are used as input for a simplified EMG-driven model to derive the force generated by 6 thigh muscles and estimate the knee joint flexion-extension moment used to control a lower limb powered orthosis. These works, however, utilize very simplified models of the human joint and the predicted somatosensory information is often not representative of the actual muscle behavior. This makes them not ideal for being integrated into the control system of assistive devices that are to support a wide range of movements. The availability of accurate and comprehensive human limbs models, combining high reliability and real-time operation, is therefore needed for the development of effective HRIs and control systems for rehabilitation robotic devices.

An additional limitation of current EMG-driven NMS models is they only predict forces of muscles crossing one joint and moments about one single degree of freedom (DOF), i.e. knee flexion-extension, elbow flexion-extension, etc. We will refer to these models to as *single-DOF EMG-driven NMS models*. This limitation poses questions on whether the estimated muscle forces are truly representative of the real muscle behavior. Indeed, muscles normally develop forces that satisfy multiple DOFs in multiple joints. Furthermore, when single-DOF EMG-driven NMS models are used to control assistive devices, only the control of one DOF in one joint only is allowed.

In [6] a whole-body NMS model was presented. However, it was not driven by EMG signals and the muscle redundancy problem, i.e. the way muscles share the load about a joint, was solved using optimization models. Optimisation models typically involve partitioning individual muscle forces based upon an objective function using a set of adjustable parameters within the model. Parameters such as activation are optimised to achieve a solution for the objective function, for example, achieving a movement with minimal joint contact force, minimal muscle stress, or minimal muscle force. Achieving a solution to satisfy equilibrium equations based on a single objective criterion give rise to questions regarding the physiological validity of optimisation models [39]. The question arises then, how do we know what the body is trying to optimise? And can an assumption on

this optimisation process be generalised across all individuals? Challis et al [40] showed that by using appropriate constraints, muscle forces can be kept within physiological boundaries using optimisation techniques, however, the inferred activation used to achieve a result is not necessarily related to the activation patterns that are actually used by the central nervous system. Buchanan et al. [41] also showed that any of a number of optimisation criteria could not adequately represent actual muscle activity in their elbow joint experiments. These problems remain if assumptions are made concerning the relative activations from individual muscles surrounding a joint.

A hybrid approach that used optimisation criteria and muscle activation patterns (measured using EMG) was presented in [42]. This is to overcome the indeterminate biomechanical model. Selected *gains* were used to change individual muscle forces and satisfy moment constraints about multiple joints using an optimisation process whilst preserving the biological muscle recruitment patterns. Although moment constraints were satisfied using this technique, the physiological basis for using a set of gains to satisfy moment constraints must be questioned.

1.4 Novelty of this Research

This research work develops advanced methods for the realistic simulation of the human movement from motion capture data. These data are used as input to the NMS model to provide dynamic and anatomical consistency in the process. A new knee joint model is developed in which functional axes can be defined and scaled to the subject's characteristics. Also, a new foot-ground contact model is created and used to derive more accurate estimates of joint loading during movement (Chapter 2).

This work proposes a novel EMG-driven NMS model that combines together the physiological accuracy of the models proposed by the biomechanists, to the fast operation of those proposed by robotics researchers. This work also demonstrates the proposed NMS model can meet the real-time deadline associated to the control of a lower limb powered orthosis (Chapters 3 and 4).

An effective way to speed up the calibration of complex NMS models is achieved

by exploiting the fast operation of the NMS model proposed in this thesis (Chapter 5).

This work shows for the first time it is possible to use EMG signals to accurately estimate muscle forces from all major muscles in the lower limb. A novel methodology is proposed that allows constraining the operation of muscles so that the forces they produce satisfy the joint moments simultaneously generated at multiple DOFs including: hip adduction-abduction, hip flexion-extension, knee flexion-extension and ankle dorsi-plantar flexion. This is achieved by the use of a novel calibration algorithm. We will refer to this to to as the *multi-DOF EMG-driven NMS model* (Chapter 6). Single-DOF models such as knee flexion-extension (FE) models [2–4, 9, 35, 43] allow estimating the muscle forces involved in the production of FE moments at the knee joint only. However, most of the muscles spanning the knee also span the hip and the ankle joints too. Therefore, the forces the muscles generate for the production of knee FE moment also have to satisfy the generation of moments about hip and ankle joints. Results obtained in this work show that the force that a muscle can generate during a specific movement can be predicted in extremely different ways when different single-DOF models are used, i.e. the force of a muscle crossing the hip joint can be estimated by a hip flexion-extension NMS model as well as by a hip adduction-abduction model as well as by a hip internal-external rotation model. If this muscle was biarticular, its force could also be predicted by a knee flexion-extension model. The problem is, it is not possible to know what single-DOF model is best using. The proposed multi-DOF NMS model allows removing this indeterminacy by providing a single solution for each muscle. Results show this model has the potential to better estimate muscle force than single-DOF models.

A novel method is developed that uses physiologically-based rationales to better scale important musculotendon parameters (Chapter 7).

1.5 Delimitations

This research develops the technology needed to achieve power orthosis continuous control and the simultaneous EMG-driven actuation of multiple DOFs in multiple

joints. The work is focused on the design and validation of the core component, that is, the EMG-driven NMS model. This work does not realize real-time synchronization with powered orthoses. Neither does it improve disabled people's mobility using robotics assistive devices. This work provides the theoretical results and the methodology needed to achieve this.

Below are summarized the key-points that delimit the boundaries within which this research work investigates:

- The EMG-driven NMS model is used to predict muscle force and joint moments using data *previously* collected during the subject's movement. This work represents the first step in the development of a neuromuscular HMI for assistive device control. The study is focused on the pure model design and validation and not on its synchronization with real-time data acquisition systems.
- The proposed multi-DOF EMG-driven NMS model is not used to control real assistive devices.
- Experiments are conducted on a population of healthy subjects.
- A motion capture system is used to collect human movement data.

1.6 Research Questions to be Addressed

This work addresses a number of research questions including:

- Is it possible to ensure dynamic consistency in the operation of the EMG-driven NMS model (Chapter 2)?
- To which extent physiological accuracy in the NMS model design has to be sacrificed to achieve real-time operation (Chapters 3, 4 and 5)?
- Can tendons be assumed infinitely stiff during walking and running with no loss in the NMS model predictive ability (Chapter 3)?
- Can estimations of musculotendon kinematics (i.e. musculotendon length and moment arms) be done with the same accuracy of third-party musculoskeletal

softwares such as SIMM [44, 45] and OpenSim [11, 46] and with the possibility of integration into custom softwares? Can fast computation time be also achieved (Chapter 4)?

- How can a NMS model be used to provide effective control strategies for powered orthoses and musculoskeletal humanoid robots (Chapters 3)?
- Do single-DOF NMS models provide reliable muscle force estimates (Chapter 6)?
- Is it possible to constrain the operation of lower limb muscles to satisfy joint moments produced about multiple DOFs in EMG-driven modeling (Chapter 6)?
- How do muscle force estimates change with respect to those obtained by single-DOF NMS models (Chapter 6)?
- Is it possible to achieve accurate estimates of the joint moments simultaneously produced about multiple DOFs using an EMG-driven NMS model (Chapter 6)?
- Is it possible to define physiologically-based rationales to better scale musculotendon parameters (Chapter 7)?
- Can pattern recognition and machine learning techniques be combined to NMS modeling and provide a superior way to extract motor information from EMG signals (Chapter 8)?

1.7 Significance of this Research

The real time execution of the EMG driven NMS model will have a substantial contribution to the design and implementation of robotic exoskeletons and powered orthoses. Indeed, a better understanding of the real-time behavior of muscles can improve the actuation of these devices and their control algorithms, resulting in enhanced biomimetic control systems. Also, the ability to directly study muscles behavior in healthy and impaired people will be readily possible.

The possibility to constrain the operation of each single muscle in the model to satisfy joint moments about multiple DOFs will allow estimating more physiologically accurate muscle forces. This will permit expanding the number of studies into how the nervous system controls muscles in both healthy and impaired populations.

The possibility of estimating the moments simultaneously produced at multiple joints can be applied to the design of more intuitive assistive devices control systems for the simultaneous actuation of multiple joints and the support of an even wider range of movements.

The NMS model can also provide effective solutions for the actuation of humanoid robots that have a musculoskeletal architecture and artificial muscles. The proposed NMS model allows taking inspiration from the way humans move and addressing the challenge of autonomous locomotion in musculoskeletal humanoids. Indeed, a better understanding of the dynamics of muscles during movement will allow designing more sophisticated systems to actuate and control artificial muscles.

This research development aims to integrate musculoskeletal dynamics into robotics systems to achieve more advanced bio-inspired control strategies. Neuromusculoskeletal modeling technology not only can offer great solutions for exoskeletons control and humanoids actuation, but can also boost research that aims to realize comprehensive virtual humans by providing a more realistic estimation of the human internal state [5].

1.8 Thesis Overview

This thesis consists of nine Chapters inclusive of this introduction. Chapter 2 illustrates the general *workflow* that goes from the collection of motion data to the creation of a digital representation of the human musculoskeletal system to achieve realistic simulations of the musculoskeletal dynamics. The novel methodologies proposed in this thesis will be illustrated. Furthermore, an overview of the main components forming the physiologically accurate single-DOF NMS model developed by the biomechanics group around David G. Lloyd is given [3, 4, 35, 43].

This model will be used as a *baseline* for comparison to the NMS model proposed in this thesis. Chapter 3 describes the development of a novel single-DOF NMS model of the knee joint that combines together physiological accuracy to real-time operation. A discussion on how the proposed NMS model can be used to control powered orthoses and musculoskeletal humanoids is given. Chapter 4 presents a novel methodology to estimate musculotendon kinematics in large musculoskeletal models. This is used within the NMS model to achieve real-time operation. Chapter 5 shows the proposed single-DOF NMS model can be used to achieve a faster calibration of the more complex NMS model developed by Lloyd et al. presented in Chapter 2. Chapter 6 extends the single-DOF NMS model (Chapter 3) to a multi-DOF NMS model of the whole human lower extremity and shows it is more robust in the estimation of muscle forces than single-DOF models. Chapter 7 presents a physiologically-based methodology to scale the resting length of tendons in NMS models showing this helps achieving better prediction performances. Chapter 8 presents the use of Support Vector Machine to classify locomotion modes from EMG patterns and suggests how this technique can be integrated with the EMG-driven NMS model. Chapter 9 summarizes the results of this research and sketches future research paths.

Chapter 2

Workflow

This work uses motion capture technology together with sophisticated algorithms for motion kinematics and dynamics computation to produce the most accurate inputs for the neuromusculoskeletal (NMS) model of the lower limb presented in this thesis. Fig. 2.1 illustrates the *workflow* that goes from the acquisition of motion data from the human subject to the execution of the NMS model to estimate somatosensory information. The next sections will first illustrate the *Human Movement* and the *Movement Modeling* steps. Then, the general structure of the single-DOF EMG-driven NMS model developed by Lloyd et al. [3, 35, 37, 43] will be presented. This is a well established model of the knee joint that is physiologically accurate and that has been extensively validated in the past. Muscles are modeled using a modified Hill-type model with non-linear elastic tendons. Within this thesis, this model is regarded as the *gold standard* with respect to the physiological and predictive accuracy because no simplifications in the modeling design have been done to achieve faster operation.

The NMS model that is proposed in this thesis has the same general structure of the elastic-tendon model proposed by Lloyd et al. However, novel components are introduced to achieve faster execution and to constrain the operation of muscles to satisfy all moments in the lower extremity joints (Chapters 3, 4 and 6). The operation of the NMS model proposed in this thesis is always compared to that of the elastic-tendon model developed by Lloyd et al.[3] and presented in this Chapter.

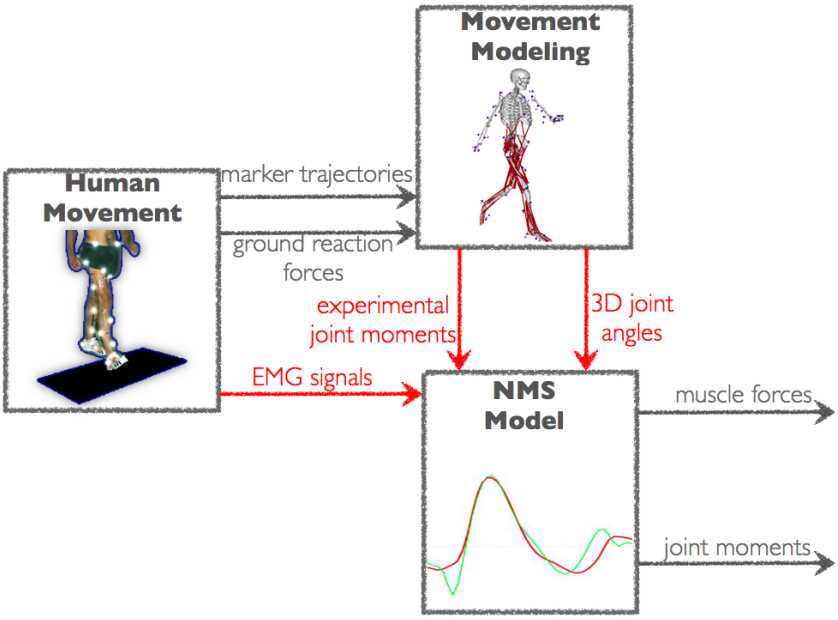

Figure 2.1: Motion data are collected from the human subject. These are used by sophisticated algorithms for the dynamic motion simulation to calculate 3D joint angles and joint moments. These are then used, together with EMG signals, as inputs for the NMS model. The NMS model input data are highlighted in red.

2.1 Human Movement

This is the first step of the workflow in which the data from the subject's movement is collected using motion capture technology and surface electromyography.

A data set for the calibration of the model is initially created. This includes: 1) static trials, in which the subject stands still, 2) swinger trials, in which the subject performs specific exercises to repeatedly flex and extend their hip, knee and ankle joints, 3) dynamic trials, in which the subject performs specific motor tasks. Data collected from the static and swinger trials are used in the *Movement Modeling* step to create a musculoskeletal model scaled to the subject's anatomical dimensions (Fig. 2.2) as described in Section 2.2. Data collected from the dynamic trials are used to calibrate the biomechanical parameters of the NMS model as described in Section 2.3.

A 12 camera motion capture system (Vicon, Oxford, UK) is used to record the human body kinematics with sampling frequency at $250Hz$. A set of reflecting markers are placed on the human body and their instantaneous three-dimensional position is then reconstructed and used to measure the movement of body segments

including: arms, trunk, pelvis, thigh, shank, and foot. Ground reaction forces (GRFs) generated during the dynamic trials are collected using a multi-axis in-ground force plate (AMTI, Watertown, USA) with a sampling frequency at $2kHz$. Double-differential surface electrodes are used to collect EMG signals from the selected muscles. A telemetered system (Noraxon, Scottsdale, USA) transfers the EMGs to a 16 channel amplifier (Delsys, Boston, USA) with sampling frequency at $2kHz$.

Both body kinematics and GRFs are low-pass filtered with cut-off frequencies ranging from 2 to $8Hz$ depending on the motor task, i.e. walking, running, etc.

Raw EMG signals are first band-pass filtered ($10-150Hz$), and then full-wave rectified and low-pass filtered ($6Hz$) subsequently. The processed signal is the *linear envelope* which is then normalized against the maximum values from EMG linear envelopes obtained from a range of extra trials including: running and squat jumps.

2.2 Movement Modeling

This is the second step in which three-dimensional joint angles and moments are recorded during the human movement. 3D joint angles and joint moments in general are not easily recordable using external sensors. To have accurate measurements of those quantities, the external sensor would have to be centered on the joint centre of rotation. For some joints, like the hip, it is practically impossible because of the amount of tissues surrounding it. Furthermore, the human joints are not ideal hinge joints. Therefore, the centre of rotation is not a fixed point but it moves as a function of the joint angle itself. The knee joint centre of rotation, for instance, moves on an elliptical surface. Therefore, the use of an external sensor would not give satisfactory results. This work therefore uses motion capture technology to drive a dynamic motion simulation of the human movement. This has the advantage of giving the possibility of modeling the morphology of the joint such as the shape of the surfaces of the bones that make up the joint, and the location of the joint centre of rotation as a function of the joint angle.

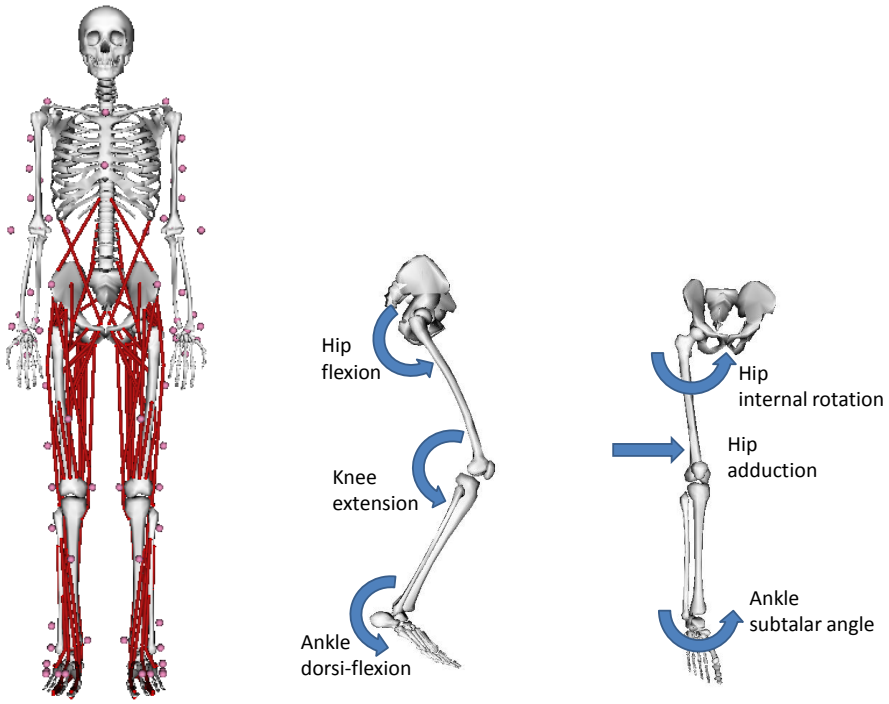

(a) (b)

Figure 2.2: (a) Model to define the subject's musculoskeletal system. (b) Angles conventions used in this thesis. Orientations with a positive sign are shown.

The freely available musculoskeletal modeling software OpenSim [11, 46] is used to customize a generic musculoskeltal model of the human body[1] (Fig. 2.2a). The musculoskeletal model is customized to include all muscles of interest and to define 6 degrees of freedom across the joints (Fig. 2.2b).

Most of the muscles in the model are described by a single musculotendon actuator (MTA). That is, muscle fibers and tendons together are modeled as a single wire which has only an origin and an end and can have internal via points that appear when the muscle line of action touches a bone as a function of the 3D joint angle (Fig. 2.3). Some muscles are instead described by multiple MTAs. That is, muscle fibers and tendons together are modeled as a multi wire complex composed of multiple single MTAs. This is to describe large muscles composed of a great complex of fibers. This model includes 34 MTAs per leg (Table 2.1). It

[1]The musculoskeletal model is freely available from the Neuromuscular Models Library: https://simtk.org/home/nmblmodels/

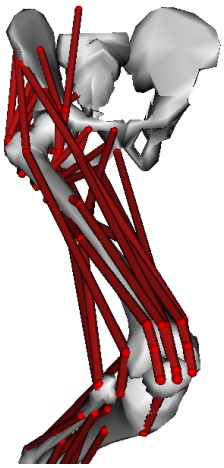

Figure 2.3: Muscles are defined as complexes of musculotendon actuators (MTAs). These are wire-like components that wrap around bones defining via points as a function of the joint angle.

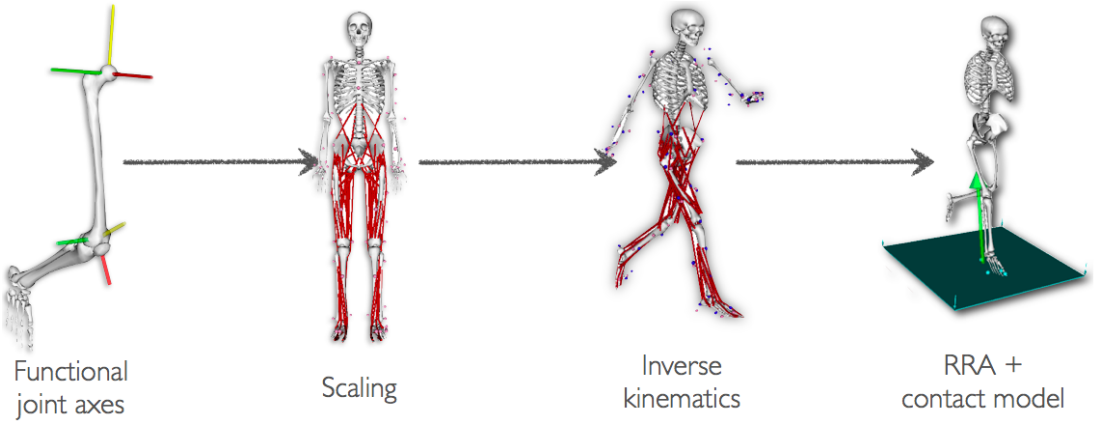

Figure 2.4: Functional axes at hip, knee and ankle are first computed. Then the model is scaled to match the subject's anthropometry. Then IK and RRA are used to measure joint angles and moments. A foot-ground contact model is used to further improve the joint moment computation.

defines 6 generalized coordinates (GCs) in the lower limb (Fig. 2.2b) including: hip flexion-extension (HF), hip abduction-adduction (HA), hip internal-external rotation (HR), knee flexion-extension (KF), ankle plantar-dorsi flexion (AF), ankle abduction-adduction (AA), and ankle internal-external rotation (AR).

The *movement modeling* process involves four steps (Fig. 2.4).

2.2.1 Optimal Joint Centres and Functional Axes

As described in [47], the repeatability of traditional kinematic and kinetic models is affected by the ability to accurately locate anatomical landmarks (ALs) to

Table 2.1: The 34 musculotendon actuators included in the model and the joints they span

Joints	Musculotendon Actuators
Hip	Adductor Brevis, Adductor Longus, Adductor Magnus1, Adductor Magnus2, Adductor Magnus3, Gluteus Maximus1, Gluteus Maximus2, Gluteus Maximus3, Gluteus Medius1, Gluteus Medius2, Gluteus Medius3, Gluteus Minimus1, Gluteus Minimus2, Gluteus Minimus3, Illiacus, Psoas
Knee	Vastus Interioris, Vastus Lateralis, Vastus Medialis, Biceps Femoris Short Head
Ankle	Peroneus Brevis, Peroneus Longus, Peroneus Tertis, Soleus, Tibialis Anterior
Hip, Knee	Biceps Femoris Long Head, Semimembranosus, Semitendinosus, Gracilis, Rectus Femoris, Sartorius, Tensor Fascia Latae
Knee, Ankle	Gastrocnemius Lateralis, Gastrocnemius Medialis

define joint centres and anatomical coordinate systems (ACS) (Fig. 2.5). The development of numerical methods that define joint centres and axes of rotation independent of ALs may therefore improve the repeatability of kinematic and kinetic data. In this thesis, the numerical methodology presented in [47] is used to derive the three-dimensional position of the centre of rotation for the hip, knee and ankle joints. Furthermore the three dimensional orientation of the flexion-extension axis of the knee joint is calculated.

To determine the three-dimensional position and orientation of each lower limb segment, clusters of three retro-reflective markers (20 mm) were firmly adhered to the subject's pelvis, thighs, shank, and feet (Fig. 2.5). For the hip joint, a functional method is employed, whereby subjects are required to consecutively move the right and left thigh through a range of flexion, abduction, adduction, and extension [47]. These data are used in a constrained optimization program written in MATLAB (Optimization Toolbox, Mathworks Inc.; Natick, MA), where spheres are fit to each thigh marker to find a left and right hip joint centre (HJC) location relative to the pelvis coordinate system and sphere radii. Fig. 2.6 shows the results of this computation.

For the knee joint, a mean helical axis is used to define the knee joint centre

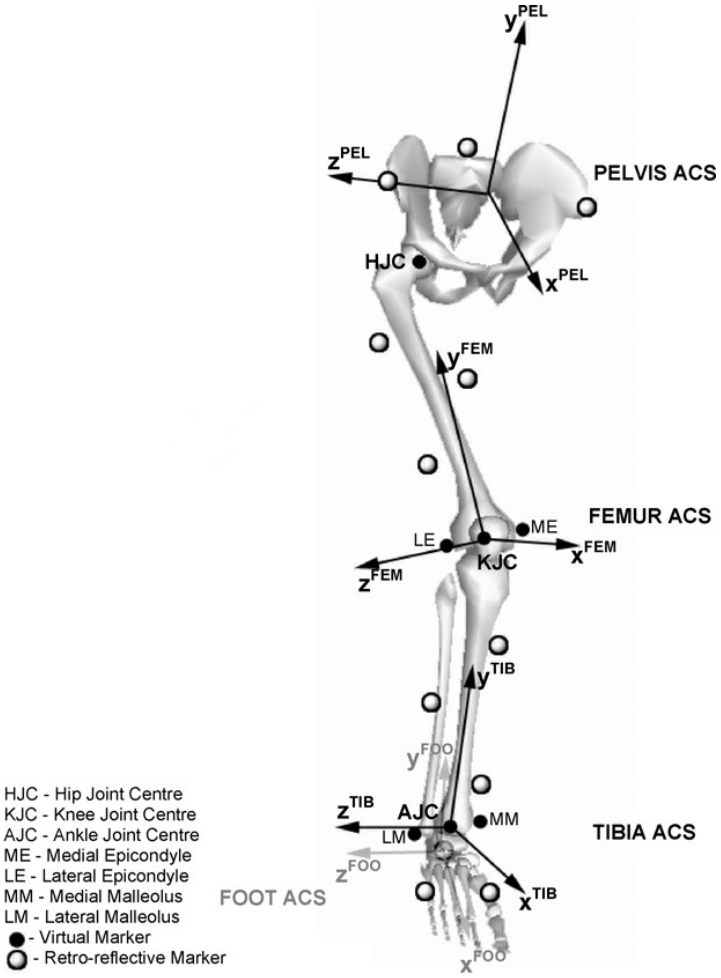

Figure 2.5: Experimental and virtual markers used in this work. The anatomical coordinate system (ACS) for each joint is also visible.

and flexion-extension axis. To achieve this, subjects stand on one leg and flex the contra-lateral thigh to enable the shank to freely flex and extend about the knee from full extension to approximately 100 degrees of flexion. This is performed for at least three cycles for each limb. Using the custom MATLAB program, the tibia markers are expressed in the femoral coordinate system and instantaneous helical axes are calculated throughout the range of motion using a singular value decomposition method from [48, 49]. A mean helical axis is then calculated for each knee, analogous to the method presented in [50] for the elbow joint. The mean helical axis is used to define the flexion-extension axis of the knee relative to the thigh coordinate system. The KJC is then defined relative to the mean helical axis, at a point along the helical axis that intersects a plane that is normal

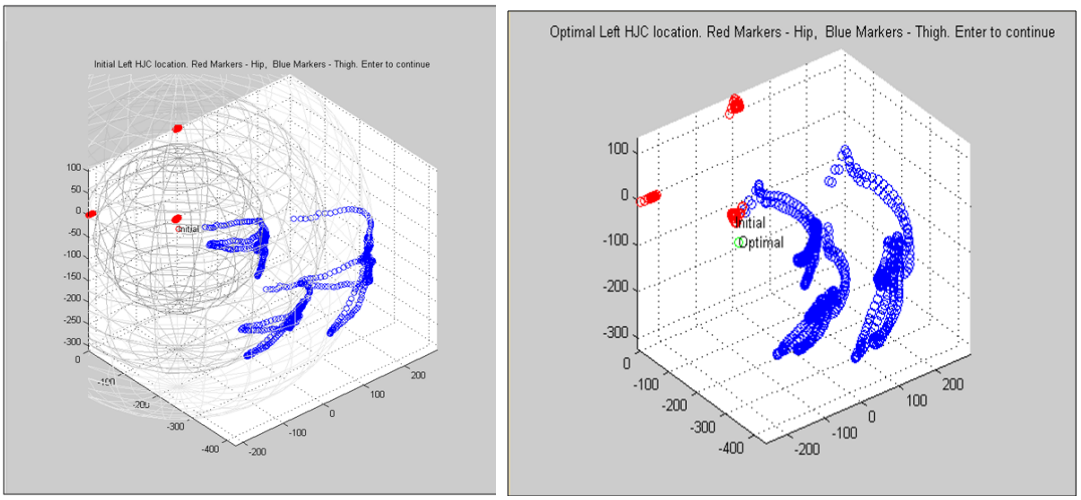

(a) (b)

Figure 2.6: Swinger trial for the calculation of the optimal hip joint centre. The blue trajectories represent the motion of the thigh markers. (a) The three-dimensional range of motion of the thigh markers is computed throughout the whole swinger trial. A sphere per marker is then created to fit the respective trajectory. (b) The optimal centre (green circle) is then calculated with respect to the pelvis anatomical coordinate system.

to the transepicondylar line, midway between the epicondyles. Fig. 2.7a shows the results of this computation. Furthermore, Fig. 2.7b shows the knee helical axes (KHA) that have been imported and visualized into the motion capture system software. An analogous procedure is used to define the ankle joint centre in which the relative movement of foot marker with respect to the shank ones is used.

The computed 3D positions of the hip, knee and ankle joint centres are then integrated in the OpenSim musculoskeletal model (Fig. 2.2).

For the integration of the 3D orientation of the knee joint flexion-extension axis, a novel procedure was developed in this thesis to define a 3-DOF knee joint in the OpenSim musculoskeletal model. The estimated mean helical axis is used to compute its 3D orientation with respect to the thigh reference frame. The OpenSim musculoskeletal model is then integrated with this information in the following way. The generic OpenSim musculoskeletal model that is used in this thesis has a knee joint that is based on the work presented by Delp et al. [44]. In this work the pelvis, thigh, shank and foot bones are digitized to create 3D meshes of polygons to define each bone surface. Based on the anatomical digitized bone surfaces the motion of the tibia with respect to the femur bone was determined as

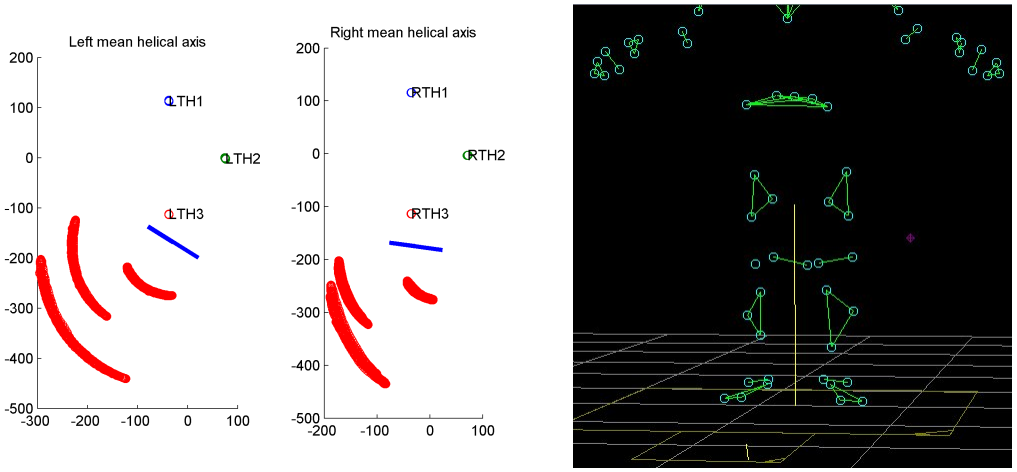

Figure 2.7: (a) The motion of the 3 shank markers (red trajectories) is calculated with respect to the left thigh (LTH1, LTH2, LTH3) and right thigh (RTH1, RTH2, RTH3) markers. Then the mean helical axes are calculated (blue lines). (b) helical knee axes placed in the marker-based model.

a function of knee joint angle. Fig. 2.8a shows the geometry used in this model for determining knee moments and kinematics in the sagittal plane. The femoral condyles were represented as an ellipse; the tibial plateau was represented as a line segment. The transformation from the femoral reference frame to the tibial reference frame was then determined so that the femoral condyles remain in contact with the tibial plateau throughout the range of knee motion. The tibia is therefore constrained to move on an elliptical surface defined by the femur medial-lateral condyles. From a numerical point of view, this is defined by two uni-dimensional spline functions that respectively associate a vertical (y-axis) and an anterior-posterior (x-axis) translation of the tibia to the current knee angle with respect to the femur reference frame. These two translations are combined with the rotation of the tibia about the origin of its reference frame as a linear function of the knee angle. As a result, the tibia moves and rotates simultaneously on an elliptical trajectory. The OpenSim model used in this thesis defines the spline functions with the assumption that the knee joint flexion-extension axis has an orientation of zero degrees. That is, it is perpendicular to the vertical axis of the femur reference frame. In this thesis a custom MATLAB routine was implemented to apply the 3D orientation of the knee helical axis to the two uni-dimensional

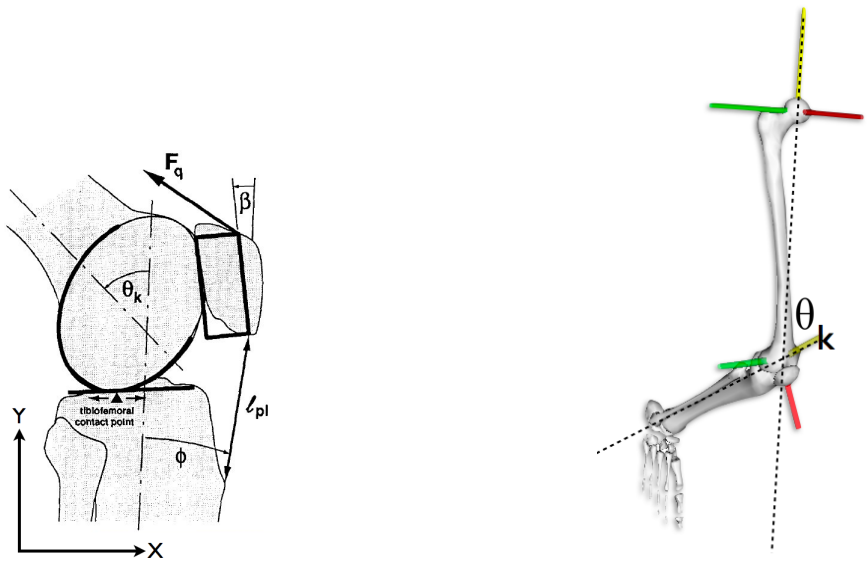

(a) (b)

Figure 2.8: (a) Geometry for determining knee moments and kinematics in the sagittal plane. θ_k is the knee angle; ϕ is the patellar ligament angle; β is the angle between the patella and the tibia; F_q, is the quadriceps force; l_{pl} is the length of the patellar ligament. From these kinematics, the moment of the quadriceps force about the instant center of knee rotation can be computed. (b) The knee joint angle is defined by the orientation of the tibia reference frame (located on the tibia head) with respect to the femur reference frame (located on the femur head). The yellow, red and green axes represent the y, x and z coordinate axes respectively. This figure shows the computation of the flexion-extension angle (about the z-axis).

spline functions defined in the OpenSim model. This allows moving the tibia on an *inclined* elliptical surface. In the OpenSim musculoskeletal model, the knee angle is defined by the orientation of the tibia reference frame with respect to the femur reference frame (Fig. 2.8b). The tibia reference frame was first rotated, in the femur reference frame, with respect to the anterior posterior axis (x-axis) according to the computed knee helical axis. This caused the tibia to move on a circle whose radius was the distance from the femur reference frame to that of the tibia. Then, the two translational spline functions were counter rotated, about the same axis using a rotation matrix. This process produced a third spline that translates the tibia on the medial-lateral axis (z-axis) as a function of the knee angle.

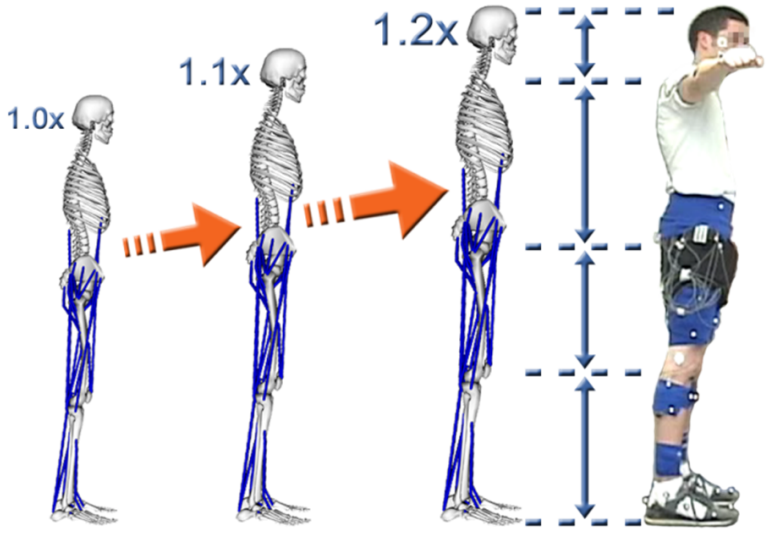

Figure 2.9: Experimental marker trajectories recorded during a static trial are used to scale the generic OpenSim musculoskeletal model to match the subject's anthropometry.

2.2.2 Scaling

Marker trajectories collected during the static trials are used in the scaling process to adjust a number of variables in the OpenSim musculoskeletal model including: 1) length of each bone and muscle, 2) position of the centre of mass of each bone, 3) mass of each segment, i.e. mass of a specific bone and all of the attached muscles. This process starts with the unscaled OpenSim musculoskeletal model (Fig. 2.9) and places a set of virtual markers on the model based on the location of the experimental markers (Fig. 2.5). The unscaled model has predefined weight, height, inertia and position of centre of mass for each body segment. A scaling factor for each segment is then calculated and used to linearly scale length and mass. Scaling factors are obtained by computing the ratio between the subject's segments mass and dimension and the generic OpenSim model segments mass and dimension. The dimension of the subject's segments are estimated by computing the distance between the centres of the joints the segment is connected to (Section 2.2.1). In the case of the femur for instance, the length of the segment is calculated by computing the distance between hip and knee joint centres. The mass of each segment is derived from the subject's total mass using anthropometric tables [11]. The scaling process is an OpenSim built-in tool [11, 46].

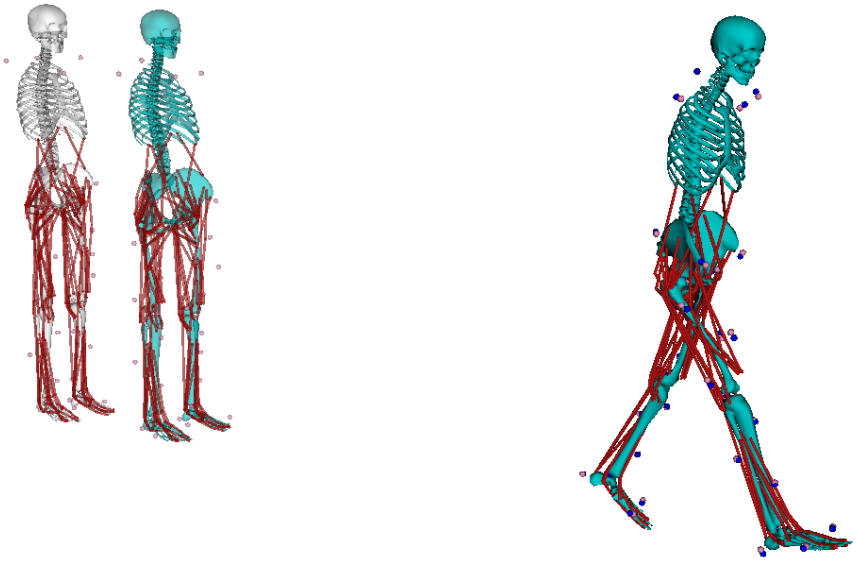

Figure 2.10: The unscaled model (grey) is first scaled to subject's real dimension. During the inverse kinematics step the scaled model (blue model) is driven so that the displacement error between virtual markers (pink markers) and the experimental ones (blue markers) is minimized at each time step.

2.2.3 Inverse Kinematics

Marker trajectories recorded during dynamic movements are used by an Inverse Kinematics (IK) model to calculate 3D joint angles (Fig. 2.10). This is done using the OpenSim Inverse Kinematics tool in which an IK algorithm solves for the joint angles that minimize the difference between the experimentally measured marker positions and the virtual markers on the model (Section 2.2.2).

2.2.4 Residual Reduction Analysis

Ground reaction forces (GRF) recorded during motor tasks are used in conjunction with the thee-dimensional joint angles computed through IK to derive the experimental joint moments. This is usually done by performing standard Inverse Dynamics (ID). However, this method does not provide optimal solutions. Due to limitations in marker trajectory acquisition and processing, there is an inherent mismatch between the recorded trajectories and the recorded GRF. As a results, in traditional ID algorithms, a non-physical external force and moment (i.e., residuals) are applied to a body in the model (e.g.,the pelvis) to resolve dynamic inconsistency between the measured kinematics and GRF. This implies that, the

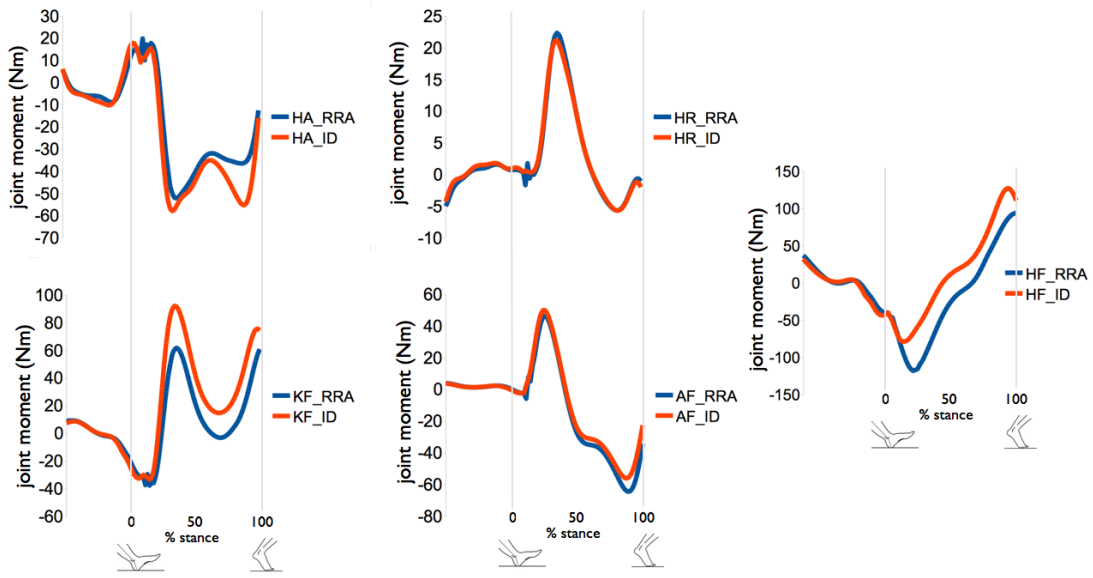

Figure 2.11: Comparison between the joint moments computed using standard inverse dynamics (ID) and residual reduction analysis (RRA).

moments computed via ID do not match the motion computed via IK. In this work Residual Reduction Analysis (RRA) is used to minimize the mismatch between trajectories and GRF and to compute the joint moments needed to track the subject's motion. RRA is an optimization procedure that slightly adjusts the joint kinematics and model mass properties until an inverse dynamic solution is found that minimizes the magnitude of the residuals [11]. Fig. 2.12 and 2.11 show how estimates of joint moments and angles change when using standard ID as opposed to RRA. Fig. 2.13 shows how the motion simulation differs when using ID and RRA. Experiments are obtained from one male subject (age:28, weight: 67Kg, height: 183cm) who performed walking trials at self selected speed. The residuals held in the pelvis body associated to the ID simulation were as follows: $FX = -19.31N$, $FY = 108.608N$, $FZ = -4.94242N$, $MX = -13.9448Nm$, $MY = -4.00663Nm$ and $MZ = 26.8262Nm$. These were significantly reduced by the RRA algorithm: $FX = -0.692733N$, $FY = -0.709131N$, $FZ = -0.104057N$, $MX = -9.7929Nm$, $MY = 0.285471Nm$ and $MZ = -18.4733Nm$. The terms F and M represent the magnitude of forces and moments respectively, that are applied to the pelvis body to resolve the dynamic inconsistency.

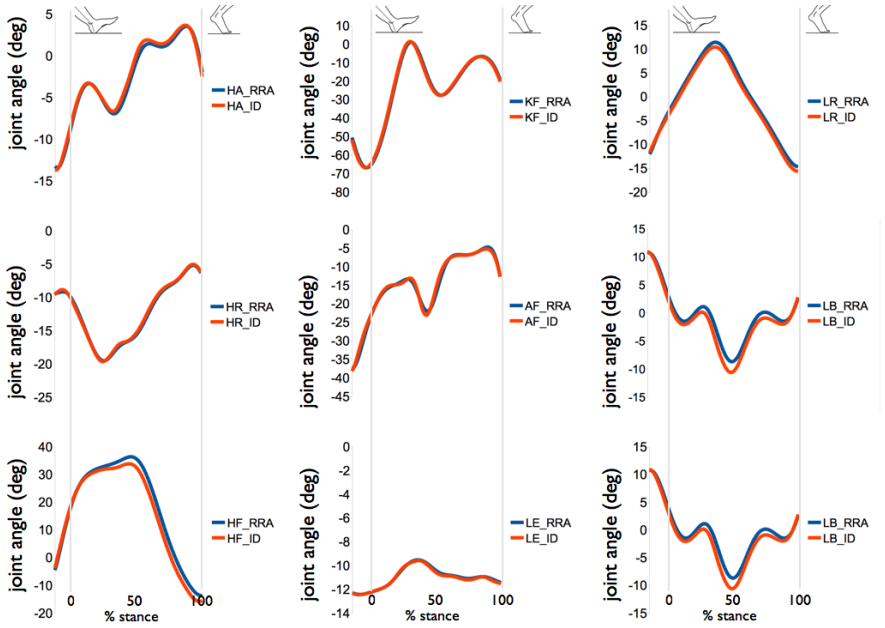

Figure 2.12: Comparison between the joint angles computed using standard inverse dynamics (ID) and residual reduction analysis (RRA).

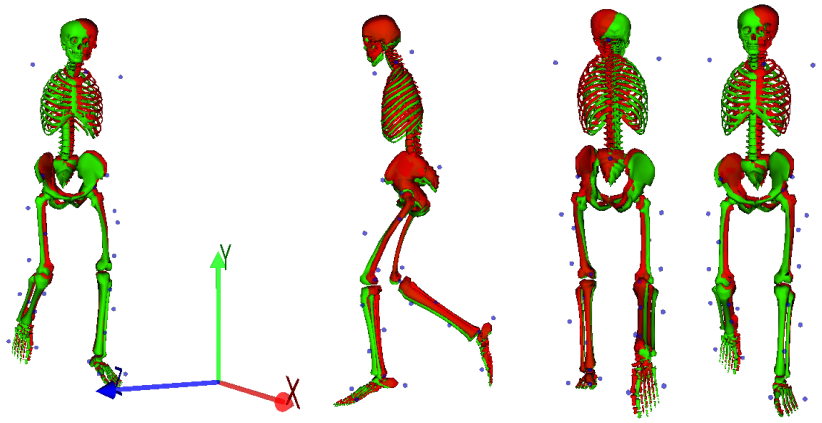

(a) (b) (c) (d)

Figure 2.13: (a) Motion simulation using standard inverse dynamics (red model) is compared to the dynamically consistent one obtained using RRA (green model). The global reference frame is shown. (b) Lateral view. (c) Posterior view. (d) Anterior view.

2.2.5 Contact Model

The RRA approach has the disadvantage that while it allows perturbing the whole-body kinematics it does not allow perturbing the feet kinematics when they are in contact with the ground. This is because RRA can only use GRFs obtained experimentally. Therefore, if the foot kinematics was changed, the experimental

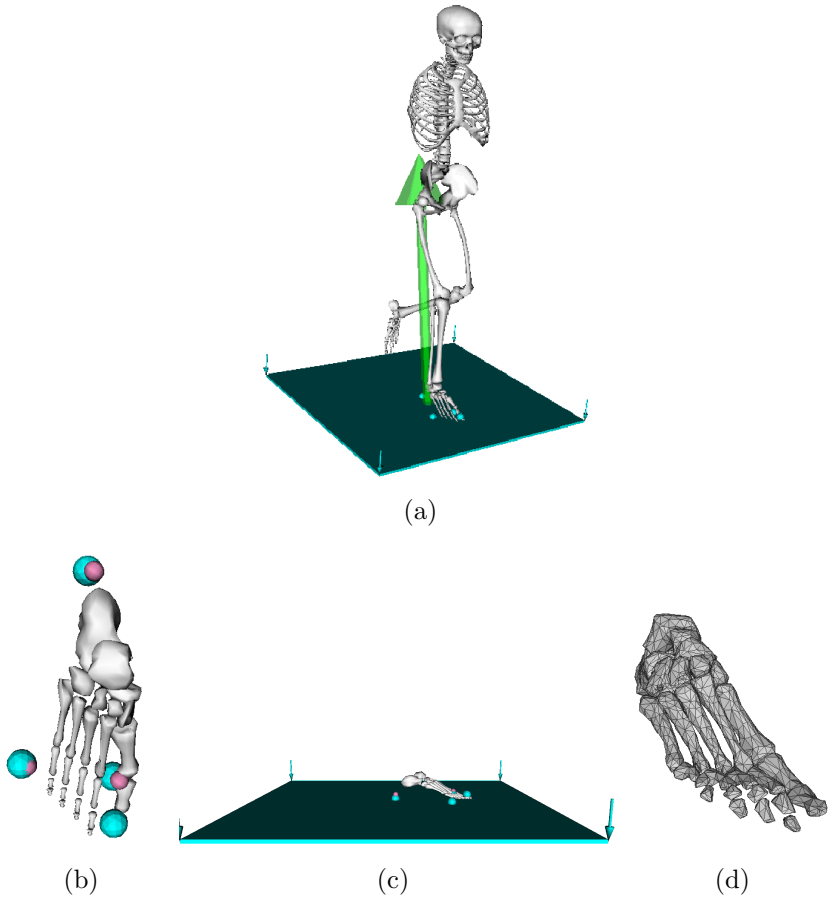

Figure 2.14: (a) Contact model working with RRA (b) Contact meshes are placed in the correspondence of the foot anatomical landmarks. (c) Contact meshes are placed on the same plane of the floor contact mesh. (d) More sophisticated meshes can be used in future implementations such as a foot-shaped mesh. This one is anatomically accurate and was obtained from the study presented in [5].

GRF would not be valid anymore and a further dynamic inconsistency would be included in the process. Furthermore, RRA assumes that by changing the whole-body kinematics but the feet kinematics, the GRF do not change. This assumption is not necessarily true.

In this thesis work, a novel foot-ground contact model was developed (Fig. 2.14a) in a custom C++ program using the OpenSim Application Programming Interface[2] (API). The foot-ground contact model allows modeling contact between objects that are defines by 3D meshes by utilizing an *elastic foundation model* [51]. It places a spring at the center of each face of each *contact mesh* it acts on. Those springs interact with all objects the mesh comes in contact with. It is then

[2]The Doxygen documentation is available at: https://simtk.org/api_docs/opensim/api_docs20b/

possible to assign different physical properties to each contact mesh including: stiffness, dissipation and static, dynamic and viscous frictions.

Four spheres were placed on the OpenSim musculoskeletal model's in the correspondence of heel, first and fifth metatarsal bones and toe (Fig. 2.14b). This was done using the 3D position of the experimental markers obtained from motion capture data. Because no experimental marker was placed on the toe, the position of the associated contact sphere was placed at $2cm$ from the first metetarsal bone. Then, the four spheres were placed on the same plane and the floor contact mesh was consequently aligned as in Fig. 2.14c. Finally, the dynamic contact parameters were assigned a meaningful physical value to define appropriate contact. In this work both floor location and contact parameter values were defined manually. In future implementations an optimization algorithm will be used to find optimal position of the floor and optimal contact parameters. The optimization procedure will minimize the difference from the experimental GRF recorded during a static standing trial and those simulated by the proposed contact model. Furthermore, more sophisticated meshes will be used (Fig. 2.14d).

Once the contact model is calibrated it is possible to use it in conjunction with RRA to also adjust the foot kinematics (Fig. 2.14a) and subsequently recompute the associated GRF. In general, at each time step, the contact model computes the the GRF generated by the RRA kinematics change. A more accurate ID solution can then be used in RRA. The contact model presented in this section was not used in the studies reported within this thesis due to lack of time. Although it is very promising, further validation is needed.

In future work, the presented contact model can be also utilized to create dynamic motion simulations of humanoid robots.

2.3 An Elastic-Tendon NMS Model of the Knee Joint

This section briefly reviews the NMS model developed by Lloyd et al. and previously presented in [2, 3, 35, 37]. Lloyd'd NMS model is used to validate the novel NMS

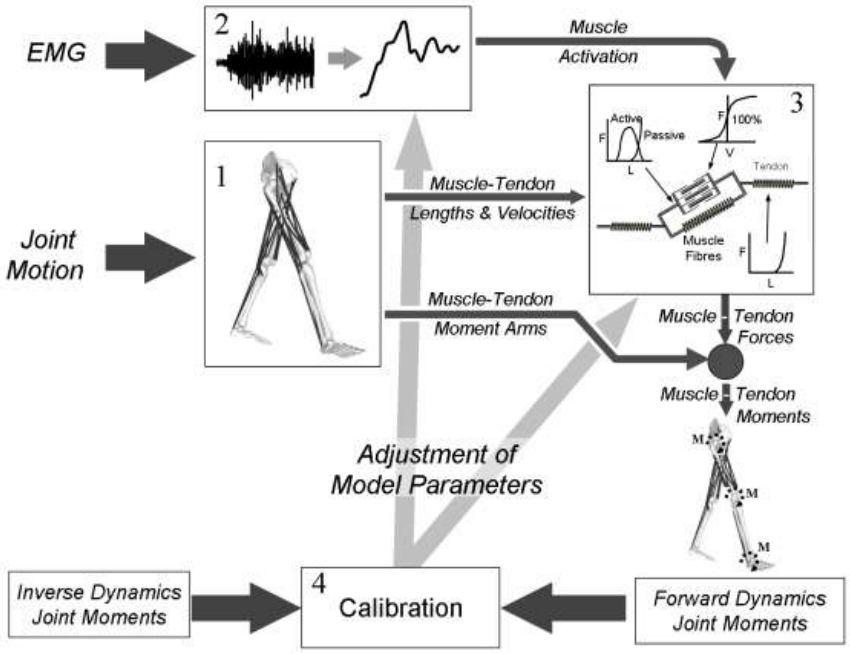

Figure 2.15: Flow chart depicting the 4-step process of Lloyd et al. EMG-Driven model [3, 4]. Musculotendon lengths, velocities, and moment arms are obtained from the SIMM anatomical musculoskeletal model (1) which along with the processed EMG (2) are incorporated into a Hill-Type muscle model (3) to estimate net muscle forces and resultant joint moments. The calibration process (4) adjusts selected parameters to minimise the difference between these joint moment estimates and those obtained from standard inverse dynamics.

model that is presented in this thesis. This comparison allows quantifying how, changes and extensions applied to the NMS model design, affect its global operation and performances.

The NMS model developed by Lloyd et al. was chosen as a *baseline* for comparison for several reasons:

1. it has been extensively validated in the past,
2. it is anatomically and physiologically accurate,
3. it represents the state of the art of the EMG-driven NMS models of the knee joint.

Lloyd's EMG-driven NMS model (Fig. 2.15) consists of 4 fundamental components: anatomical musculoskeletal model (Fig. 2.15-(1)), Muscle Activation model (Fig. 2.15-(2)), Muscle Dynamics model (Fig. 2.15-(3)), Calibration (Fig. 2.15-(4)). It uses these in conjunction with raw EMG and segmental movement to estimate

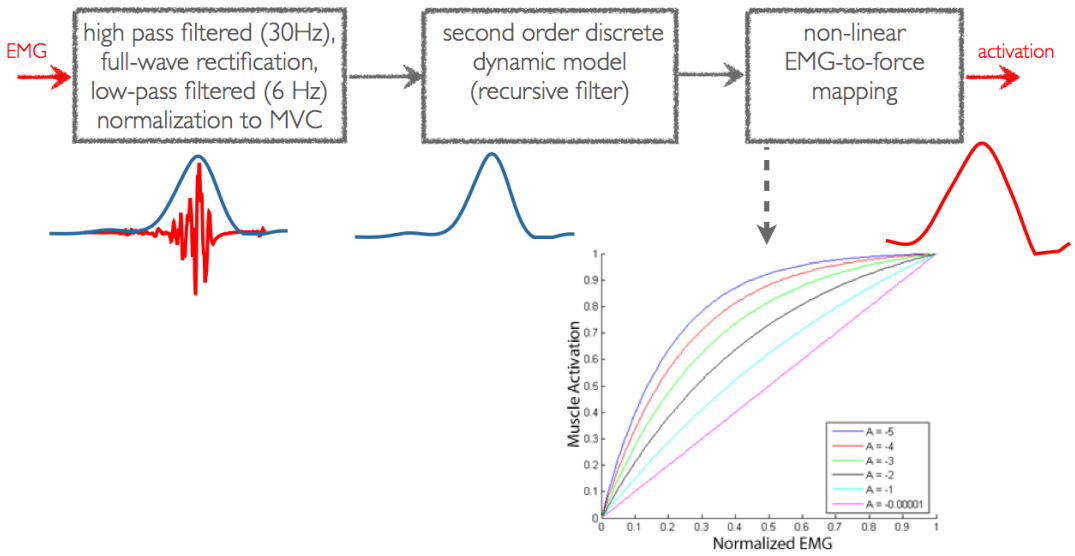

Figure 2.16: Raw EMGs are low-lass filtered (30Hz), full-wave rectified and low-pass filtered (6Hz). Signals are then normalized to maximal voluntary contraction (MVC) to obtain the normalized linear envelope. A second order recursive filter is applied to model the electromechanical delay and to include the muscle's twitch response [3]. Signals are then non-linearly mapped to account for the non-linear relationship between EMG amplitude and muscle force [3].

individual muscle force and subsequently joint moments and soft tissue loading. This is a forward dynamic model because it estimates muscle force directly from muscle EMG signals in an open-loop fashion.

2.3.1 Musculoskeletal Model

The musculoskeletal model of the lower limb (Fig. 2.15-(1)) is created using the SIMM Biomechanics Software Suite (Musculographics, Inc.) [45] based on the results presented in [37, 44]. It consists of line segment representations of 13 musculotendon actuators (MTAs) spanning the knee joint including: semimembranosus, semitendinosus, biceps femoris long head, biceps femoris short head, sartorius, tensor fascia latae, gracilis, vastus lateralis, vastus medialis, vastus intermedius, rectus femoris, gastrocnemius medialis, and gastrocnemius lateralis. Only two muscles crossing the knee are not included: the plantaris and the popliteus. They are assumed to have a negligible contribution to the total flexion-extension (FE) moment due to their relatively small physiological cross sectional area (PCSA). The lengths of the modeled bones and MTAs are linearly scaled to the actual

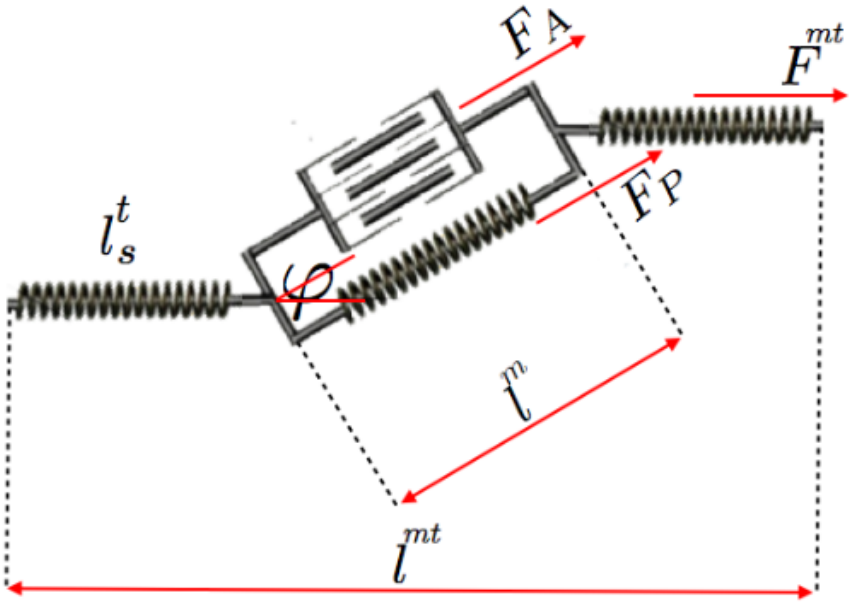

Figure 2.17: Hill-type elastic-tendon muscle model. Each tendons is represented by a single elastic passive element. The fibre is represented by an active contractile element in parallel with a passive element. The two-element fibre is placed between the two tendons. The fibre is oriented with respect to the tendon according to the pennation angle φ. l^{mt} is the musculotendon length. l^m is the fibre length. l_s^t is the tendon slack length. F_A is the force produced by the fibre active element. F_P is the force produced by the fibre passive element. F^{mt} musculotendon force, i.e. the fibre force projected on to the tendon line of action.

subject's size. This muscuoskeletal model is used in SIMM to perform a kinematic driven simulation to determine muscletendon lengths, l^{mt}, velocities, v^{mt}, and moment arms, r during movement. These values are then input in the Muscle Dynamics model together with muscle activation to estimate muscle force (Section 2.3.3).

2.3.2 Muscle Activation

Raw EMG signals are processed as in Section 2.1 to obtain normalized linear envelopes. Then, a second order recursive filter is applied to characterize the muscle electromechanical delay and twitch response [3]. We will refer to the processed signals to as, $u(t)$. Then, a non-linear map is applied to account for the non-linear relationship between EMG amplitude and muscle force [3] (Fig. 2.16). To achieve this step, an exponential relationship is used which includes a single parameter A

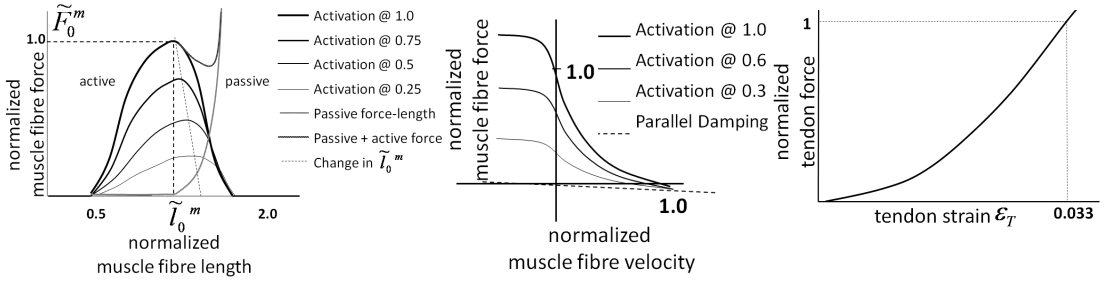

(a) (b) (c)

Figure 2.18: (a) Active and passive force length curves. Values are normalised by F_0^m and l_0^m with 1.0 being 100% activation. Optimal muscle fibre length was scaled with activation by a relationship experimentally determined in [52] (b) Normalised force-velocity relationship. Note the parallel damping element added to prevent singularities when activation or isometric force = 0.0 of the inverted force-velocity relationship [36]. (c) Exponential tendon force-strain relationship.

to control the extent of the non-linear relationship [2]:

$$a(u(t)) = \frac{e^{Au(t)} - 1}{e^A - 1} \tag{2.1}$$

where A is the non-linear shape parameter and it is constrained to $-5 < A_i < 0$, with 0 being a linear relationship.

2.3.3 Muscle Dynamics

A Hill-type muscle model is used to represent each musculotendon actuator (MTA), and consists of a contractile element in series with a non-linear elastic-tendon [1, 53] (Fig. 2.17). The tendon is modeled using an exponential force-strain curve (Fig. 2.18c). This is scaled by tendon slack length l_s^t and maximal isometric force at optimal fibre length F_0^m. It is used to interpolate musculotendon forces [1]. The muscle fibre is composed of an active force-generating contractile element in parallel with a passive elastic one. The contractile element consists of a generic active force-length function $f_A(\tilde{l}^m)$ (Fig. 2.18a, active curve) and a force-velocity function $f_V(\tilde{l}^m)$ (Fig. 2.18b). A passive parallel damping element (d^m) is added to $f_V(\tilde{l}^m)$ as suggested by [36] to prevent any singularities of the mass-less model when activation or isometric force are zero. The passive elastic component in the muscle fibre is modeled using the exponential relationship $f_P(\tilde{l}^m)$ in Fig. 2.18a

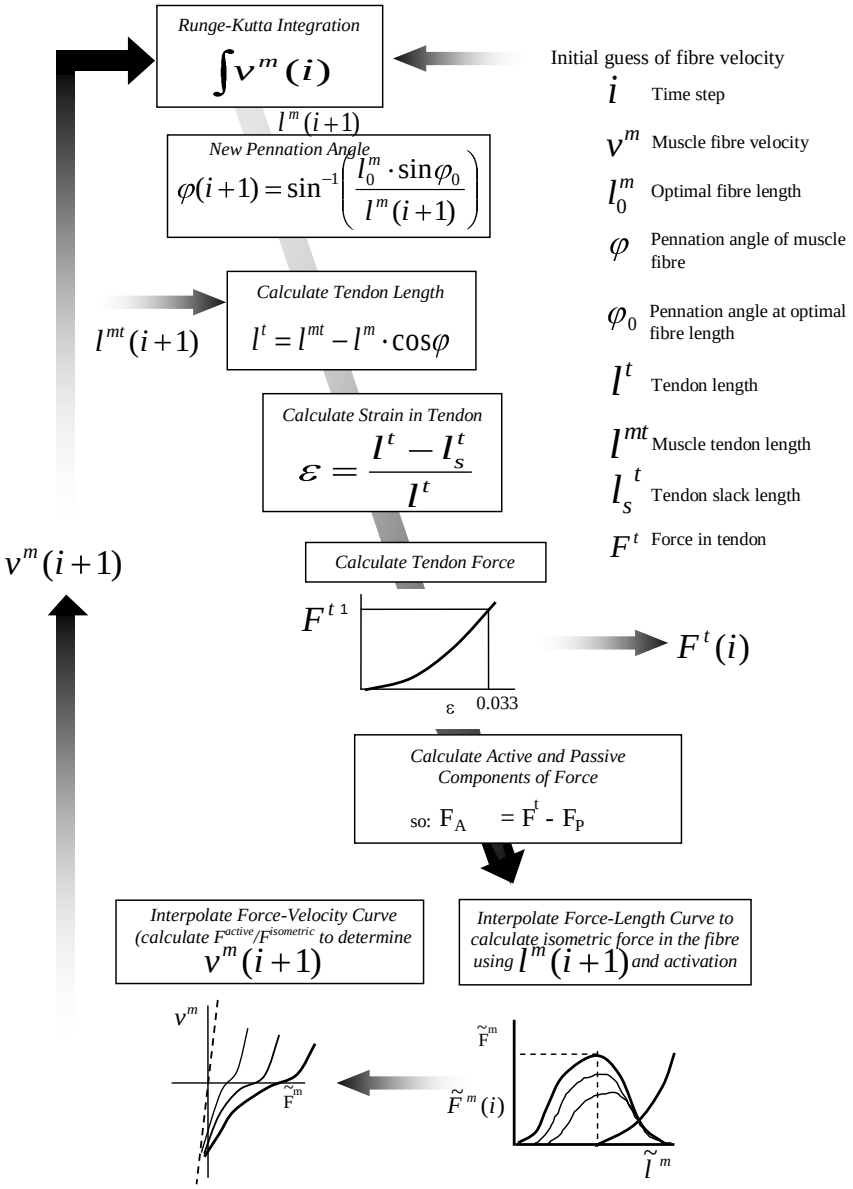

Figure 2.19: Schematic diagram of muscle dynamics

(passive curve). The final MTA force depends on a number of parameters including: maximum isometric muscle force at optimal fibre length F_0^m, optimal muscle fibre length l_0^m, instantaneous pennation angle φ, instantaneous muscle fibre length l^m, instantaneous fibre contraction velocity v^m, and instantaneous muscle activation $a(u)$. It is the contractile element of the model that represents the culmination of the forward dynamics component of the EMG-driven NMS model, as the muscle fibre velocities are numerically integrated to predict the time evolution of the muscle fibre length. The dependence of l_0^m on muscle activation [54] is modeled using a linear relationship [3]:

$$new\_l_0^m(t) = l_0^m \cdot (\gamma \cdot (1 - a(t)) + 1) \tag{2.2}$$

where:

- γ = percentage change in optimal fibre length
- $new\_l_0^m$ = new optimal fibre length
- l_0^m = current optimal fibre length
- $a(t)$ = activation at time t

The effect of this relationship is illustrated in Figure 2.18a. The percentage change in optimal fibre length, γ, is altered in the calibration process between 0 and 20% as a function of activation (Section 2.3.4). Muscle fibre lengths are calculated by forward integration of the fibre velocities obtained from the force-velocity and force-length relationships using a Runge-Kutta-Fehlberg algorithm. Using a method developed by Loan [55], initial muscle fibre lengths and fibre velocities are determined by calculating the stiffnesses of muscle fibre and tendon, and apportioning the total muscle tendon velocity to the muscle fibre and tendon based on their relative stiffnesses. A schematic diagram of the complete muscle model is shown in Figure 2.19.

Muscle fibre force can then be expressed as:

$$F^m = (f_A(\tilde{l}^m) \cdot f_V(v^m) \cdot a(u) + f_P(\tilde{l}^m) + d^m \cdot \tilde{v}^m) \cdot F_0^m \cdot \delta \tag{2.3}$$

where the term δ is the muscle strength coefficient (Section 2.3.4) whereas all other terms have been defined previously. The force produced by the MTA, F^{mt}, can then be derived by projecting the fiber force F^m onto the tendon line of action as follows:

$$F^{mt} = F^m \cdot cos(\varphi) \tag{2.4}$$

Indeed, the pennation angle, φ defines the angle at which fibers are oriented with respect to the tendon (Fig. 2.17).

Net knee joint flexion-extension (FE) moments (M) are obtained by summing the product of each MTA's force by its flexion-extension moment arm r:

$$M = \sum_{i=1}^{N} r_i F_i^{mt} \tag{2.5}$$

where $r_i F_i^{mt}$ represents the individual FE moment generated by the i^{th} muscle.

2.3.4 Validation and Calibration

To validate a model, it is usually desirable to compare the output of that model with data measured empirically. Unfortunately, the methodological difficulties in measuring individual muscle forces prevent any direct validation of the EMG-driven model on humans. An indirect validation process is instead used to validate and calibrate the model to an individual. The validation process involves comparing the predicted net knee flexion-extension moments with the net moments measured experimentally. If the muscle forces are accurate, then the model estimates of net joint moments should be equal to the external moments measured experimentally.

Lloyd et al. used standard Inverse Dynamics to calculate experimental knee FE moments. It is here clear the importance of utilizing dynamically consistent joint moments in the calibration. If this is not done, the calibration will constrain muscles to satisfy join moments that are not truly representative of the actual joint dynamics.

The aim of the calibration process is to obtain a set of model parameters for an individual to accurately estimate the net FE moments at the knee. The calibration process uses a set of calibration trials to *learn* the muscle dynamics across a

wide range of muscle contractile conditions. Starting from a set of uncalibrated parameters a simulated annealing algorithm [56] is used to alter the selected parameters so that the moments estimated by the NMS model fit the net joint moments experimentally measured and minimize the sum of squared difference between the estimated and experimental moments. Once the calibration process has completed it is possible to use the subject-specific calibrated parameters to estimate muscle forces and joint moments during the subject's movement. It is worth noting that once calibrated, the NMS model only requires EMG signals and joint angles and can execute in open-loop. That is, no *tracking* is required to match the experimental joint moments. If properly calibrated, the model will naturally track novel data with no need for optimization. Tracking the experimental moment is required during the calibration step only. This feature allows deceasing the amount of information required during the model run-time execution and maximize its speed.

The adjustable parameters used in the calibration process are divided into two groups. One group includes activation parameters, chosen from the Muscle Activation model and the other group includes muscle parameters from the Muscle Dynamics model. Activation filtering parameters are constrained in the calibration process to realize a stable positive solution to the discrete linear dynamic model and used to determine the gain and recursive coefficients of the recursive filter. These coefficients are dimensionless and are varied between -1 and 1. They take into account changes in muscle excitation levels due to different EMG electrode placement, skin preparation, and impedance. It is assumed that these values may differ between individuals, different muscles, and different testing sessions. The non-linear muscle activation shape factor A in (2.1) is also altered in the calibration process between -5 and 0 (2.1). The non-linearity of the EMG to force relationship has been well documented and has shown that the inclusion of this parameter within a transfer function improves model estimates of stress from EMG data [57]. Parameters in the Hill-type Muscle model that are adjusted include:

1. muscles strength coefficients

2. resting tendon slack length

3. muscle optimal fiber length

The strength coefficients allow scaling the relative maximum isometric force a muscle can produce to account for well documented individual differences in muscle strength, i.e. Physiological cross-sectional area and difference in strength between different muscles. To maintain relative strength across all muscles, global gains were used as opposed to individual muscle gains. The inclusion of muscle dependent force coefficients is physiologically valid to account for strength differences between individuals and has been used previously in EMG-Driven models. However, care must be taken when increasing the number of parameters within an optimisation process as this may compromise the physiological construct of the model, as each parameter becomes a *fix* for a general solution to be obtained. Constraints on muscle gain coefficients were used to prevent unrealistic muscle forces being estimated by the model. These were applied such that each strength coefficient was allowed to vary from 0.5 to 1.5. In the NMS model presented in this Chapter, strength coefficients grouped muscles into three categories: knee extensors, knee flexors and gastrocnemious muscles.

Resting tendon slack length (l_s^t) directly defines the length of the fibers and the force they can produce. Furthermore, there is very little information in the literature in regards to tendon slack lengths of lower limb musculature. The reason for this lack of information is mostly due to the difficulty in measuring these values and the ill-defined junction between muscle and tendon. This further motivated the need for calibrating this parameter. Initial values were obtained from [37] and constrained such that: $l_s^t = initial\_value \pm 5\%$.

Optimal fibre length (l_0^m) is also calibrated as it has been shown to vary between individuals and to have a strong impact on the behavior of each muscle [37]. Initial values were obtained from [37] and constrained such that: $l_0^m = initial\_value \pm 2.5\%$.

The objective function used in the calibration algorithm is defined as follows:

$$min \sum_{N_t} \frac{\frac{M^2 - \hat{M}^2}{var(\hat{M})} + Penalty}{N_t} \tag{2.6}$$

$$Penalty = \sum_{i=1}^{N_t} \sum_{j=1}^{N_m} P(i,j) \tag{2.7}$$

$$P(i,j) = \begin{cases} 0, & \text{if } 0.5 < \tilde{l}^m(i,j) < 1.5 \\ 0.5, & \text{otherwise} \end{cases} \tag{2.8}$$

where $\hat{M}$ and M are the measured and predicted knee FE moments respectively. The $var(\hat{M})$ term is the variance of $\hat{M}$ over all time steps N_t. The N_m term represents the number of muscles in the NMS model. A penalty is included in the objective function to penalize instances of $\tilde{l}^m$ being less than 0.5 or greater than 1.5. This is to discourage the algorithm from adopting solutions that results in the muscle operating in a range that is not physiological. The structure of this penalty factor is such that it is incremented for every time point that any muscle has $\tilde{l}^m$ outside of the range $0.5 < \tilde{l}^m < 1.5$. The magnitude of this increment is set such that a muscle operating outside of the specified range for the entire trial would approximately double the cost function value.

2.4 Differences to Lloyd's NMS model

The model developed by Lloyd at al. [3] is used in this thesis as a *baseline* for comparison. From here on we will refer to it to as the *baseline NMS model* or to as the *elastic-tendon NMS model*.

While the structure of the NMS model proposed in this thesis is like that of the baseline model, it also differs in many parts including:

1. Anatomical musculoskeletal model. Section 2.2 presents the methodology used in this thesis. Section 2.3.1 presents the methodology used in the baseline NMS model.

2. Hill-type muscle model. Chapter 3.5 presents the methodology used in this thesis. Section 2.3.3 presents the methodology used in the baseline model.

3. Musculotendon kinematics computation. Chapter 4 presents the methodology used in this thesis. Section 2.3.1 presents the methodology used in the baseline model.

4. Number of DOFs. Chapter 6 presents the methodology used in this thesis. Section 2.3.1 presents the methodology used in the baseline model.

5. Calibration. Chapters 5, 6 and 7 present the methodology used in this thesis. Section 2.3.4 presents the methodology used in the baseline model.

2.5 Conclusions and Future Work

In this chapter the general workflow that was used in this research work was presented. This included: 1) the acquisition and processing of data from the subject's movement, 2) the creation of a dynamic musculoskeletal simulation to estimate joint kinematics and moments, 3) the execution of the NMS model.

Advanced methods were developed and used to scale a generic OpenSim musculoskeletal model to match the subject's anthropometry and anatomy and to define optimal centres and axes in the hip, knee and ankle joints. Advanced motion simulation methods were used to calculate three-dimensional joint kinematics and moments and to ensure dynamic consistency between kinematics and kinetics. To further improve this process a foot-ground contact model was also implemented. These methods were used to generate the best input data for the NMS model developed and presented in this thesis. The aim of this specific work was that of introducing anatomical and dynamic consistency into EMG-driven modeling. The quality of the data used to calibrate the EMG-driven NMS model strongly affects its operation *post-calibration*. Because the EMG-driven NMS model is physiologically accurate and it uses real muscles excitation signals (i.e. EMG signals), the hypothesis is that by providing calibration data that better represent the dynamics of the human movement, the model will *learn* more naturally the prescribed muscle dynamics. Future work will therefore compare the NMS model performances when both traditional and advanced techniques are used to obtain calibration data.

The last two sections of the chapter illustrated the general structure of the NMS model developed by Lloyd et al. and the main differences with respect to the model presented in this thesis.

Chapter 3

A Stiff-Tendon Neuromusculoskeletal Model of the Knee Joint

In this Chapter motion capture technology is used together with a novel neuromusculoskeletal (NMS) model of the knee joint and sophisticated algorithms for motion kinematics and dynamics computation, to estimate somatosensory information during the human movement. Although the NMS model represents the single knee joint, it has been designed so that it is straightforward to extend to whole-body level with minor loss of computational time performances. This Chapter shows the proposed NMS model is as accurate as the complex models previously presented in the literature. It shows it achieves superior computational time performances. It validates the model on a population of 6 male subjects and directly compares its behavior to that of the model previously developed by a leading research group in musculoskeletal modeling. The Chapter illustrates how the proposed model can be used as a human-machine interface for the control of a powered orthosis of the lower limb and discusses how it can be used for the actuation of humanoid robots equipped with artificial muscles. This research development aims to integrate musculoskeletal dynamics into robotics systems to achieve more advanced bio-inspired control strategies.

3.1 Introduction

The development of computer simulation methods based on biologically relevant neuromusculoskeletal (NMS) models has gained particular emphasis in recent years in the field of robotics for effectively helping understand mechanisms of motion in humans [25, 58]. The need for better understanding the role of muscle function during movement is regarded as a key-point for the design of robotic systems that can robustly embody humans ability of moving. This trend can be identified as *Musculoskeletal Robotics* [59].

Indeed, the human musculoskeletal system provides form, support and stability to the body. The extraordinary capacity to efficiently use muscles allows us to realize challenging tasks including: 1) the ability to actively move in a huge variety of unknown environments, 2) the ability to add compliance to our movements and make interaction with humans and real-world objects, 3) the ability to realize multi-modal locomotion, i.e. different locomotion modes such as walking, running or hopping.

As a result, several bio-inspired humanoid robots have been proposed in which artificial muscle and tendon structures are attached to different parts of the humanoid body just like real muscles are attached in the human body [12, 13, 60–62]. This gives the robot more degrees of freedom of actuation than could be achieved with motorized rotary joints and the potential ability of moving around and interacting with the physical world in the same way our flesh bodies do [60, 62]. Despite this great advancement in the musculoskeletal design, no effective solutions have been proposed yet to activate the artificial muscles and actuate the humanoid robots. In this context, the development of accurate musculoskeletal software models can help defining the humanoids artificial muscles contraction dynamics. For this purpose, human muscle contraction dynamics can be used as a means of bio-inspired control system for humanoids.

The need for understanding muscle contraction dynamics also plays a central role in the design of assistive devices such as powered orthoses and exoskeletons. In this case, a better understanding of the real-time behavior of human muscles can improve the actuation of these devices and their control algorithms, resulting

in enhanced biomimetic control systems [6, 8]. Citing Nakamura et al.: *when the man-machine interface obtains access to the somatosensory information, machines would make the first step to understand humans. Such implicit communication between humans and machines could be termed as a cognitive-level communication* [6]. Bringing human musculoskeletal models into robotics will open the door to a new generation of human-machine interfaces (HMIs) for a more intuitive device control.

Therefore, it is crucial to develop models that reflect the action of muscles while minimizing processing time in musculoskeletal robotics research.

This Chapter presents a novel neuromusculoskeletal (NMS) model of the knee joint that is used together with motion capture technology and sophisticated algorithms for motion kinematics and dynamics computation, to estimate *somatosensory* information during the human movement (Fig. 2.1). Although the model represents a single joint, it has been designed so that it is straightforward to extend to whole-body level with minor loss of computational time performances. Chapter 6 will present an extension to the lower extremity level. The somatosensory information includes activation, force, length and contraction velocity of the muscles spanning the knee joint. This information is also used to estimate the knee flexion-extension moments as well as contact forces between bones generated during movement. The Chapter also shows the proposed model can be used as a human-machine interface (HMI) for the real-time control of a powered orthosis of the lower limb. It is then discussed how the NMS model can be used for the actuation of humanoid robots equipped with artificial muscles.

A great body of research has been previously conducted in the field of neuromusculoskeletal modeling. In the literature there have been adopted either simplified neuromusculoskeletal models that are suitable for applications with real-time constraints or very detailed and physiologically accurate models that are not efficients from a computational point of view.

Biomechanists have developed complex models of the human joints that combine together kinematic and kinetic data with neural signals to study human muscle behavior in vivo [1–3, 35, 36]. These models are extremely accurate in the way they represent physiological properties of the musculoskeletal system. To

enable the estimation of muscle force and joint moment, musculoskeletal models usually require explicit expressions of muscle-tendon kinematics including: musculotendon length, three-dimensional muscle moment arms, muscle fiber length and contraction velocity.

A main limitation of these models is they usually do not integrate these operations into a common framework. Third party musculoskeletal geometry software is used to estimate musculotendon length and three-dimensional muscle moment arms and include: SIMM [44, 45], OpenSim [11, 46] and AnyBody [63]. These are driven by graphical user interfaces (GUIs) and are difficult to implement in custom software or micro controllers due to their extreme detail of complexity in modeling the pathways of the musculo-tendon complexes. This prevents the NMS model, that uses them, to be entirely executed on line.

A second limitation is their complexity. These NMS models have complex muscle models in which tendons and fibers are represented as elastic bodies capable of stretching and contracting. An ordinary differential equation (ODE) has to be integrated at each time step to estimate the instantaneous value of muscle fiber length and contraction velocity (Section 2.3). This usually requires a great amount of computational time which quickly grows with the number of muscles in the model. Therefore, these models are unsuitable for robotics applications with real-time constraints.

Only recently, robotics researchers have developed models that are suitable for real-time applications [6, 8–10, 15, 38, 64]. These works, however, either utilize very simplified models of the human joints or they do not integrate information of the human musculoskeletal system at all. In general, real-time performances are obtained by simplifying the model design. One main simplification is that of using simple musculoskeletal geometry models that estimate musculotendon length and muscle moment arms on a plane only, i.e. the joint flexion-extension plane. This leads to inaccurate estimations of musculotendon kinematics and represents a critical point because small errors in their values can result in large errors in musculotendon force and joint moment prediction.

A second simplification is that of including a very limited number of muscles spanning a specific joint. This implies the impossibility of correctly estimating

the moments developed by the user at that joint. In fact joint moments can only be correctly estimated if all muscles spanning that joints are considered and their force is estimated.

Another limitation is that of not taking into consideration the change in muscle force due to fibers contraction velocity. This plays an important role when the subject transitions from one locomotion mode to another, i.e. from walking to running.

Furthermore these models allow calibrating a small number of subject-specific parameters thus making the scaling process less able to adapt to different subjects.

Finally, validation of the model is not paid much attention and the model is usually evaluated on one subject only and on a small number of motor tasks. In general, the degree of simplification often makes these models unsuitable for being integrated into the control system of assistive devices that are to support a wide range of movements.

This Chapter shows the proposed NMS model is accurate and achieves superior computational time performances and proposes a solution that addresses the limitations of the complex but slow models developed by biomechanists and the fast but simplified ones developed by robotics engineers [65–67].

A novel methodology is proposed to produce accurate estimates of musculo-tendon length and three-dimensional muscle moment arms eliminating the need for using an off-line GUI-driven software. This allows executing the entire NMS model on line and.

Fast operation of the NMS model is achieved by designing a novel muscle model that allows estimating muscle fiber length and contraction velocity much faster than the NMS models developed by biomechanics and with comparable predictive accuracy.

The muscle redundancy problem is solved using electromyographic (EMG) signals produced by the human muscles during movement. Previously presented approaches [6, 9] assume the muscles share the load about a joint based on some objective function that has to be carefully chosen before hand or based upon statistical assumptions. This is a limitation because muscles in general use different criteria depending on the subject and on the movement and it is often impossible

to assess the appropriateness of the chosen optimization criteria or statistical approach.

A robust validation methodology of the model is adopted. The NMS model is used on a population of 6 male subjects who performed 75 of motor tasks. The prediction accuracy was assessed by comparing the proposed methodology to the well established model developed by biomechanists Lloyd et al. [2, 3, 35, 37, 47]. Real-time operation was assessed by running the proposed NMS model on an embedded system that could be used for the real-time control of a powered orthosis.

This research development aims to integrate musculoskeletal dynamics into robotics systems to achieve more advanced bio-inspired control strategies. Neuromusculoskeletal modeling technology not only can offer great solutions for exoskeletons control and humanoids actuation, but can also boost research that aims to realize more realistic virtual humans by providing a more realistic estimation of human internal state [5].

3.2 Workflow

Fig. 2.1 gives a schematic view of the three steps that involve the acquisition of data from the human movement, the use of sophisticated algorithms for the dynamic simulation of the human motion and the execution of the neuromusculoskeletal (NMS) model for the estimation of somatosensory information.

3.3 Human Movement

This is the first step in which the data needed for the model calibration and validation are collected and processed.

A data set for the calibration of the model is initially created which includes: 1 static trial, 3 swinger trials, 2 walking trials and 2 running trials per subject. Data collected from the static trial are used to scale the anatomical dimensions of the musculoskeletal model (Fig. 3.1). Data collected from the swinger trials are used to compute the optimal centre of the hip, knee and ankle joints.

Data collected from the 4 dynamic trials are used to calibrate the biomechanical

parameters of the *Muscle Activation Model* (Section 3.5.2) and those of the *Muscle Dynamics Model* (Section 3.5.3).

A different data set is instead used for the validation of the NMS model. This includes 10 walking trials ($2meters/second$) and 3 running trials ($5meters/seconds$) per subject. The validation is performed as described in Section 3.5.5.

A 12 camera motion capture system (Vicon, Oxford, UK) is used to record the human body kinematics with sampling frequency at $250Hz$. A set of reflecting markers are placed on the human body and their instantaneous three-dimensional position is then reconstructed and used to measure the movement of body segments including: trunk, pelvis, thigh, shank, and foot. Ground reaction forces (GRFs) generated during the dynamic trials are collected using a multi-axis in-ground force plate (AMTI, Watertown, USA) with a sampling frequency at $2kHz$. Double-differential surface electrodes are used to collect EMG signals from the selected muscles. A telemetered system (Noraxon, Scottsdale, USA) transfers the EMGs to a 16 channel amplifier (Delsys, Boston, USA) with sampling frequency at $2kHz$.

Both body kinematics and GRFs are low-pass filtered with cut-off frequencies ranging from 2 to $8Hz$ depending on the trial.

Raw EMG signals are first band-pass filtered ($10-150Hz$), and then full-wave rectified and low-pass filtered ($6Hz$) subsequently. The processed signal is the *linear envelope* which is then normalized against the maximum values from EMG linear envelopes obtained from a range of extra trials including: running and squat jumps.

3.4 Movement Modeling

The second step in the process, depicted in Fig. 2.1, uses the scaled musculoskeletal model (Fig. 3.1) to perform an accurate motion dynamic simulation using motion data collected at step one. This produces three-dimensional joint angles and joint moments generated during the human movement. This work uses the freely available OpenSim software [46] to perform such a simulation. The simulation is driven by GRFs and three-dimensional marker trajectories.

Before the simulation is performed, the real dimensions of the subject have to

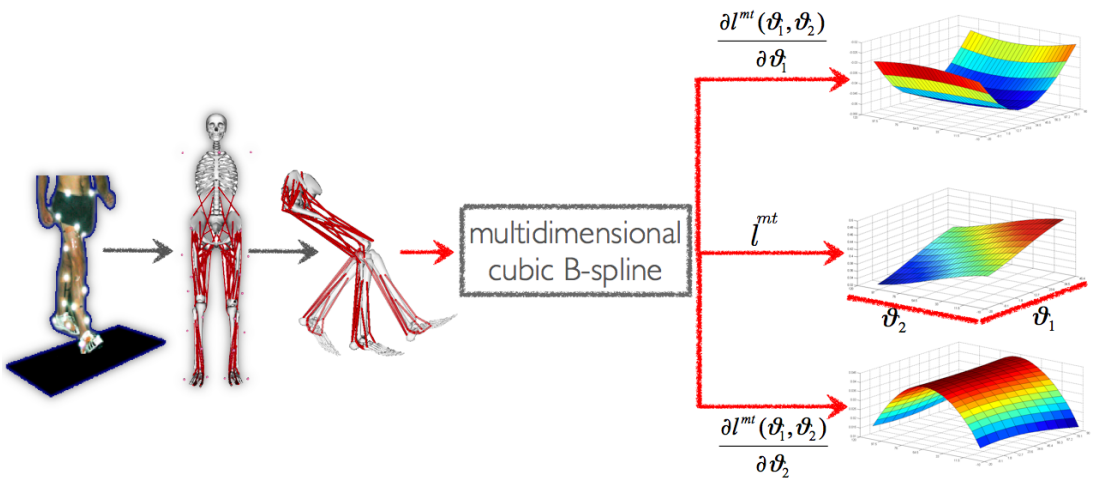

Figure 3.1: Experimental marker trajectories recorded during a static trial are used to scale the generic OpenSim musculoskeletal model to match the subject's anthropometry (also see Fig. 2.2.2). Discrete combinations of joint angles are used to obtain nominal values of musculotendon length (l^{mt}). These are used to create the coefficients for a multidimensional B-spline function per muscle that can interpolate the discrete l^{mt} nominal values. The spline function can then be differentiated with respect to the generalized coordinate (θ_i) of interest to obtain the respective moment arm. The process is here shown in the 2-dimensional case.

be taken into account. Optimal joint centres and axes are computed as previously described in Section 2.2.1. The OpenSim musculoskeletal model is scaled as previously described in Section 2.2.2. Three-dimensional joint angles and moments are measured using Inverse Kinematics and Residual Reduction Analysis as previously explained in Sections 2.2.3 and 2.2.4 respectively.

3.5 NMS Model

The third step in the process depicted in Fig. 2.1 is the execution of the NMS model. This is a digital representation of the human neuro-musculoskeletal organization. It reproduces the transformations that take place from the generation of the EMG signals to the production of muscle forces and knee joint flexion-extension moments. It comprises 5 main components (Fig. 3.2). The main structure is similar to that of the baseline model (Section 2.3). However, the here proposed NMS model introduces novel components including a musculotendon kinematic model

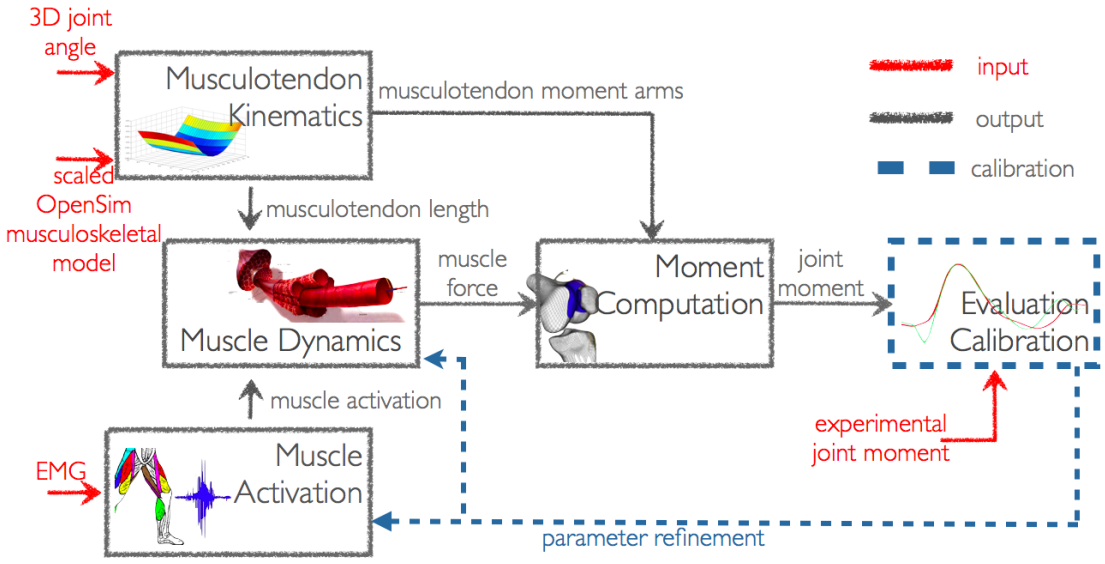

Figure 3.2: Schematic view of the NMS model structure. Model inputs are highlighted in red. Main outputs are muscle force and estimated joint moment.

(Section 3.5.1) and a stiff-tendon muscle model (Section 3.5.3). The EMG-driven NMS model presented in this Chapter was entirely implemented in a C++ custom program and no additional toolboxes were used.

3.5.1 Musculotendon Kinematics

The musculotendon kinematics (MTK) model uses the scaled musculoskeletal model depicted in Fig. 3.1 to describe the organization of the muscular and skeletal systems and to define the way muscles and bones interact with each other towards the generation of joint motions. The MTK model is fed with 3D joint angles and generates instantaneous estimates of musculotendon lengths l^{mt}, and moment arms r. It enables the subsequent estimation of musculotendon force F^{mt} and joint moments. Models of the musculoskeletal geometry have been used in the biomechanics community to estimate musculotendon kinematics including software packages such as SIMM [45], OpenSim [46] and AnyBody [63]. These are usually driven by graphical user interfaces (GUIs) and are difficult to implement in custom software and/or micro controllers. To overcome these issues this Chapter develops an alternative approach that can be easily integrated in custom programs.

The freely available musculoskeletal software OpenSim is used in this work to precompute subject-specific values of l^{mt} at discrete joint configurations. That is, the musculoskeletal model in Fig. 3.1 is set at different discrete joint configurations and the length of each musculotendon actuator (MTA) is evaluated. A single multidimensional cubic spline per MTA is then used to interpolate the discrete values and thus generate l^{mt} estimates at any joint configuration. Estimates of r are obtained by calculating the partial derivative of the l^{mt} spline with respect to the DOF of interest (Fig. 3.1). A detailed description of this method is provided in Chapter 4.

OpenSim Musculoskeletal Model: A freely available musculoskeletal model (Fig. 3.1) is used[1] in OpenSim and customized to include only the muscles crossing the knee joint and to define 6 generalized coordinates (GCs) in the lower limb. The selected muscles include: semimembranosus (sm), semitendinosus (st), biceps femoris long head (bflh), biceps femoris short head (bfsh), sartorius (sar), tensor fascia latae (tfl), gracilis (gra), vastus lateralis (vl), vastus medialis (vm), vastus intermedius (vi), rectus femoris (rf), medial gastrocnemius (mg), and lateral gastrocnemius (lg). The modelled GCs include: hip flexion-extension (HF), hip abduction-adduction (HA), hip internal-external rotation (HR), knee flexion-extension (KF), ankle plantar-dorsi flexion (AF), ankle subtalar angle (SA). By adding more muscles to the musculoskeletal model it is possible to easily extend it until the whole-body level.

Multidimensional Cubic Spline: The problem of finding musculotendon length as a function of d joint angles generalized coordinates $(\theta_1, ..., \theta_d)$ may be formulated as determining the coefficients for the generic d-dimensional spline function $s_{d,n}(\theta_1, ..., \theta_d)$. The terms $x_0(\theta_1, ..., \theta_d), ..., x_n(\theta_1, ..., \theta_d)$, with $x_i, 0 \leq i \leq n$, correspond to n discrete configurations of the d joint angles $(\theta_1, ..., \theta_d)$. To each joint angle configuration there is a correspondent value of musculotendon length. These musculotendon length values are the spline interpolation data and are used to calculate the spline coefficients. The moment arm spline function can be found by

[1]Available to download from the musculoskeletal library: http://www.simtk.com

differentiating $s_{d,n}(\theta_1, ..., \theta_d)$ with respect to the specific GC of interest.

To achieve better performances in terms of memory storage and computational time *B-Spline basis functions* are used [68]. In general, a spline with $n+1$ nodes,

$$a = x_0 < x_1 < ... < x_n = b \in \mathbb{R} \tag{3.1}$$

where

$$\Delta_n = [a = x_0, x_1, ..., x_n = b]$$

can be written as a linear combination of $n+3$ cubic polynomials (B-Spline functions) $\{u_1, u_2, ..., u_{n+3}\}$ that define a *basis*. That is, any one-dimensional cubic spline can be written as a linear combination of basis cubic polynomials u_i:

$$s_{1,n}(x) = \sum_{i=l}^{m} c_i u_i(x) \tag{3.2}$$

with some coefficients c_i, where $x \in \mathbb{R}$ is the point at which the spline is evaluated. Furthermore $l = \left\lfloor \frac{x-a}{h} \right\rfloor + 1$ and $m = min(l+3, n+3)$. The h term is the *fixed-distance* between the discrete nodes in (3.1). With this arrangement, to compute a single spline value, $m - l + 1$ coefficients c_i and basis u_i are needed where $m - l + 1 \leq 3$. If the bounded interval Δ_n and the interpolation data $y_i \in \mathbb{R}, i = 0, ..., n$ are given, a spline interpolates the data if it satisfies the $n+1$ conditions on the nodes: $s_1(x_i) = y_i$ for $i = 0, ..., n$. In the general d-dimensional case a total number of $N_c = \prod_{i=1}^{d}(n_i + 3)$ coefficients are needed to *construct* a spline on the experimental data whereas the evaluation of a single spline value requires $\prod_{i=1}^{d}(m_i - l_i + 1) \leq 3^d$ coefficients and bases.

B-Spline functions provide a straightforward way to compute partial derivatives. The partial derivative of a bivariate cubic spline function takes the form:

$$\frac{\partial s_{2,n}(x,z)}{\partial x} = \sum_{i_1=l_1}^{m_1} \sum_{i_2=l_2}^{m_2} c_{i_1 i_2} \dot{u}_{i_1}(x) v_{i_2}(z) \tag{3.3}$$

where x and z are real-valued variables on the bounded intervals $\Delta_{n1} = [a_1, b_1]$ and $\Delta_{n2} = [a_2, b_2]$. The terms $u_{i_1}(x)$ and $v_{i_2}(z)$ are basis functions for the two variables

respectively and $\dot{u}_{i_1}(x)$ is the x-basis function first derivative. The $(n_1+3)(n_2+3)$ coefficients $c_{i_1 i_2}$ for the non-differentiated spline function can therefore be *reused* to estimate its derivative.

3.5.2 Muscle Activation

EMG linear envelopes are further processed and converted into muscle activation. This is a percentage value that expresses how much a specific muscle is activated toward the generation of force. The transformation from EMG to activation accounts for the non-linear relationship between EMG and muscle force (Section 2.3.2). Fig. 2.16 shows the transformations involved from the acquisition of the raw EMG signal to the derivation of muscle activation. The final activation time series are obtained for 10 of the 13 muscles previously listed in Section 3.5.1 following the procedure described in [3]. Muscle activation from *vi* is estimated as an average of the *vm* and *vl* activation, whilst *st* is assumed to have the same activation as *sm* and *bfsh* is assumed to have the same activation as the *bflh*.

3.5.3 Muscle Dynamics

It calculates the force developed by each musculotendon actuator (MTA) in the model. Section 2.3.3 described the structure of the elastic-tendon Hill-type muscle model also depicted in Fig. 2.17. A brief summary will be given here and the modifications that lead to the infinitely stiff-tendon model will be presented.

Each MTA consists of an active force generating component in series with two passive elastic ones. These three components can be viewed as non-linear springs whose force production ability is defined by specific functions (Fig. 2.18a, 2.18b and 2.18c).

The active force generating component represents the muscle fibers. It is widely accepted that the muscle fiber force depends on three factors. The first one, $f_A(\tilde{l}^m)$, is the non-linear *active force-length function* that expresses the ability of muscle fibers to produce force at different lengths. The second factor, $f_P(\tilde{l}^m)$, is the non-linear *passive force-length function* that represents the passive element of the fibers producing resistive force when stretched and compressed. These first two

components relate the instantaneous length of the fibers (l^m) to the force produced in the muscle. The third factor, $f_V(v^m)$, is the non-linear *force-velocity function* that expresses the ability of muscle fibers to produce force as a function of the fiber contraction velocity. Fiber length (l^m) and velocity (v^m), in this specific work, are derived from the musculotendon length (l^{mt}) and velocity (v^{mt}) output from the MTK model. The remaining two *elastic passive components* represent the tendons. These are modeled to act like rubber bands. As the muscle fiber force grows, the tendon gets stretched. When the tendon resting length is exceeded, the tendon produces a resistive force that is non-linearly related to the amount of tendon strain. Muscle fiber force and elastic-tendon force are then combined together with muscle activation level computed by the *Muscle Activation* model to estimate the total force produced by the MTA. To estimate the force produced by the MTA at each time step, the equilibrium of the three-element system has to be calculated using an ordinary differential equation (ODE). This involves the execution of several computation steps including: the estimation of the current musculotendon velocity, the apportion of it to the the muscle fibers and tendon (based on their relative stiffness), and the integration of the derived fiber and tendon contraction velocities. When several samples of l^m need to be estimated, the numerical integration of the ODE considerably increases the computational time involved (Fig. 2.19).

To reduce the computational time, the elastic tendon was replaced with an infinitely stiff one. The force produced by the MTA depends now on the action of the muscle fibers only. This simplification was introduced under the hypothesis it does not affect the model prediction ability. Indeed, according to [1] the tendon is rather stiff. The strain, i.e. the percentage of length variation with respect to its resting length, is only the 3.3% of the tendon length when the muscle generates the maximum isometric force as shown in Fig. 2.18c. In the following of this Chapter we will refer to this model to as the Stiff-tendon Hill-type Muscle (SHM) model and to the previous one to as the Elastic-tendon Hill-type Muscle (EHM) model.

The force produced by the muscle fibers alone, is expressed in the SHM model

in the same way it is expressed in the EHM. This can be written as follows:

$$F^m = (f_A(\tilde{l}^m) \cdot f_V(v^m) \cdot a(u) + f_P(\tilde{l}^m) + d^m \cdot \tilde{v}^m) \cdot F_0^m \cdot \delta \tag{3.4}$$

where d^m represents a passive parallel damping element that was added to the force-velocity relationship to account for the muscles damping characteristics as suggested in [36]. The term $a(u)$ is the muscle activation as a function of the post processed EMG signal u. The term F_0^m expresses the force generated by the muscle when fibers are at their optimal length, while the term δ is the muscle strength coefficients. The force produced by the musculotendon unit, F^{mt} can then be derived by projecting the fiber force F^m onto the tendon line of action as follows: $F^{mt} = F^m \cdot cos(\varphi)$, where the term φ is the pennation angle. This is the angle at which fibers are oriented with respect to the tendon. The computation of F^m and F^{mt} can then be done when the instant values of l^m and v^m are known at all times.

The SHM model is designed so that the tendon length (l^t) is constant regardless of the force projected onto the tendon and is always equal to the resting tendon slack length l_s^t, i.e. $l^t = l_s^t$. Because of this, the muscle model has now one non-linear spring only and the computation of its instantaneous length does not require the integration of an ODE anymore. In fact l^m is calculated as in (3.5):

$$l^m = \sqrt{(l_0^m \cdot sin(\varphi_0))^2 + (l^{mt} - l^t)^2} \tag{3.5}$$

where φ_0 is the pennation angle at optimal fiber length. The fiber contraction velocity v^m can then be found by differentiation. As shown in Sec. 3.7, SHM has better time performances with respect to the EHM, with no loss of accuracy.

3.5.4 Moment Computation

The net knee FE moments, M_{KFE}, are finally computed as the sum of the product of each MTU force, F^{mt}, by its FE moment arm (r_{KFE}) as in (3.6):

$$M_{KFE} = \sum_i F_i^{mt} \cdot r_{KFE,i} \tag{3.6}$$

where i is the i^{th} muscle in the model.

3.5.5 Validation and Calibration

The NMS model presented in this Chapter is calibrated and validated likewise the procedure described in Section 2.3.4.

3.6 Validation Procedure

Experiments were performed at the Gait Laboratory of the School of Sport Science Exercise and Health of the University of Western Australia. Data were collected from 6 healthy male subjects (mass = $81.73 \pm 16.4Kg$, height = $175.75 \pm 6.39cm$, age= 30.67 ± 7.84years) who gave informed consent. The validation comprised of three tests.

The first test compared the behavior of the stiff-tendon muscle model (SHM) to that of the elastic-tendon muscle model (EHM). This was done for the purpose of validating our hypothesis that the human tendon, in the lower limb muscles, is rather stiff and its contribution to the production of muscle force and knee FE moments can be neglected in the experiments conducted in this study. To quantify how stiff the tendon actually was during the dynamic trials, the tendon strain (ϵ_T) was calculated using the EHM model, where ϵ_T is defined by the following equation:

$$\epsilon_T = \frac{l^t - l_s^t}{l_s^t} \times 100 \tag{3.7}$$

and where all the terms in (3.7) are defined in Section 3.5. The term ϵ_T represents the percentage of tendon length variation with respect to its resting length. The instantaneous tendon strain associated to each muscle was computed at each instant of time for all dynamic trials of all subjects. For each muscle, the average tendon strain was then calculated. To quantify the impact of assuming the tendon infinitely stiff (i.e. its length always equals the resting length), the percentage of the variation of the muscle fibre length calculated using SHM with respect to

EHM was computed using the following equation:

$$\Delta_F = \frac{l_s^m - l_e^m}{l_e^m} \times 100 \tag{3.8}$$

where l_s^m is the fibre length calculated using SHM, i.e. assuming the tendon infinitely stiff, and l_e^m is the fibre length calculated using EHM, i.e. assuming the tendon is elastic. This is an important quantity because the force produced in the musculotendon unit directly depends on the force produced by the muscle fibers. Therefore, assessing how the fibre length varies when assuming the tendon infinitely stiff or elastic, helps quantifying how important the role of the tendon is in the NMS model design. The fibre length variation associated to each muscle was computed for all trials of all subjects at each instant of time. For each muscle, the average length variation was then calculated. Finally, the impact of assuming the tendon infinitely stiff on the model ability of predicting knee FE moments was quantified. Knee FE moments were estimated during the *stance phase*. This is defined as the period of time between the *heel-strike* and *toe-off* events and it represents the interval during which the foot is in contact with the ground floor and the lower limb is supporting the entire body. The stance phase represents about 60% of the gait cycle. The remaining 40% is associated to the swing of the leg, that is the *swing phase*. Moments estimated by the SHM and EHM models and those obtained experimentally were time normalized using a cubic spline. This allowed comparing results associated to different trials and subjects. The time normalized moments estimated by SHM, EHM, and those experimentally recorded were respectively averaged across all trials from all subjects. This produced three *ensemble average curves* of the knee FE moments. The SHM ensemble average curve was then compared to that associated to EHM and to that associated to the experimental moments. This allowed assessing how the predicted knee FE moments changed with an infinitely stiff tendon and with an elastic one. Furthermore, it allowed quantifying whether or not the assumption of an infinitely stiff tendon produced a loss of accuracy in the prediction of the joint moments. Statistical coefficients including *Pearson Correlation* and *Root Mean Squared Error* were also used to better assess the prediction accuracy.

The second test assessed the accuracy of the Musculotendon Kinematics (MTK) Model. The model uses multidimensional cubic splines that are created from nominal values of musculotendon length l^{mt} obtained from OpenSim (Section 3.5.1). Therefore, the accuracy of the model is defined based on the capability of reproducing the original OpenSim values of both l^{mt} and r. The range of motion of the lower limb joints about all associated GCs were sampled into equidistant nodes that were input, together with the selected musculoskeletal model, into OpenSim to compute the *experimental* l^{mt} and r. Nominal values of l^{mt} only, were used to calculate the coefficients for both the l^{mt} and the r spline functions (Section 3.5.1). The fitting accuracy was assessed both on the nodes used for coefficients calculation as well as on a novel set of evaluation points located midway between each pair of consecutive nodes. As a measure of error in estimated values we used the *Mean Fitting Error* (MFE) and its *standard deviation* (σ):

$$MFE = \frac{1}{N}\sum_{i=1}^{N}\left|\hat{X}_i - X_i\right|, \tag{3.9}$$

where $\hat{X}$ is the OpenSim-generated value of l^{mt} or r. The term X is the corresponding estimated value from the MTK model. N is the number of points at which the fitting function was evaluated. The created splines can now be used to predict the musculotendon kinematics for any possible combination of 3D joint angles (Fig. 3.1). A more detailed description of this process is provided in Chapter 4. The impact of the fitting error on the knee FE moment prediction was also investigated. Moments calculated using OpenSim-generated values of l^{mt} and r were compared to the moments obtained using estimates of l^{mt} and r from the MTK model. Moments were time normalized and two ensemble average curves were produced: one for the joint moments obtained from OpenSim estimates of l^{mt} and r (M_{OSIM}), and one obtained from estimates of the MTK model (M_{MTK}). The ensemble average curves were obtained from all dynamic trials of all subjects during the stance phase. The percentage of the variation of M_{MTK} with respect to M_{OSIM} was then computed:

$$\Delta_M = \frac{M_{MTK} - M_{OSIM}}{M_{OSIM}} \times 100 \tag{3.10}$$

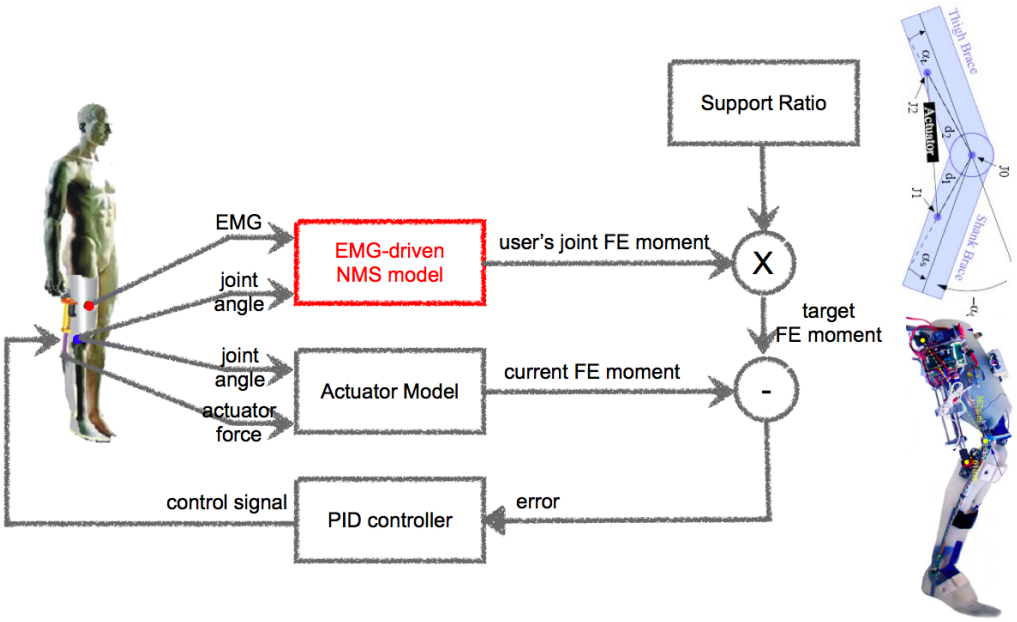

Figure 3.3: The EMG-driven NMS model can be integrated in the control loop for the actuation of a lower limb powered orthosis as previously presented in [9]. The powered orthosis itself is visible aside along with a schematic view of its mechanical structure.

The third test investigated whether the stiff-tendon muscle (SHM) model executed faster than the elastic-tendon muscle (EHM) model. Finally, the time performances of the entire NMS model were investigated for the purpose of assessing whether the proposed SHM model can be used in robotics applications with real-time constraints. In this work we assume the specific application is the control of a powered orthosis for the lower limb, using EMG signals to establish an interface between the human and the machine as in [9]. Fig. 3.3 gives a schematic view of the control scheme. The powered orthosis control system can use the EMG-driven NMS model to estimate the force the user's muscles can produce and the resulting user's moments produced at the knee joint. When muscle forces are not strong enough to allow for a proper joint movement, they can be amplified to produce the *target FE moment* at the knee. This is the moment the subject should produce to properly carry out the desired movement. The powered orthosis controller can then be fed with the difference between the target moment and the current moment produced by the user wearing the powered orthosis. This difference defines the amount of extra moment the orthosis actuation system should add to obtain the target motion. The muscle amplification factor that

leads to the target moment can be initially defined by a medical doctor who had previously analyzed the patient. However, automated procedures for the calibration of this parameter can be implemented. Alternatively, if the subject is healthy, the amplification factor can be used to further facilitate the user's movement and to augment their motor ability. For this to work, by the time the human muscles contract, the NMS model has to provide a prediction on the amount of force produced by each muscle and the FE moments produced at the knee joint to be supported. This will allow actuating the orthosis as soon as the human muscles activate. Recent studies have established that there is a delay between the time instant the neural system generates EMG signals in the muscles and the time instant when muscles contract mechanically and generate moments around the joints. This is called the electromechanical delay (EMD). In the lower limb muscles, the EMD is in the order of $10ms$ [27]. If the EMD is exploited in the control algorithm of the powered orthosis, a non invasive and seamless integration between the human operator and the assistive device is achievable and the device can become a natural extension of the operator's body. The real-time constraint for the proposed NMS model is therefore the EMD. That is, the NMS model has to be able to produce estimates of muscle forces and joint moments in less than $10ms$. Tests were performed on an embedded system (Digital Logic, Switzerland) equipped with a $1.6Ghz$ Atom CPU with $512MB$ RAM. This choice was motivated by the fact of verifying whether the proposed NMS model would run on a hardware architecture with low computation resources that could be actually used for the control of a powered orthosis. The computational time of the NMS model needed to produce one estimate of muscle force and one estimate of knee FE moment, was calculated as the average time needed for computing one thousand estimates.

3.7 Results

Results from the first tests are shown in Fig. 3.4. Fig. 3.4a shows that the tendon strain associated to all muscles in the model was always less than 2% during all the dynamic trials. This validated our hypothesis and suggested the contribution of the

Table 3.1: Comparison of computational time performances (mean ± sdev) in ms

SHM	EHM	MTK	NMS(SHM, MTK)	NMS(EHM, MTK)
0.07 ± 0.00068	17.5 ± 0.072	1.1 ± 0.043	3.6 ± 0.064	21.1 ± 0.11

tendon to the production of muscle force and joint moment could be potentially neglected in our experiments.

Fig. 3.4b shows that the fibre length variation associated to all muscles in the model was always less than 9% during all dynamic trials. This suggested that the impact of assuming the tendon infinitely stiff might not lead to drastic changes in the predicion of muscle force with respect to the model with elastic tendons.

Fig. 3.4c shows that the SHM model predicted FE knee moments that were very closely related to the reference knee FE moments. Both predicted and reference moment curves had peaks that occurred at the same time instants. A small discrepancy was noticeable at the edges of the graph and it was mostly due to filtering issues. For each time step, filter algorithms needed to process data over a predefined time window. At the edges of the data time series the window is not full and therefore approximation errors were introduced. The Pearson correlation coefficient R was 0.932. This means that the SHM model generated estimates that were highly correlated to reference values over all subjects' trials. The root mean squared error $RMSE$ was $7.898Nm$. This means the SHM model introduced an error that, on average, was less than the 10% of the range of variation observed in the reference values (i.e. $86.673Nm$). The maximum absolute error (e_{max}) was equal to $21.494Nm$. It occurred at 73% of the stand phase and was located at the edge region where the observed data was less significant due to the filtering issues. The minimum absolute error (e_{min}) was equal to $0.114Nm$ and occurred at 47% that was the peak region. This proved that the model was capable of providing high performances within the most significant part of the observed data.

Fig. 3.4c also shows the predictive ability of the EHM model. Surprisingly, this was found to be slightly lower, on average, than that provided by the SHM. Statistical coefficients assumed poorer values with respect to the SHM ones: $R = 0.893$, $RMSE = 9.714Nm$. However, minimum and maximum absolute

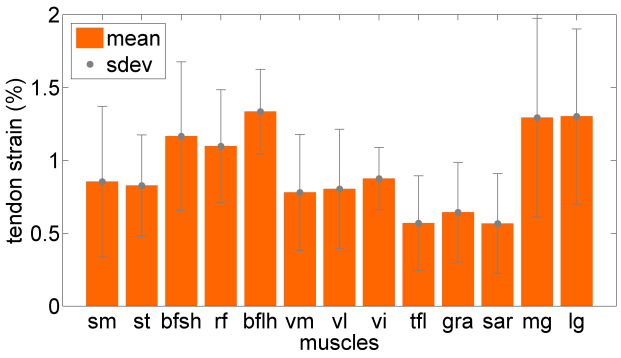

(a)

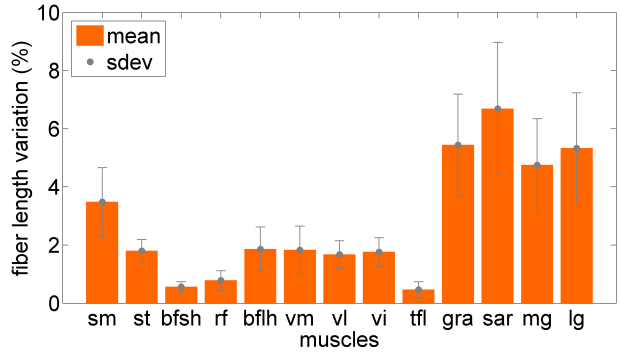

(b)

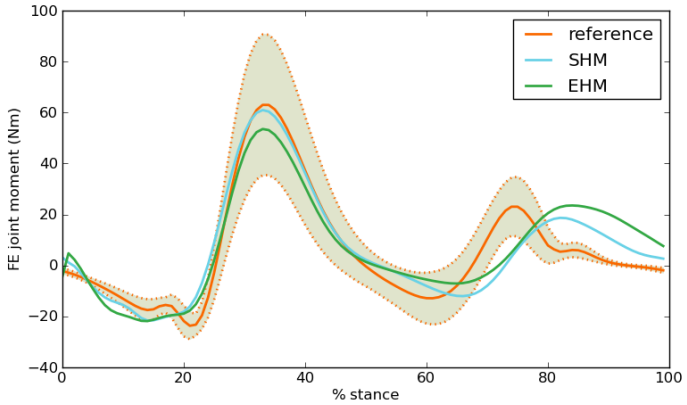

(c)

Figure 3.4: Average values of tendon strain (a) and fibre length variation (b) averaged all dynamic trials for all subjects. Tendon strain and fibre length variation are calculated as in (3.7) and (3.8) respectively. In (c) the ensemble average of the reference FE knee moment is compared to that estimated by the SHM and to that estimated by the EHM. The standard deviation of the ensemble average of the reference knee FE moment is represented by the dotted lines and shaded area.

errors provided better results: $e_{max} = 19.031Nm$ and $e_{min} = 0.012Nm$. The proposed results showed that by assuming the tendon infinitely stiff, the model prediction accuracy did not decrease in our experiments but slightly increased with respect to the case in which the tendon was modeled as an elastic body.

Results from the second tests are shown in Fig. 3.5. Fig. 3.5a and 3.5b show that the MTK model was able to produce estimates of l^{mt} and r with negligible fitting errors which always were less then $0.004mm$ and $0.25mm$ respectively.

Fig. 3.5c shows that the l^{mt} and r fitting errors introduced by the MTK model produced a percent variation in the predicted knee FE moments that was always less than the 2.5% of the moments obtained using OpenSim-generated estimates of l^{mt} and r.

The proposed results showed that the MTK model produces accurate estimates of l^{mt} and r and can be reliably used instead of GUI-driven third-party software such as OpenSim to allow for an on-line execution of the entire NMS model.

Results from the third test are shown in Table 3.1. The SHM model executed in $0.07ms$, that is 250 times faster than the EHM model execution time, i.e. $17.5ms$. This proved that modeling the tendon as an infinitely stiff body leads to a substantial improvement in the computational time performances.

Table 3.1 also reports the time needed by the MTK model to execute. Because the spline coefficients for each muscle are pre-calculated off-line, the total time needed for the MTK model to execute is associated to the evaluation of both l^{mt} and r multidimensional spline functions for all muscles in the model. Spline functions can be uni-dimensional in the case of uniarticular muscles crossing the knee joint only, three-dimensional, in the case of biarticular muscles crossing the ankle and knee joints and four-dimensional in the case of biarticular muscles crossing the hip and knee joints. Spline function evaluation is done using generalizations to higher dimensions of (3.2) and (3.3). The multidimensional spline evaluation time grows as a function of the number of dimensions. In our tests, it ranged from $0.001ms$ (uni-dimensional spline) to $0.08ms$ (four-dimensional spline).

Finally, Table 3.1 reports the time needed by the entire NMS model to execute. Execution time significantly differed when using the NMS model with SHM and MTK ($NMS(SHM, MTK)$) with respect to using the NMS model with

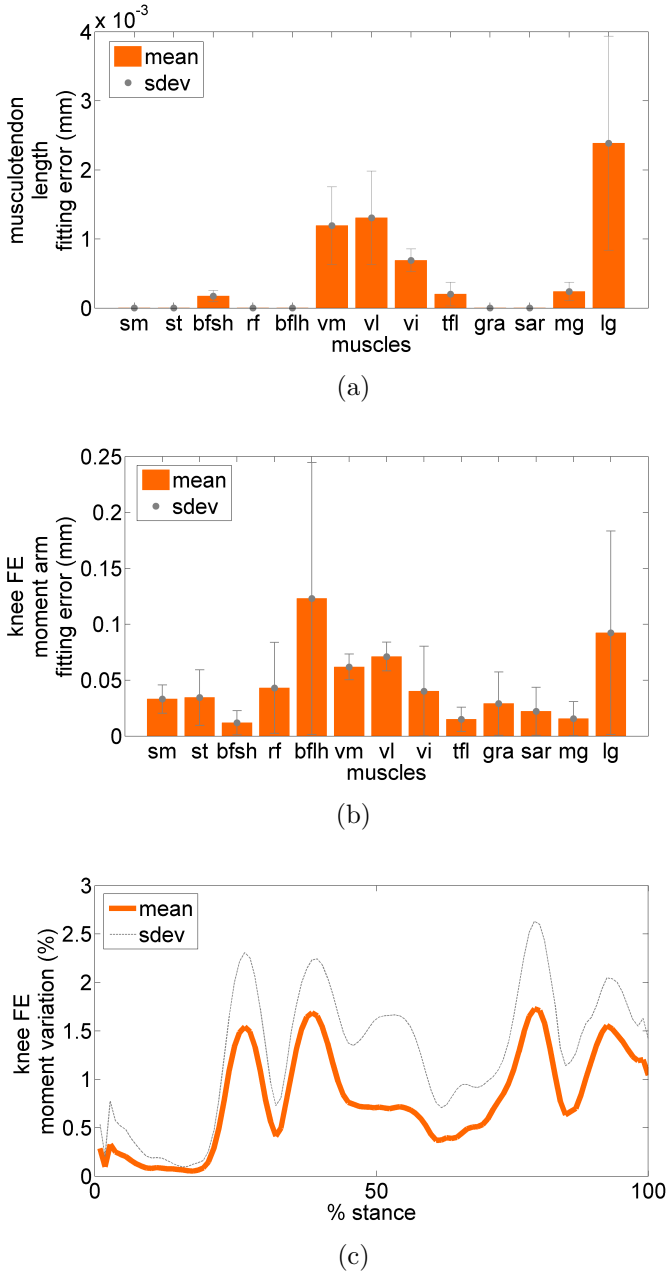

Figure 3.5: Mean fitting error and standard deviation for musculotendon length (a) and for FE moment arms (b) computed for all muscles in the model. In (c) the percentage variation of the knee FE moments is estimated using (3.10). The upper standard deviation is shown (dotted line) to quantify the maximum variation in knee FE moment due to the use of MTK as opposed to OpenSim.

EHM and MTK ($NMS(EHM, MTK)$). The $NMS(SHM, MTK)$ arrangement demonstrated to execute in less than $4ms$ and showed to have computational time performances that were suitable for the real-time control of the powered orthosis

where the real-time deadline was set to be $10ms$ (Section 3.6). On the contrary, the $NMS(EHM, MTK)$ arrangement needed more than $20ms$ to execute and was therefore regarded as unsuitable for the real-time control of the orthosis.

Finally we assessed the time needed to calibrate the $NMS(SHM, MTK)$ model (Sec. 2.3.4) on each subject separately and we compared it to that needed by the $NMS(EHM, MTK)$. For each subject the NMS models were calibrated on 4 trials (Section 3.3). While $NMS(SHM, MTK)$ was calibrated in just 6 minutes and 37 seconds it took 15 hours and 48 minutes for the $NMS(EHM, MTK)$.

3.8 Musculoskeletal Humanoids Actuation

In the previous sections we illustrated how the proposed NMS model can be used for the real-time control of a powered orthosis. However, the NMS model can also provide effective solutions for the actuation of humanoid robots that have a musculoskeletal architecture and artificial muscles.

The proposed NMS model allows taking inspiration from the way humans move and addressing the challenge of autonomous locomotion in musculoskeletal humanoids. A direct biological observation of how humans activate their muscles and actuate their joints can therefore be done using the proposed NMS model. The model can be used to experimentally estimate the muscle forces generated by the human subject during dynamic motor tasks. The estimated muscle force patterns during a specific movement can then be mapped and used to actuate the humanoids artificial muscles and produce the observed movement in the robot. The human-humanoid mapping has to take into account the different number of muscles in the humanoid robot, the different mass properties and size of the humanoid limbs and the different number of DOF in the humanoid joints.

A similar approach can be based on the recent studies suggesting that muscle activation patterns are generated by a functional module located in the spinal cord primarily based on global kinematics parameters that define the orientation of the human limbs [24]. The proposed NMS model can be used to establish a function that relates joint angle and moments to the corresponding force produced by the muscles crossing that joint. This can be done by observing a broad range of

dynamic motor tasks from a great number of human subjects. It is then possible to derive average muscle force patterns of the whole subject population using the proposed EMG-driven NMS model. Finally it is possible to create a function that maps a specific combination of joint angle and moment to the corresponding muscle force level. This can be done for each muscle spanning the specific joint. It is then possible to prescribe a specific force to each artificial actuator depending on the angle and moment that has to be produced by the humanoid joint.

Finally the proposed NMS model can play a very important role in determining joint stiffness in humanoid robots. This is a very important parameter that has been intensively used for the design of compliant humanoids and artificial limbs. Indeed, joint stiffness can be easily expressed as a function of the activation of the antagonistic muscles crossing a specific joint.

3.9 Conclusions and Future Work

This Chapter presented a novel neuromusculoskeletal model of the knee joint that was used to estimate somatosensory information during the human movement. The presented model proved to be as accurate as the detailed ones developed in the biomechanics community but with superior computational time performances. Our proposed NMS model was directly compared to the well known model developed by Lloyd et al. [2, 3, 35, 37, 47]. A robust validation methodology was also provided in which data obtained from 6 male subjects who performed a total of 78 motor tasks were used to assess the time performances and prediction accuracy of the NMS model. This work demonstrated the proposed NMS model has computational time performances that make it suitable for the control of powered orthosis. That is, the NMS model computation loop executes in less than $10ms$ which is the electromechanical delay (EMD) in the lower limb muscles. The EMD was identified as the real-time deadline that is necessary to achieve intuitive real-time orthosis control. Computational time tests were performed on an embedded system that can be used as the orthosis control unit. The Chapter then illustrated a control strategy in which the model can be effectively used as an intuitive EMG-driven human-machine interface following research previously done in [9]. The NMS

model can be easily extended to whole-body level and this can play a crucial role for the the actuation of humanoid robots with artificial muscles.

Results demonstrated the NMS model can achieve faster execution and calibration time by integrating the proposed stiff-tendon muscle model (SHM) and musculotendon kinematics model (MTK) within a common framework. The lower prediction performances of the elastic-tendon model (EHM) are related to the fact that the model does not always correctly estimate the amount of stiffness in the musculotendon actuator. This can be related to calibration issues or to limitations in the elastic-tendon model design. On the contrary, the SHM does not rely on tendon stiffness to compute the muscle force and joint moments. Results suggested that assuming the tendon length always constant might better represents the real tendon dynamics that actually occurred in the experiments and might be a better approximation than that provided by the elastic-tendon model. Further studies have to be carried out to assess whether this assumption is valid for a wider range of movements including: squat, jump, fast running, side stepping and cross-over cutting manoeuvres.

Fast operation in calibration can be further exploited in future research to develop more advanced algorithms for the continuous calibration of the model biomechanical parameters. As the NMS model executes, the continuous calibration algorithm will keep refining those parameters that vary with muscle fatigue such as: optimal fibre length, maximum isometric force, maximum EMG. This will allow designing more advanced powered orthosis control systems that will be able to adapt to the user's conditions on the fly.

The time complexity of the NMS model is bound to increase as a function of the number of muscles. The superior computational time performances provided by the SHM model with respect to the EHM not only allow executing within the real-time deadline but also will allow including a greater number of muscles in the model. This in turn will allow estimating the moments generated at multiple joints including: hip, knee and ankle and controlling powered orthosis for the simultaneous support of those joints (Chapter 6).

Furthermore, integration of pattern recognition technology in the NMS model will be used to extrapolate more information out of the EMG signals (Chapter 8).

This research development aims to integrate musculoskeletal dynamics into robotics systems to achieve more advanced bio-inspired control strategies.

Chapter 4

Estimation of Musculotendon Kinematics

This Chapter presents a robust and computationally inexpensive method to estimate lengths and three-dimensional moment arms for a large number of musculotendon actuators of the human lower limb using a single multidimensional B-spline function per muscle. This is the method that is used in the Musculotendon Kinematics (MTK) Model briefly illustrated in Section 3.5.1. Also see Fig. 3.1 and 3.2.

This Chapter presents a more detailed explanation of this methodology and compares it to the approach currently used in the literature which is based on polynomial regression. Compared to the polynomial regression method, the multi-dimensional spline method produced lower errors for estimating musculotendon lengths and moment arms at the generalized coordinate boundaries. The fitting accuracy was also less affected by the dependant number of degrees of freedom and by the amount of experimental data available. Furthermore, a single spline function can be used to estimate both musculotendon length and moment arms as opposed to polynomial regression where different equations had to be chosen depending on the shape of the surface to be fitted. Finally, the spline method was further tested in conjunction with an EMG-driven musculoskeletal model for the estimation of muscle force under different contractile conditions. This confirms the spline methodology is actually suitable for the integration in predictive models.

4.1 Introduction

The development of mathematical models of human physiology and biology is enabling a better understanding of whole body function from the genome to the tissue and organ levels [5]. Musculoskeletal-level models and simulation tools are providing effective ways to study muscle contribution to human movement and this is offering possibilities to investigate how in vivo tissue loading is implicated in the mechanisms of musculoskeletal injury and disease [4, 11]. The availability of comprehensive and fast musculoskeletal models may also play an important role in establishing intuitive Human-Machine Interfaces (HMIs) at the neuromuscular level and providing new solution to implement effective control systems for assistive devices [8]. Therefore it is crucial to develop models that reflect the action of muscles while minimizing processing time in musculoskeletal modeling research. Musculoskeletal models usually require computation of musculotendon kinematics including musculotendon length (l^{mt}) and three-dimensional muscle moment arms (r) that enable the estimation of musculotendon forces (F^{mt}) and joint moments (Section 3.5). The estimation of these musculotendon kinematics is critical because small variations in their values can result in large variations in musculotendon force [35]. It is therefore important to develop methods that are capable of producing estimates that accurately reflect results obtained from experimental techniques such as MRI or ultrasound. This introduces reliability and consistency in the modeling process and assures results are directly related to the experimental data set that was used. Models of the musculoskeletal geometry can be used to estimate musculotendon kinematics including software packages such as SIMM [44, 45], OpenSim [11, 46] and AnyBody [63]. These are usually driven by graphical user interfaces and are difficult to implement in custom software and/or micro controllers. To overcome these issues, an alternative approach has been proposed in the literature to fit the musculotendon kinematics using polynomial regression on both l^{mt} and r [69]. That is, different polynomial regression equations (P^{eq}) were individually fitted to experimental values of both l^{mt} and r thus requiring the gathering of both sets of experimental data. In this Chapter we develop a novel inexpensive model that can produce accurate estimates of l^{mt} and r

and that can be integrated into large scale musculoskeletal models and custom programs. The aim was to determine if a single piecewise multidimensional cubic spline could be used to generate estimates for both l^{mt} and r from nominal values of musculotendon length only, corresponding to discrete combinations of generalized coordinates (GC) that specify joint kinematics. Nominal values for l^{mt} can be obtained from experimental data using MRI or ultra-sound technologies. Alternatively, nominal values can be derived from models of the musculoskeletal geometry [3, 4, 11, 44]. An additional aim of the paper was that of comparing our methodology to polynomial regression equations and assessing whether spline can provide more robust solutions. The EMG-driven NMS model previously presented in Chapter 3 was used to quantify to which extent l^{mt} misfits compromised the capability of the EMG-driven model to predict F^{mt} [3].

4.2 Methods

This section presents the two musculoskeletal biomechanical models of the human lower-limb that were used (Table 4.1) and the theory of the proposed spline-based approach. This was entirely implemented by the author of this Thesis in a custom program and no additional toolboxes where used[1]. More details about spline interpolation and the generalization to the multidimensional case can be found in [68]. Please refer to Menegaldo et al. [69] for details about polynomial regression.

4.2.1 Musculoskeletal Models

The first model (*LowerLimb4307*) had 43 musculotendon actuators (MTAs) and 7 generalized coordinates (GCs), i.e. 7 joint angles [44]. The lengths and moment arms for each MTA depended on all GCs associated to the corresponding joints. The *LowerLimb4307* model had a maximum number of 4 GCs per MTA corresponding to the biarticular muscles crossing hip and knee. This model was used by Menegaldo et al. [69] to study fitting accuracy of polynomial regression equations and was also used in this study as the comparison to our method. The second model

[1]The software C++ implementation, MATLAB interface, User's Manual and all original data will be made freely available to download at http://www.massimosartori.net/

Table 4.1: Generalized coordinates (GCs) and their range of motion (ROM). Angles that define the ROM of each GC are expressed in degrees. The Metatarsus-phalangeal angle is not used in the *LowerLimb1310* model because the muscles included in this model do not cross the Metatarsus-phalangeal joint.

LowerLimb4307 Model		Min	Max
Hip Rotation	(HR)	-20	20
Hip Adduction	(HA)	-50	15
Hip Flexion	(HF)	-10	95
Knee Flexion	(KF)	-10	95
Subtalar Angle	(SA)	-20	20
Ankle Flexion	(AF)	-30	30
Metatarsus-phalangeal angle	(MA)	-30	30

LowerLimb1310		Reduced		Extended	
		Min	Max	Min	Max
Hip Rotation	(HR)	-20	20	-30	20
Hip Adduction	(HA)	-50	15	-50	30
Hip Rotation	(HR)	0	95	-10	95
Knee Rotation	(KR)	-5	5	-10	10
Knee Adduction	(KA)	-3	3	-5	5
Knee Flexion	(KF)	0	120	-10	120
Subtalar Angle	(SA)	-10	10	-20	20
Ankle Adduction	(AA)	-10	10	-20	20
Ankle Flexion	(AF)	-30	30	-40	30
Metatarsus-phalangeal angle	(MA)	-30	-30	30	30

(*LowerLimb1310*) had 13 MTAs and 10 GCs [35, 43] with a maximum number of 6 GCs associated with the biarticular muscles crossing hip and knee and those crossing knee and ankle. This model was used to study the fitting capabilities of spline functions and polynomial regression equations with a wider range of conditions.

4.2.2 Multidimensional Cubic B-Splines

Generally a cubic spline consists of a series of 3rd order polynomial segments spliced together to preserve continuity of the first and second derivatives. The

points at which polynomials are spliced together,

$$a = x_0 < x_1 < ... < x_n = b \in \mathbb{R} \tag{4.1}$$

are called *nodes*, where

$$\Delta_n = [a = x_0, x_1, ..., x_n = b]. \tag{4.2}$$

If Δ_n and the interpolation data $y_i \in \mathbb{R}, i = 0, ..., n$ are given, a spline interpolates the data if it satisfies the $n+1$ conditions on the nodes: $s_1(x_i) = y_i$ for $i = 0, ..., n$, where s_1 represents a 3rd order one-dimensional spline function on the bounded interval Δ_n. To achieve better performances in terms of memory storage and computation time *B-Spline basis functions* were used. In general, a spline with $n+1$ nodes can be written as a linear combination of $n+3$ cubic polynomials (B-Spline functions) $u_1, u_2, ..., u_{n+3}$ that define a *basis*. That is, any one-dimensional cubic spline can be written as:

$$s_1(x) = \sum_{i=l}^{m} c_i u_i(x) \tag{4.3}$$

with some coefficients c_i, where $l = \left\lfloor \frac{x-a}{h} \right\rfloor + 1$ and $m = min(l+3, n+3)$. With this arrangement, to compute a single spline value, only $m - l + 1$ coefficients c_i and basis functions u_i are needed out of the $n+3$ ones, where $m - l + 1 \leq 3$. In the general d-dimensional case a total number of $N_c = \prod_{i=1}^{d}(n_i + 3)$ coefficients are needed to *construct* a spline on the experimental data whereas the evaluation of a single spline value requires $\prod_{i=1}^{d}(m_i - l_i + 1) \leq 3^d$ coefficients and basis functions. B-Spline basis functions provide a straightforward way to compute partial derivatives. The partial derivative of a bivariate cubic spline function takes the form:

$$\frac{\partial s_2(x,z)}{\partial x} = \sum_{i_1=l_1}^{m_1} \sum_{i_2=l_2}^{m_2} c_{i_1 i_2} \dot{u}_{i_1}(x) v_{i_2}(z) \tag{4.4}$$

where x and z are real-valued variables on the bounded intervals $\Delta_{n_1} = [a_1, b_1]$ and $\Delta_{n_2} = [a_2, b_2]$. The terms $u_{i_1}(x)$ and $v_{i_2}(z)$ represent basis functions for the two variables respectively and $\dot{u}_{i_1}(x)$ is the x-basis function first derivative. The

$(n_1 + 3) \cdot (n_2 + 3)$ coefficients $c_{i_1 i_2}$ for the non-differentiated spline function can therefore be used to estimate its derivative.

The estimation of musculotendon lengths and moment arms can be done using the B-spline function previously defined. The problem of finding musculotendon length as a function of d joint GC-angles, $(q_1, ..., q_d)$ may be formulated as determining the $(n_1 + 3) \cdot ... \cdot (n_d + 3)$ coefficients $c_{i_1 i_2 ... i_d}$ for the generic d-dimensional spline function $s_d(q_1, ..., q_d)$ where the $y_{i_1,...i_d}$ interpolation data are given by l^{mt}. The moment arm spline function can then be found by differentiating $s_d(q_1, ..., q_d)$ with respect to the specific GC of interest.

4.2.3 Validation Procedure

The validation is comprised of three tests. In the first one, the same input data, biomechanical model and procedure as published by Menegaldo et al. [69] were used for a direct comparison to our methodology. The second test was performed to study spline and polynomial regression equations under a wider range of experimental conditions. In the third test the impact of l^{mt} misfit on muscle force estimation was assessed.

In all tests, the range of motion (ROM) of each GC was sampled into equidistant nodes that were input, together with the selected biomechanical model, into OpenSim to compute the *experimental* l^{mt} and r. Coefficients were then computed for the polynomial regression equations, P^{eq} using nominal values of both l^{mt} and r. Data for l^{mt} only were used to compute the coefficients for the spline function. The fitting accuracy was assessed both on the nodes used for coefficients calculation as well as on a novel set of evaluation points located midway between each pair of consecutive nodes. In this work, the accuracy of a model is defined based on the capability of reproducing the original values of l^{mt} and r that were generated using OpenSim. This is because the coefficients of both spline functions and polynomial regression equations were obtained using nominal values produced by OpenSim. Therefore, the accuracy of a spline function as well as that of a polynomial regression equation depends on how well they are able to replicate the same dataset that was used to calculate their coefficients. The third test also involved the collection of experimental data from gait analysis trials, reported

previously by Winby and collegaues [35, 43].

The evaluation of the *LowerLimb4307* model was performed using the ROM of each GC sampled at 20 points (Table 4.1). However, when four GCs were used, only 15 nodes per GC were used for coefficients computation.

The evaluation using the *LowerLimb1310* model concentrated on the biarticular muscles and tested three different sets of GC across the lower limb joints. Tests on 4 GCs included: hip internal-external rotation (HR), hip adduction-abduction (HA), hip flexion-extension (HF) and knee flexion-extenion (KF) for the thigh muscles and KF, ankle adduction-abduction (AA), subtalar flexion-extension angle (SA), ankle dorsi-plantar flexion (AF) for the shank muscles. With 5 GCs, internal-external rotation (KR) was added and the 6 GC tests also included knee adduction-abduction (KA). In this model no muscles crossing the metatarso-phalangeal joint were included therefore the metatarso-phangeal angle (MA) was not used. All tests were executed with the two different ROM arrangements as defined in Table 4.1, i.e. reduced and extended. The ROM of each GC was sampled at 10 nodes both with the reduced and extended arrangements. As a result, the distance from one node to another was greater in the extended ROM. These tests assessed how the fitting accuracy was affected by a number of experimental conditions including: the distance between interpolation nodes, the number of dimensions (GCs) to interpolate and distance of the evaluation points from the interpolation nodes.

The impact of using the spline model on muscle force estimations was evaluated using the *LowerLimb1310* model in conjunction with the EMG-driven NMS model presented in Chapter 3.5. In the current study, two different tests were performed where muscle forces were computed using musculotendon length estimates generated using OpenSim, polynomial regression and the spline-based approach respectively. Muscle force derived using OpenSim estimates of l^{mt} were assumed to be the gold standard and were compared to the muscle force derived by estimates produced by spline and P^{eq}.

In the first muscle force test no EMG signals and kinematic data on real subjects were recorded. The musculotendon lengths and KF moment arms as a function of 4 GCs were estimated as described previously. The estimated musculotendon

lengths were then used in the EMG-driven model to calculate the isometric muscle force produced at each data point. Since this test assumed isometric conditions, no velocity effects were modeled therefore F^{mt} was only a function of muscle fiber length and muscle activation. Each muscle was assumed to be maximally activated at each GC configuration. This represented the worst-case scenario because when the muscle is maximally activated, the effects of the musculotendon length fitting errors on muscle force are amplified.

The second test studied the impact of l^{mt} fitting error in dynamic conditions. Data were collected from one male subject who gave informed consent and who performed 15 gait and 5 jogging trials. Kinematic and ground reaction force data were input into a RRA model to calculate knee flexion-extension moments (Section 3.4). The EMG-driven model was then scaled and calibrated to the subject (Sections 3.4 and 3.5). OpenSim was used to generate values of l^{mt} for each sampled time instant. The same was done using spline functions and polynomial regression. EMG signals were used to determine the activation in the muscles and the Hill-type model was used to estimate F^{mt}. A measure of force prediction error due to musculotendon misfit was calculated. This test also assessed whether during jogging trials, the effect of l^{mt} fitting error on muscle force prediction was magnified by the increased muscle activation as opposed to walking.

As a measure of the differences in estimated values from the different methods the *Mean Fitting Error* (MFE) and its *standard deviation* (σ) were used:

$$MFE = \frac{1}{N}\sum_{i=1}^{N}\left|\hat{X}_i - X_i\right|, \tag{4.5}$$

where, $\hat{X}$ is the OpenSim-generated value of l^{mt} or r. The term $\hat{X}$ can also refer to F^{mt} calculated using OpenSim-generated l^{mt}. The term X is the corresponding estimated value from the P^{eq} or spline methods. N is the number of points at which the fitting function has been evaluated. Additionally, the percentage of the MFE relative to the OpenSim-generated value averaged on all angle configurations ($E[\hat{X}]$) was computed:

$$\%\epsilon = \frac{MFE}{E[\hat{X}]} \times 100 \tag{4.6}$$

Confidence Interval (CI) at at 90% and 95% of the MFE was estimated using Chebyshev's Theorem, which can be conservatively applied to any probability distribution with known mean and standard deviation:

$$MEE = MFE + 3.16\sigma, (90\%) \tag{4.7}$$

$$MEE = MFE + 4.47\sigma, (95\%) \tag{4.8}$$

The number of errors that has fallen inside the previously defined CIs was counted for all muscles and proposed in a histogram form.

As discussed, computation time is important for neuromuscular skeletal modeling so it can be potentially used in real-time applications. Therefore, computation time was evaluated on repeated tests where the number of GC was increased from 1 to 6. In each test, the reported time needed to compute a single estimate of l^{mt} or r was the average time computed from the evaluation of 10000 estimates. A desktop computer with a $2.26GHz$ Intel Xeon CPU and $3GB$ RAM memory was used. Both spline and polynomial regression equations evaluation routines were implemented in C++ to better compare their relative speeds.

4.3 Results

The tibialis anterior muscle was chosen to demonstrate the performance of the spline method. In the *LowerLimb4307* model the tibialis anterior kinematics depended on two GCs (AF and SA) and the variation of l^{mt} and r errors are easy to visualize in 3D. Fig. 4.1a shows the space distribution of the spline fitting error associated to the prediction of l^{mt} is uniform throughout the workspace and is substantially smaller than that associated to P^{eq} which reaches larger values at the boundaries[2]. In Fig. 4.1c the P^{eq} fitting error associated to the prediction of r_{AF} is clearly visible and it gets larger at the boundaries reaching a maximum of $0.15cm$. Fig. 4.1e shows a very good agreement between the OpenSim-generated surface associated to r_{SA} and that generated by the spline function. The error

[2]The polynomial regression equations that were chosen to generate the results presented in this work are the ones that produced the smallest fitting error.

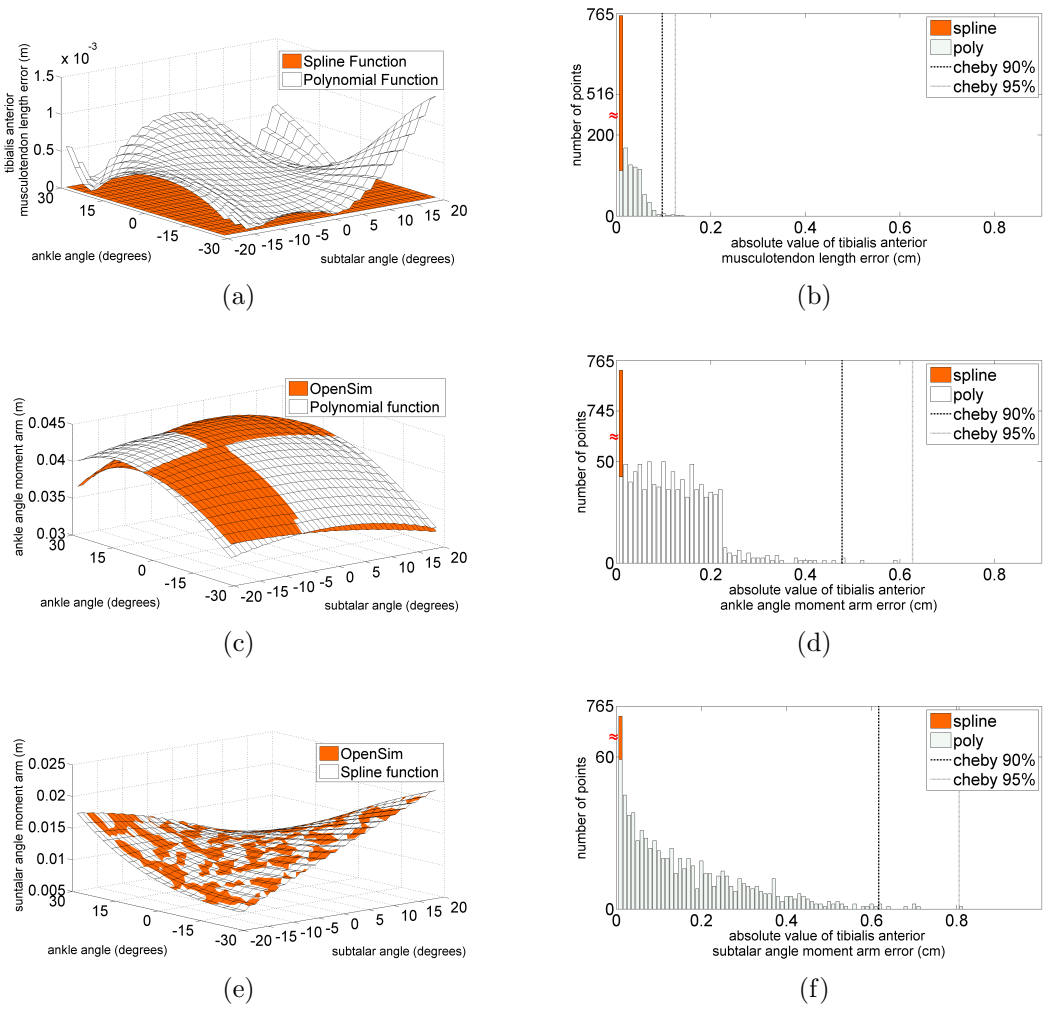

Figure 4.1: All graphs report values for the tibialis anterior muscle. (a) The two surfaces represent the space distribution of the difference between the musculotendon length computed using OpenSim and those estimated by the P^{ep} and by the spline function respectively. (c) The distribution of the AF moment arms (r_{AF}) computed using OpenSim and using P^{eq} respectively. (e) The distribution of the SA moment arm (r_{SA}) computed using OpenSim and using the spline function respectively. Histograms (b), (d) and (f) show the fitting error distribution associated to l^{mt}, r_{AA} and r_{SA} respectively. The y-axis has been broken to focus on the most informative part of the graph.

(distance) between the two surfaces is uniform throughout the workspace and it reaches a maximum that is in the order of $8 \times 10^{-4} cm$. The histograms in Figs 4.1b, 4.1d and 4.1f, showed that spline generated errors were always contained in an error class that was smaller than the first (smallest) polynomial regression equation error class. Similar results were obtained with all the other muscles as reported in Table 4.2. The spline method provided MFEs that were three orders

Table 4.2: Mean fitting error (MFE) and standard deviation (σ) expressed in meters for both polynomial regression equation (P^{eq}) and spline methods. Values are associated to the estimation of musculotendon length and moment arms and were obtained by averaging MFE and σ of all muscles in the *LowerLimb4307* model during the first test as described in Section 4.3.

$(MFE \pm \sigma)$	P^{eq}	spline
l^{mt}	$7.2^{-4} \pm 6.4^{-4}$	$1.1^{-7} \pm 3.2^{-7}$
r_{HR}	$2.1^{-3} \pm 1.6^{-3}$	$1.8^{-6} \pm 3.3^{-6}$
r_{HA}	$2.8^{-3} \pm 2.2^{-3}$	$3.4^{-6} \pm 1.2^{-5}$
r_{HF}	$2.9^{-3} \pm 2.3^{-3}$	$3.8^{-6} \pm 1.4^{-5}$
r_{KR}	$4.7^{-4} \pm 5.1^{-4}$	$1.2^{-5} \pm 4.1^{-5}$
r_{SA}	$9.4^{-4} \pm 9.1^{-4}$	$6.7^{-6} \pm 1.9^{-5}$
r_{AF}	$4.4^{-4} \pm 7.2^{-4}$	$2.0^{-6} \pm 3.8^{-6}$
r_{MA}	$1.6^{-4} \pm 9.3^{-5}$	$9.3^{-7} \pm 9.9^{-7}$

Table 4.3: Error measures on *semimembranosus* musculotendon length interpolation expressed in meters. The term $P_n^{eq_m}$ represents the m-th polynomial regression equation as a function of n generalized coordinate (GC). The term s_n represents the n-dimensional spline function. Both polynomial regression and spine approaches have been used to estimate l^{mt} using different ranges of motion (ROM) for the GCs listed in Table 4.1. Furthermore, l^{mt} has been estimated both on the interpolation nodes (*on*) and a novel set of nodes placed midway between the interpolation nodes (*off*). Error measures have been used to quantify the fitting accuracy including: Mean fitting error (MFE), error standard deviation (σ) and 95% confidence inerval using a Chebychev distribution (CI).

Reduced ROM				
	MFE	σ	C.I.(95%)	
P_4^{eq1}	2.15E-03	1.74E-03	9.92E-03	on
s_4	2.39E-10	1.69E-10	9.97E-10	
P_4^{eq1}	1.86E-03	1.42E-03	8.19E-03	off
s_4	6.93E-06	7.18E-06	3.90E-05	
P_5^{eq1}	2.16E-03	1.68E-03	9.69E-03	on
s_5	2.46E-10	1.75E-10	1.03E-09	
P_5^{eq1}	1.87E-03	1.34E-03	7.85E-03	off
s_5	6.92E-06	7.17E-06	3.90E-05	
P_6^{eq1}	2.17E-03	1.68E-03	7.49E-03	on
s_6	2.56E-10	1.83E-10	1.07E-09	
P_6^{eq1}	1.86E-03	1.33E-03	7.81E-03	off
s_6	1.35E-05	1.88E-05	9.74E-05	

Extended ROM				
	MFE	σ	C.I.(95%)	
P_4^{eq0}	2.35E-03	2.22E-03	1.23E-02	on
s_4	2.25E-10	1.60E-10	9.42E-10	
P_4^{eq0}	1.91E-03	1.71E-03	9.54E-03	off
s_4	1.62E-05	2.11E-05	1.11E-04	
P_5^{eq0}	2.45E-03	2.26E-03	1.26E-02	on
s_5	2.31E-10	1.66E-10	9.74E-10	
P_5^{eq0}	2.02E-03	1.72E-03	9.71E-03	off
s_5	1.62E-05	2.11E-05	1.11E-04	
P_6^{eq0}	2.53E-03	2.28E-03	1.27E-02	on
s_6	2.51E-10	1.82E-10	1.06E-09	
P_6^{eq0}	2.08E-03	1.74E-03	9.86E-03	off
s_6	2.66E-05	3.52E-05	1.84E-04	

of magnitude smaller then the errors obtained using polynomial regression.

The test on the *LowerLimb1310* model showed that, with the same conditions, the spline method provided better performance than P^{eq} (Table 4.3). The use of

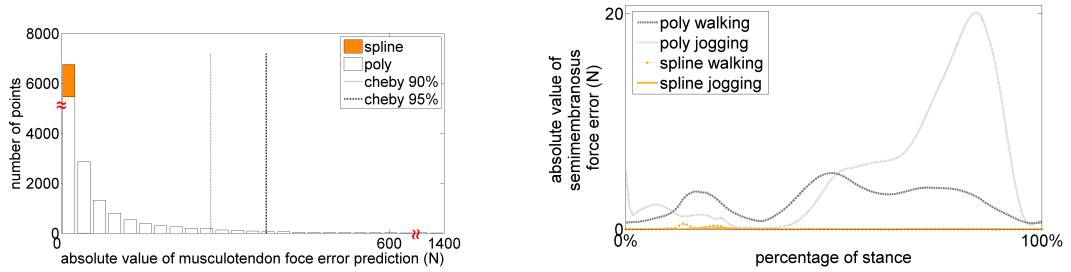

(a) (b)

Figure 4.2: (a) The error associated to the prediction of the maximal isometric F^{mt}. The histogram combines values for all muscles in the *LowerLimb1310* obtained during the third test. A set of error classes have been defined, each one representing a different error range and the number of points falling into each class have been counted and graphed. The x an y axes have been broken to focus on the most informative part of the graph. (b) The *semimembranosus* force prediction errors during all gait and jogging trials are estimated and the average errors are here reported.

an extended ROM, significantly affected P^{eq} accuracy. Furthermore, a different regression equation had to be used on the extended ROM even though, experiments were done on the same muscle and and kinematic variable. The spline method was less affected than the P^{eq} by the distance between interpolation nodes, and their associated difference measures were always at least three orders of magnitude smaller. When the number of GCs was increased, splines were not significantly affected whereas P^{eq} fitting accuracy showed higher variability. In general, spline functions evaluated on the interpolation nodes produced negligible errors ($10^{-10}m$) thanks to the $(n+1)$ interpolation conditions that assure perfect fit on-nodes (Section 4.2.2). When evaluated off-nodes, errors were still very small, i.e. in the order of $10^{-5}m$. Interestingly, P^{eq} produced slightly bigger errors when evaluated on the interpolation nodes although always in the order of $10^{-2}m$. As shown in Table 4.4, the percentage mean fitting error $\%\epsilon$ associated to the HA moment arm (r_{HA}) showed that the non-differentiated spline, that was individually fitted to $r_{HA}\left(s_4^{ha}\right)$ provided the best results. However, $\partial s_4^{lmt}/\partial q_{HA}$ still produced very small values of $\%\epsilon$ in the order of 0.1% of $E[r_{HA}]$ with better performances off-nodes. Errors associated to P^{eq} were higher and corresponded to a *thick* 10% of $E[r_{HA}]$.

The l^{mt} fitting error impacted the estimates of muscle force. Estimations of l^{mt} using P^{eq} reached a MEE of $1.23cm$ with four GCs and an extended ROM

(Table 4.3). On the other hand, splines produced a MEE of only $0.01cm$. When muscles were maximally activated, a $1cm$ difference in l^{mt} with respect to the true length can result in variations of hundreds of newtons (N) in the estimation of the isometric musculotendon force. The force errors stemming from P^{eq} fell into error classes of hundreds of newtons whereas spline related errors were always less than $20N$ and always contained in the first (smallest) error class (Fig. 4.2a). In the *LowerLimb1310* test, errors of all muscles from the spline-based approach provided superior results than P^{eq} (Fig. 4.2a). During tests involving dynamic motor tasks, errors in force prediction associated to P^{eq} were highly dependent on the muscle activation level as opposed to errors associated to the spline method (Fig. 4.2b). The force prediction instantaneous error during walking reached a maximum error of $6N$ using P^{eq} which increased up to almost $20N$ during jogging, while the spline errors were not affected by the increased muscle activation and was always less than $1N$.(Fig. 4.2b).

The computation time needed to evaluate one point on the spline function depends on the number of GCs [68]. This dimension dependency was observed in the computational time tests although computational costs were always reasonably low. Computational time ranged from $10^{-5}ms$ (one-dimensional case) to $10^{-2}ms$ (six-dimensional case) both for spline and for its derivative. The P^{eq} computation time was always in the order of $10^{-6}ms$ as the number of coefficients is not a function of the number of GCs.

4.4 Conclusions and Future Work

In this study, multidimensional cubic B-splines were used to estimate musculotendon kinematics for a set of lower-limb musculotendon actuators. The proposed methodology was compared to previous research work that used polynomial regression [69]. A single spline function could be used to estimate both l^{mt} and r with only very small errors compared to the original data. Contrary to this, different P^{eq} had to be chosen according to the surface to be fitted. If 6 GCs were involved, 7 different regression equations had to be chosen (i.e. one for l^{mt} and six for r) and their coefficients had to be calculated. This requires in general more

Table 4.4: Percentage of the mean fitting error (MFE) relative to the OpenSim-generated value averaged over the N data points $\%\epsilon$. Values are from the estimation of the *semimembranosus* muscle hip adduction-abduction moment arms (r_{HA}). The term P_n represents the polynomial regression equation used for the estimation of r_{HA} as a function of n generalised coordinates (GCs). The term s_n^{HA}represents the n-dimensional spline function used for the direct estimation of r_{HA}. The term s_n^{lmt} represents the n-dimensional spline function used for the direct estimation of the *semimembranosus* musculotendon length. The term $\frac{\partial s_n^{lmt}}{\partial q_{HA}}$ represents the first partial-derivative of s_n^{lmt} with respect to the hip adduction-abduction GC (q_{HA}) and represents the approach that is presented in this research work. Values of $\%\epsilon$ were calculated using an extended (E) and a reduced (R) range of motion (ROM) for q_{HA} as in Table 4.1. Furthermore, $\%\epsilon$ has been calculated when r_{HA} was estimated on the interpolation nodes (*on*) and on a novel set of nodes placed midway between the interpolation nodes (*off*).

	R/on	*R/off*	*E/on*	*E/off*
P_4	10.35	8.39	12.01	9.94
$\partial s_4^{lmt}/\partial q_{HA}$	0.18	0.05	0.26	0.06
s_4^{ha}	4.6E-08	1.5E-03	5.3E-08	3.8E-03
P_5	10.34	8.38	12.00	9.93
$\partial s_5^{lmt}/\partial q_{HA}$	0.18	0.04	0.26	0.06
s_5^{ha}	4.8E-08	1.5E-03	5.5E-08	3.8E-03
P_6	10.34	8.38	12.00	9.95
$\partial s_6^{lmt}/\partial q_{HA}$	0.18	0.05	0.26	0.07
s_6^{ha}	5.0E-08	2.0E-03	5.9E-08	6.3E-03

experimental data to be available whereas the spline-based approach provides a single solution to the problem.

Fitting accuracy was analyzed under different conditions including: number of experimental nodes, number of GCs, distance of evaluation points from experimental nodes. Splines always provided fitting errors of at least three orders of magnitude smaller than errors associated to P^{eq}.

Muscle force estimates were not affected by the use of the spline method to estimate musculotendon kinematics. There was tight agreement between the forces determined using the NMS model driven by the OpenSim and spline generated l^{mt}. This occurred for both isometric maximal contraction and dynamic trials. On

the other hand, forces produced using P^{eq} showed large discrepancies during the isometric tests. During dynamic tests the force discrepancy significantly increased with muscle activation.

Computational requirements associated to both spline and polynomial regression were compared. The computational time of P^{eq} is not a function of the number of GCs and was always in the order of $10^{-6}ms$. Because the number of spline coefficients is a function of the number of GCs (Section 4.2), the computational cost associated to the spline approach varies with the number of GCs too. However, results showed that good performances were obtained even with 6 GCs where the time needed to estimate a single data point for l^{mt} and for the 6 moment arms was estimated to be in the order of $0.1ms$ per muscle. The splines' first derivatives could be estimated at the same computational cost needed for the non-differentiated spline. Computational performances provided by the proposed spine method make this approach suitable for applications with real-time requirements.

The use of splines is not limited to fitting l^{mt} data from muscluotendon models such as SIMM or OpenSim. Alternatively, l^{mt} could be determined from the centroids of three dimensional muscles based on MRI data [70, 71] or from three dimensional geometric modeling of musculoskeletal systems [72–74]. These methods allow modeling muscles as complex of fibers with different contraction properties, mass distributions and shapes. However, the amount of information needed to represent these models and the associated computational requirements would prevent any direct implementation into real-time systems or micro controllers. The approach proposed in this Chapter allows creating a multivariate function that can reliably replicate the behavior of complex systems at low computational cost.

In summary, the results obtained using the spline-based approach are promising and further demonstrate the methodology can be reliably integrated in complex neuromusculoskeletal models for the prediction of muscle force for a large number of musculotendon actuators as previously shown in Chapter 3.

Chapter 5

Fast Calibration of the Elastic-Tendon NMS Model

Chapters 3 and 4 presented the design of the proposed EMG-driven NMS model based on infinitely stiff tendons. In some applications however, it may be useful to have accurate estimates of the instantaneous tendon and muscle fibre lengths. In such a situation, an elastic-tendon NMS model may be the best choice. The main problem though, is the time required to properly calibrate it. Indeed, as explained in Chapter 3 the calibration of the single-DOF knee joint model may take several hours. This time is bounded to significantly increase with the number of muscles and DOFs in the model but also with the number of calibration trials that are used. The required calibration time can therefore easily become unmanageable even with powerful machines.

This Chapter illustrates an alternative solution to the use of standard global optimization algorithms (Section 2.3.4) to optimize the model. We will refer to the NMS model that uses an elastic-tendon Hill-type muscle model to as the EHM. We will instead refer to the NMS model that uses a stiff-tendon Hill-type muscle model to as the SHM.

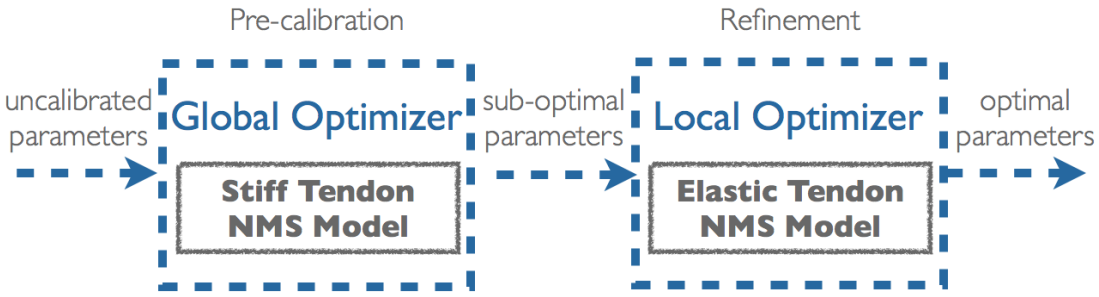

Figure 5.1: Proposed procedure for the fast calibration of the elastic-tendon NMS model.

5.1 Methods

Chapter 3 showed that the SHM proposed in this thesis achieves faster execution and calibration time with no loss of accuracy in the prediction of knee flexion-extension (FE) moments with respect to the EHM. Because of this, it is reasonable to hypothesize that the set of parameters obtained for the SHM may represent a good *sub-optimal* solution for the EHM. If this hypothesis holds, it could be possible to create a faster calibration procedure for the EHM that comprises two steps:

1. Pre-calibration: the global optimization criteria (i.e. simulated annealing) presented in Section 2.3.4 is used to calibrate the stiff-tendon model. The resulting parameter set represents the initial sub-optimal solution for the elastic-tendon model. The simulated annealing procedure will be referred to as the *standard calibration procedure*.

2. Refinement: the fast local optimization criteria (i.e. downhill simplex) presented in [75] is used to further refine the initial sub-optimal solution to obtain an optimal parameter set for the EHM. The pre-calibration step allows localizing and avoiding all the locally optimal solutions in the work space. The local optimization algorithm is then used to explore the neighborhood of the sub-optimal solution and quickly converge towards the closest optimum.

Fig. 5.1 gives a schematic view of the proposed calibration procedure.

5.2 Validation Procedure

Experiments were performed at the Gait Laboratory of the School of Sport Science Exercise and Health of the University of Western Australia. Data were collected from one male subject (age: 28, weight: 67, height: 183 cm) who gave informed consent and who performed 5 walking trials at self-selected speed. The same data collection protocol and the same modeling process described in Chapter 2 were used. The data collected during the 5 walking trials were used to calibrate the elastic-tendon model presented in Section 2.3. A total number of 19 parameters were adjusted during the calibration process. These included: muscle-specific tendon slack length, global EMG-to-activation shape factor and recursive filter coefficients and muscle strength coefficients (Section 2.3.4).

The validation procedure comprises three tests. In all tests knee FE moments are estimated during the stance phase. Outputs are time-normalized using a cubic spline and averaged over the 5 walking trials to produce a single ensemble average knee FE moment curve. Furthermore, the mean fitting error (MFE), as described in (3.9), is used as an additional measure of error in the estimated moments. The first test assesses whether the set of parameters obtained from the standard calibration of the SHM actually represents a good *sub-optimal* solution for the EHM. This represents the pre-calibration step. The knee FE moments estimated by the pre-calibrated EHM (P-EHM) are then compared to those obtained by the standard-calibrated stiff (C-SHM) and elastic (C-EHM) tendon models.

The second test assesses whether the refinement step further improves the solution found during the pre-calibration step. For this purpose, the refined pre-calibrated solution (RP-EHM) is compared to that obtained from C-EHM and C-SHM. Furthermore, to prove that the refinement step alone does not lead to satisfactory solutions, the elastic-tendon NMS model (EHM) is calibrated using the local downhill simplex algorithm starting with an uncalibrated parameter set. We will refer to this model to as D-EHM (i.e. downhill simplex calibrated EHM model).

The third test assesses whether the proposed calibration procedure is faster than the standard one. For this purpose the calibration time is measured and

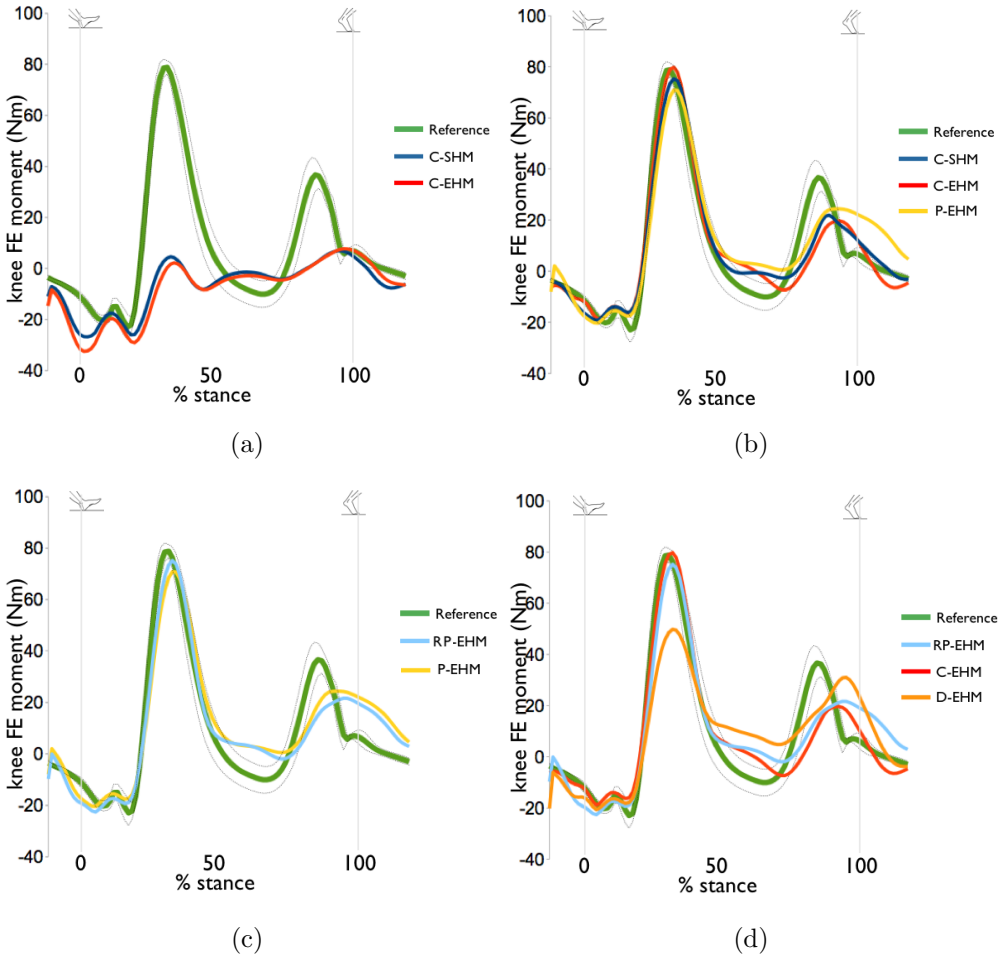

Figure 5.2: (a) Stiff and elastic-tendon models using the uncalibrated parameter set. (b) Standard-calibrated elastic (C-EHM) and stiff (C-SHM) models are compared to the pre-calibrated elastic-tendon model (P-EHM). The reference knee FE moment curve is also shown along with its standard deviation (dotted lines). (c) The refined pre-calibrated elastic-tendon model (RP-EHM) is compared to the pre-calibrated elastic-tendon model (P-EHM). (d) The refined pre-calibrated elastic-tendon model (RP-EHM) is compared to the standard-calibrated elastic-tendon model (C-EHM) and to the downhill simplex calibrated elastic-tendon model (D-EHM).

compared for both procedures. Tests are performed on an embedded system (Digital Logic, Switzerland) equipped with a $1.6Ghz$ Atom CPU with $512MB$ RAM.

5.3 Results

Fig. 5.2a shows the behavior of both stiff and elastic-tendon models using the uncalibrated parameter set. This represents the starting point for the optimization

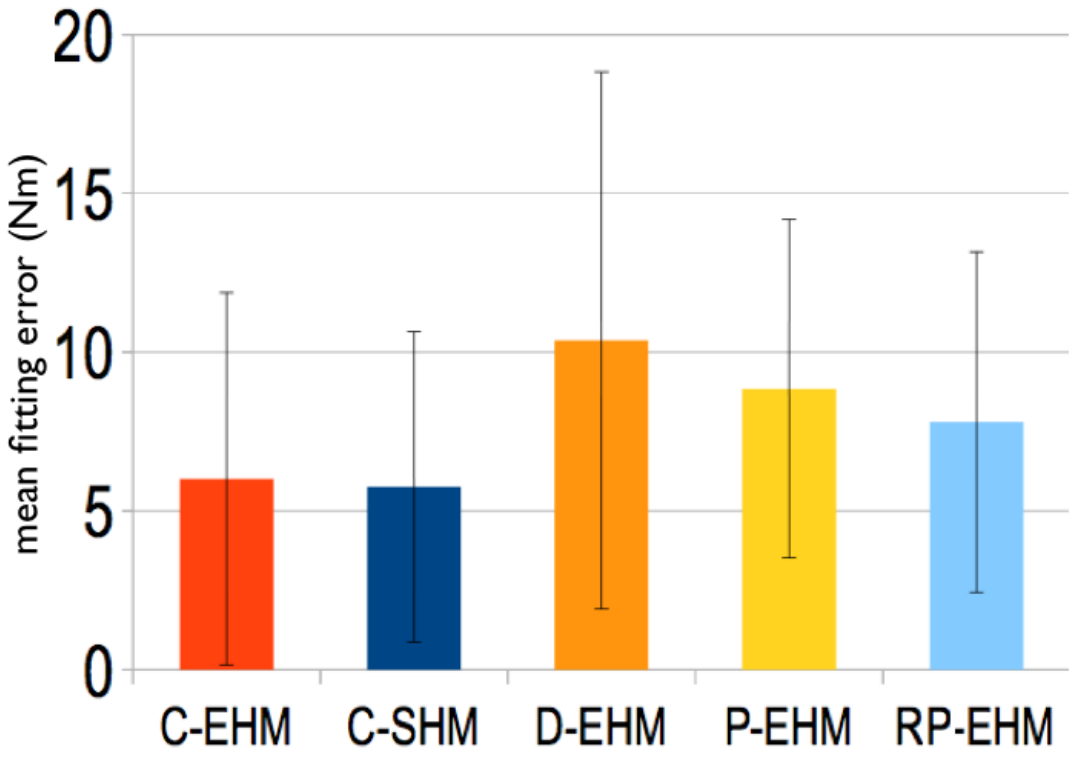

Figure 5.3: Mean fitting error (MFE) associated to: standard-calibrated elastic (C-EHM) and stiff-tendon (C-SHM) models, downhill simplex calibrated elastic-tendon model (D-EHM), pre-calibrated elastic-tendon model (P-EHM), refined pre-calibrated elastic-tendon model (RP-EHM). The standard deviation of the MFE is represented by the lines on top of each bar.

procedures.

Fig. 5.2b shows the results from the first test. The P-EHM performs very similarly to the C-EHM and C-SHM models with slightly higher fitting errors (Fig. 5.3). This proves the pre-calibration step provides a sub-optimal solution which represents a good starting point for refinement.

Fig. 5.2c and 5.2d show the results from the second test. The refinement step improved the solution associated to the P-EHM producing an even more similar curve to that associated to the C-EHM models (Fig. 5.2c). Using the downhill simplex algorithm to calibrate the elastic-tendon model from scratch does not lead to satisfactory solutions (Fig. 5.2d) thus proving this method only converges towards the *closest* locally optimal solution. This further validates the proposed idea of combining a global optimization approach with a fast local one (Section 5.1). The RP-EHM generates a knee FE moment curve that closely fits that generated by the C-EHM model. Furthermore, the RP-EHM further decreases its

Table 5.1: Comparison of computational time performances (h=hour, m=minute, s=second)

C-EHM	C-SHM	D-EHM	P-EHM	RP-EHM
19h,13m	8m,7s	55m,13s	8m,7s	63m,20s

MFE with respect to the P-EHM and reaches a similar value to that associated to the C-EHM (Fig. 5.3).

Table 5.1 shows the results associated to the third test. The time needed to calibrate the elastic-tendon model using the standard calibration procedure (C-EHM) is approximately 19 hours. The time needed using the methodology proposed in this Chapter (RP-EHM) is significantly lower, i.e. approximately 63 minutes.

5.4 Discussion

It is worth noting that the pre-calibrated elastic-tendon model (P-EHM) performed very well with a MFE of $8.8 \pm 5.3Nm$. The time for its calibration is the time required to calibrate the stiff-tendon model using the standard calibration approach that is approximately 8 minutes. The refined pre-calibrated elastic-tendon model (RP-EHM) performed slightly better than the P-EHM, i.e the associated MFE was $7.8 \pm 5.3Nm$. However, the time for calibration was much higher (63 minutes). This work shows that the stiff-tendon model alone can be used to calibrate the elastic-tendon model in just 8 minutes as opposed to the 19 hours required from the standard calibration and the 55 minutes required by the refinement step. Furthermore, the loss of prediction accuracy is significantly low. The standard-calibrated elastic-tendon model achieved a MFE of $6.01 \pm 5.9Nm$ which is only $2.79Nm$ lower to that associated to the P-EHM and $1.79Nm$ lower than that associated to the RP-EHM.

5.5 Conclusions and Future Work

In this Chapter a novel methodology was presented to achieve faster calibration of the elastic-tendon model. Results showed the proposed methodology allows calibrating the elastic-tendon model achieving the same calibration accuracy of the standard calibration procedure but in significantly less time.

This result is particularly significant when an elastic-tendon model is to be used to simulate the behavior of a large number of musculotendon actuators or when the NMS model has to be calibrated on a large number of trials. Indeed, the calibration time is a function of the number of MTAs and DOF in the model as well as number of calibration trials.

Future research will further assess the potential of the proposed calibration methodology on the multi-DOF NMS model presented in Chapter 6. Furthermore, the low calibration time associated to the stiff-tendon model will be exploited to implement an on-line calibration algorithm that keeps refining the model parameters as it executes. This will allow coping with time-varying parameters associated to muscle fatigue including the muscle maximal isometric force. This will allow creating NMS model that automatically adapt to the subject's physical conditions.

Chapter 6

A Neuromusculoskeletal Model of the Human Lower Extremity

The previous Chapters presented the single-DOF EMG-driven NMS model developed in this thesis. The model can estimate the force from 13 musculotendon actuators (MTAs) crossing the knee joint and the moments about the flexion-extension (FE) DOF. It was compared to the previously developed single-DOF NMS model based on elastic tendons (Section 2.3). It was demonstrated the single-DOF NMS model proposed in this thesis achieves faster execution and calibration time with no loss of accuracy in the prediction of knee flexion-extension (FE) moments. It was also proved the model can be used to implement fast calibration of the elastic-tendon model.

This Chapter further extends the work presented in the previous Chapters. A novel neuromusculoskeletal (NMS) model of the human lower limb is here presented. The model uses EMG signals from 16 muscles to estimate forces from 34 muscles and moments at the hip, knee and ankle joints. We will refer to the model presented in this Chapter to as the *multi-DOF EMG-driven NMS model*. Results show the multi-DOF model is capable of constraining the operation of the muscles to satisfy the moments generated at all joints and about all degrees of freedom during the human movement. This allows better estimating muscle forces providing a single solution to the problem with respect to current NMS models proposed in the literature that only constrain the operation of muscles

to satisfy moments produced at one joint only. This technology can be applied to the design of more intuitive human-machine interfaces for the simultaneous EMG-driven actuation of multiple joints in powered orthoses.

6.1 Introduction

The study of how muscles activate, generate force and actuate multiple joints simultaneously is crucial to understand the mechanisms behind human movement [25]. This is becoming an important topic in the design of wearable assistive device control systems such as powered orthoses. In recent years a body of research has been conducted on connecting the control system to biological signals generated by the operator that are directly linked to the desire of motion [8, 9, 15]. EMG signals represent a good candidate for extracting motor information from the lower limb and establishing an intuitive HMI for assistive device control (Chapter 1).

In this context, EMG-driven neuromusculoskeletal (NMS) models of the human limbs provide a way to implement continuous active control of assistive devices as opposed to pattern recognition and machine learning methods (Section 1.1).

To date though, only single-DOF EMG-driven NMS models have been proposed. That is, muscle forces are used to predict moments about a single DOF of a single joint. In [6] a whole-body NMS model was presented. However, it was not driven by EMG signals and the muscle redundancy problem, i.e. the way muscles share the load about a joint, was solved based on some objective function that had to be carefully chosen before hand. This is a limitation because muscles in general use different criteria depending on the subject and on the movement and it is often impossible to assess the appropriateness of the chosen optimization criteria. Furthermore, not using EMG signals has the drawback that to perform a movement, the operator has to be able to initiate the movement *before* he or she can receive support from the system.

This Chapter shows it is possible to use EMG signals to accurately estimate muscle forces from all major muscles in the lower limb. A novel NMS model is proposed which allows constraining the operation of muscles so that the forces they produce can satisfy the moments simultaneously generated at multiple DOFs

in multiple joints including the hip, knee and ankle joints. This is achieved by the use of a novel calibration algorithm (Section 6.3.5). Single-DOF models such as knee flexion-extension (FE) models allow estimating the muscle forces involved in the production of FE moments only. However, most of the muscles spanning the knee also span the hip and the ankle joints too. Therefore, the forces the muscles generate for the production of knee FE moment also have to satisfy the generation of moments about hip and ankle joints.

Single-DOF models, therefore, constrain the operation of muscles to satisfy the moments generated at a single joint and about a single DOF only. Because of this, Single-DOF models can usually fit the experimental *single-DOF joint moment* with good accuracy. However, the underlying behavior of the simulated muscles is questionable as it may not be truly representative of the real muscle behavior. Results in this Chapter show that the force a muscle can generate during a specific movement can be predicted in extremely different ways when different single-DOF models are used and it is not possible to know what single-DOF model gives the best estimates. The multi-DOF NMS model presented in this Chapter allows removing this indeterminacy by providing a single solution for each muscle. Results show the multi-DOF model has the potential to better estimate somatosensory information than single-DOF models.

This research has the potential to help design effective HMIs that can provide a better estimation of the human internal state. This research develops the technology needed to achieve power orthosis continuous control and the simultaneous actuation of multiple DOFs in multiple joints. This is a crucial requirement when the assistive device is to be used for the support of the lower limb. Indeed, all functional motor activities such as walking and climbing stairs involve the simultaneous actuation of hip, knee and ankle joints. This will also allow supporting an even wider range of movements.

6.2 Methods

Experiments were performed at the Gait Laboratory of the School of Sport Science Exercise and Health of the University of Western Australia. One healthy, male

subject volunteered for this investigation (age: $28 years$, height: $183 cm$, mass: $67 kg$). The subject was taken through the testing protocols and informed consent was obtained prior to data collection.

A data set for the calibration of the model is initially created which includes static and swinger trials. Furthermore, a number of dynamic trials are performed by the subject including: walking, jogging, step jumps and lateral hops. Data collected from the static and swinger trials are used to create a musculoskeletal model that is scaled to the subject's real dimensions (Section 2.2). The musculoskeletal model that is used in this work is customized to include all the muscles of interest and to define 6 degrees of freedom across the joints: hip adduction-abduction (HAA), hip flexion-extension (HFE), hip internal-external rotation (HRO), knee flexion-extension (KFE), ankle dorsi-plantar flexion (AFE), ankle subtalar angle (ASA). Data collected from the dynamic trials are used to calibrate the NMS model parameters (see Section 6.3.5).

A data set for the validation of the model (see Section 6.3.5) is then created which includes 10 repeated trials per motor task: fast walking (FW), running (RN), sidestepping (SS) and crossover (CO) cutting maneuvers. These tasks were chosen as they involve the activation of all the lower limb muscles and the subsequent production of moments across all joints.

A 12 camera motion capture system (Vicon, Oxford, UK) is used to record the human body kinematics with sampling frequency at $250 Hz$. A set of reflecting markers are placed on the human body and their instantaneous three-dimensional position is reconstructed and used to measure the movement of body segments including: trunk, pelvis, thigh, shank, and foot. Ground reaction forces (GRFs) generated during the motor tasks are collected using a multi-axis in-ground force plate (AMTI, Watertown, USA) with a sampling frequency at $2 kHz$. Both body kinematics and GRFs are low-pass filtered with cut-off frequencies ranging from 2 to $8 Hz$ depending on the trial. Marker trajectories recorded during dynamic trials are used to drive the scaled musculoskeletal model. OpenSim Inverse Kinematics (IK) tool is used to derive three-dimensional joint angles. GRFs are used in conjunction with the thee-dimensional joint angles computed through IK to derive the experimental joint moments. OpenSim Residual Reduction Analysis (RRA)

tool is used to compute the experimental joint moments.

Double-differential surface electrodes are used to collect EMG signals from 16 selected muscles including: Gluteus Maximus (*gmax*), Gluteus Medius (*gmed*), Tensor Fascia Latae (*tfl*), Medial Hamstrings (*medham*), Lateral Hamstrings (*latham*), Rectus Femoris (*recfem*), Sartorius (*sar*), Gracilis (*gra*), Adductor Magnus (*addmag*), Vastus Medialis (*vasmed*), Vastus Lateralis (*vaslat*), Gastrocnemius Lateralis (*gaslat*), Gastrocnemius Medialis (*gasmed*), Tibialis Anterior (*tibant*), Peroneus (*per*) and Soleus (*sol*). A telemetered system (Noraxon, Scottsdale, USA) transfers the EMGs to a 16 channel amplifier (Delsys, Boston, USA) with sampling frequency at $2kHz$. Raw EMG signals are first band-pass filtered ($10 - 150Hz$), and then full-wave rectified and low-pass filtered ($6Hz$) subsequently. The processed signal is the *linear envelope* which is then normalized against the maximum values from EMG linear envelopes obtained from a range of extra trials including: running and squat jumps.

6.3 NMS Model

The multi-DOF EMG-driven NMS model comprises 5 main components (Fig. 6.1). The main structure is similar to that of the single-DOF model previously presented (Chapter 3). The multi-DOF NMS model extends each single component to allow the estimation of forces from 34 muscle tendon actuators (see Table 2.1) and the joint moments about the following 4 DOF: hip adduction-abduction (HAA), hip flexion-extension (HFE), knee flexion-extension (KFE), ankle dorsi-plantar flexion (AFE). The NMS model proposed in this Chapter is entirely implemented in C++ likewise that presented in Chapter 3.

6.3.1 Musculotendon Kinematics

The musculotendon kinematics model estimates lengths and three-dimensional moment arms of the musculotendon actuators (MTA) included in the model as a function of the 3D angles of the joints each specific MTA crosses and was presented in Chapter 4 (also see Fig. 3.1). Most of the muscles in the model are described by a single MTA. That is, muscle fibers and tendons together are

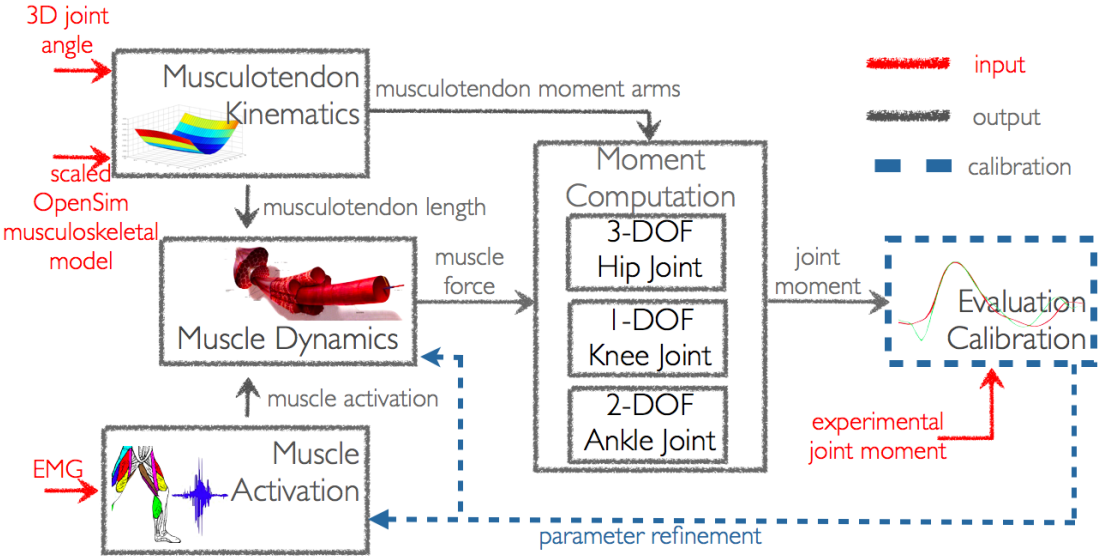

Figure 6.1: Schematic view of the NMS model structure. Experimental joint moments are input only for calibration purposes before the execution of the model (Section 6.3.5). The scaled OpenSim musculoskeletal model is used to create the muscle spline coefficients before the execution of the model 6.3.1. EMG signals and 3D joint angles are *continuosly* input and evaluated as the model executes.

modeled as a *single wire* which only has an origin and an end and can have internal *via points* that appear when the muscle line of action comes in contact with a bone, depending on the current 3D joint angle (Fig. 2.3). Some muscles are instead described by multiple MTAs. That is, muscle fibers and tendons together are modeled as a *multi wire* complex composed of multiple single MTAs. This is to describe large muscles composed of a great complex of fibers such as the Gluteus Maximus muscle (see Table 2.1). Using the scaled musculoskeletal model, a set of nominal values are established for the length of each MTA at predefined joint angles. A multidimensional spline function is then used to fit the experimental data and derive a multivariate function that can estimate values in between the experimental nominal values. Muscle moment arms are obtained by differentiating the musculotendon length spline function with respect to the generalized coordinate of interest. Spline coefficients are pre-calculated off-line prior to the NMS model execution (Chapter 4).

6.3.2 Muscle Activation

Muscles linear envelopes are processed and converted into muscle activation. This is a percentage value that expresses how much a specific muscle is activated towards the generation of force. The transformation from EMG to activation accounts for the non-linear relationship between EMG and muscle force and a more detailed description of the transformation involved as been presented previously (Section 2.3.2).

EMG signals recorded from 16 muscles (see Section 6.2) are used to estimate the activation of 34 musculotendon actuators (MTAs). EMG signals that could be experimentally recorded from those muscles that are modeled as a single wire are assigned to their respective MTA. These include: *vaslat*, *vasmed*, *sol*, *tibant*, *tfl*, *recfem*, *sar*, *gra*, *gaslat*, *gasmed*. EMG signals that could be experimentally recorded from those muscles that are modeled as a multi wire complex are assigned to all the MTAs that compose each muscle complex. That is, *addmag* EMG signals are used to drive: *addmag1*, *addmag2*, *addmag3*. The *gmax* EMG signals are used to drive: *gmax1*, *gmax2* and *gmax3*. The *gmed* EMG signals are used to drive: *gmed1*, *gmed2* and *gmed3*. The *per* EMG signals are used to drive: Peroneus Longus (*perlong*), Peroneus Brevis (*perbrev*), Peroneus Tertis (*perter*). The *medham* EMG signals are used to drive: Semimembranosus (*semimem*) and Semitendinosus (*semiten*). The *latham* EMG signals are used to drive: Biceps Femoris Short Head (*bicfemsh*) and Biceps Femoris Long Head (*bicfemlh*). The EMG signals for the remaining muscles can not be experimentally recorded because they are located too deep under the skin surface. However, muscles that are innervated in the same zone associated to those muscles whose EMG activity can be recorded, are assumed to produce similar EMG activity and contraction patterns. Therefore, the *addmag* EMG signal is used to also drive: Adductor Brevis (*addbrev*) and Adductor Longus (*addlong*). In the case of muscles that are innervated in two points, a linear combination of the EMG signals associated to the two innervations locations is used. Therefore a linear combination of the *vasmed* and *vaslat* EMG signals is used to drive the Vastus Interioris (*vasint*) MTA. Finally, a linear combination of the *gmax* and *gmed* EMG signals is used to drive the Gluteus Minimum (*gmin*) muscle that is composed of 3 MTAs. The Illiacus and Psoas

muscles are not driven by EMG signals and their activation is not computed in this current implementation of the model. However, these muscles still contribute to the production of force at the hip joint because the passive force generated during stretching and compression is calculated by NMS model anyway.

Some muscles of the lower extremity have not been included in the model because either too small and therefore negligible or too deep under the skin surface. However, the selected MTAs generate the majority of the moment in all selected joints about all considered DOFs. That is, the muscles in the model that have a HAA moment arm cover the 91% of the total physiological cross sectional area (PCSA). Muscles that have a HFE moment arm cover the 87% of the total PCSA. Muscles with a KFE moment arm in the model cover the 95% and muscles in the model that have an AFE moment arm cover the 80% of the total PCSA.

6.3.3 Muscle Dynamics

It uses the values computed in the previous two blocks to calculate the force developed by each MTA in the model as previously described in Section 3.5.

6.3.4 Moment Computation

This component evaluates the moments produced about all the DOFs of each joint included in the model. The estimated muscle forces are combined with the corresponding moment arms to calculate the torque about a specific DOF.

6.3.5 Validation and Calibration

To validate a model, it is usually desirable to compare the output of that model with data measured empirically. Unfortunately, the methodological difficulties in measuring individual muscle forces prevent any direct validation of the NMS model on humans. An indirect process was therefore designed. This involves comparing the net moments from muscles crossing the hip, knee and ankle joints with the net moments measured experimentally. If the muscle forces are accurate, the net joint moments estimated by the model should be equal to the external moments measured experimentally.

The calibration process is critical for the proper operation of the model. It defines how muscles activate in response to EMG signals and generate moments about multiple DOFs. Biarticular muscles crossing the hip and knee joints for instance, have to produce a force that satisfy moments about up to 4 DOFs (HROT, HAA, HFE and KFE). The aim of the calibration process therefore is to obtain a set of parameters for each muscle to accurately estimate the net experimental moments at the hip, knee, and ankle across all corresponding DOFs (Section 6.2). An optimization procedure has been designed to alter the initial uncalibrated parameters until the error function (Section 2.3.4) associated to the joint moment prediction is minimized. The calibration process repeatedly calls an optimization routine. The steps involved in the calibration of a 4-DOF NMS models are here summarized:

1. objective function: $min(E_{KFE})$. Adjust parameters for all muscles crossing the knee joint (13 MTAs).

2. objective function: $min(E_{KFE} + E_{HFE})$. Adjust parameters for all muscles crossing the knee joint (13 MTAs) and the hip joint (23 MTAs).

3. objective function: $min(E_{KFE} + E_{HFE} + E_{HAA})$. Adjust parameters for all muscles crossing the knee joint (13 MTAs) and the hip joint (23 MTAs).

4. objective function: $min(E_{KFE} + E_{HFE} + E_{HAA} + E_{AFE})$. Adjust parameters for all muscles crossing the knee joint (13 MTAs) and the hip joint (23 MTAs) and the ankle joint (8 MTAs).

where E_X is the error function associated to the prediction of the moments about the X^{th} DOF with $X \in \{HAA,\ HFE,\ KFE,\ AFE\}$. At each step, the error function is extended by including a new DOF. The parameter set to be calibrated is also extended by adding the parameters associated to a new set of muscles. The first call uses an uncalibrated set of parameters. At each step the optimization process utilizes the optimal solution produced by the previous step. The optimization process is designed so that it can only produce a better solution than the initial one. This assures that by adding a new DOF to the objective function, the fitting accuracy provided from the previous calls is always guaranteed. At each call,

the parameters associated to the currently added muscles are calibrated in order to fit the joint moments associated to the currently added DOF. Furthermore, the parameters associated to the muscles added by the previous steps are also re-calibrated. This ensures that muscle behavior accounts for the new DOF added to the process. If this was not done the biarticular muscles calibrated at *Step 1* would satisfy the knee FE moments only and would not be able to satisfy the hip adduction-abduction and hip flexion-extension moments added in *Step 2* and *Step 3* respectively. The same applies to each step. Once calibrated, the NMS model only requires EMG signals and joint angles as inputs. GRF and experimental joint moments are needed during the calibration step only.

6.4 Validation Procedure

The validation procedure is comprised of three tests. In all tests the NMS model outputs, i.e. muscle force and joint moments, are estimated during the *stance phase*. Outputs are then time-normalized using a cubic spline. Time-normalized muscle force predicted from each motor task respectively, i.e. fast walking (FW), running (RN), side-stepping (SS), cross-over (CO) are averaged over the 10 repeated trials and an ensemble average force curve per muscle is produced for each of the 4 motor tasks. The same procedure is applied to the time-normalized experimental and predicted joint moments.

The first test assesses whether the force generated by the same MTA is predicted in a different way by using different single-DOF NMS models. This is done for the purpose of validating the hypothesis that single-DOF models introduce indeterminacy and the impossibility to know what model to use for the estimation of a specific muscle force. For this purpose, the ensemble average force curves of the biarticular MTAs Gastrocnemius Lateralis and Medialis are predicted during FW both using a KFE NMS model and an AFE NMS model. The ensemble average force curves of the biarticular MTAs Semimembranosus and Semitendinosus are predicted during RN both using a HFE and a KFE NMS model. Finally the ensemble average force curves of the uniarticular MTAs Gluteus Medius 1, 2 and 3 are predicted during SS both using a HFE and a HAA NMS

model.

The second test assesses the ability of the proposed multi-DOF NMS model to predict joint moments about 4 DOFs including: HAA, HFE, KFE and AFE. The ensemble average curves associated to the predicted joint moments are directly compared to those associated to the experimentally measured moments (Section 6.3.5) as well as to those associated to the moments predicted by the respective single-DOF models i.e. HAA NMS model, HFE NMS model, KFE NMS model and AFE NMS model. This is done for the purpose of assessing the impact, of adding more DOFs to a NMS model, on its prediction capability. Furthermore, it validates whether the proposed calibration scheme (Section 6.3.5) is capable of producing a set of parameters that constraints the operation of the muscles to satisfy the joint moments produced about all the DOFs of all the joints they span. As an additional measure of error, the *Mean Fitting Error* (MFE) and its *standard deviation* (σ) are used : $MFE = \frac{1}{N}\sum_{i=1}^{N}\left|\hat{M}_i - M_i\right|$, where $\hat{M}$ is the ensemble average curve associated to the experimentally measured joint moments. The term M is the corresponding estimated value either from the multi-DOF NMS model or from the single-DOF NMS model. N is the number of points the ensemble average curves are composed of.

In the third test the forces of the muscles crossing the knee joint are predicted both using the proposed multi-DOF NMS model and the single-DOF KFE NMS model model during running trials. Forces estimated by both models are then compared.

6.5 Results

Results from the first tests are showed in Fig. 6.2. The Gastrocnemius Medialis force estimated by the KFE NMS model reached drastically higher values than those estimated by the AFE NMS model. Also the Gastrocnemius Lateralis force estimated by the KFE NMS model assumed higher values than that estimated by the AFE model. The Semimembranosus and Semitendinosus forces estimated by the KFE NMS models reached significantly higher values than those estimated by the HFE NMS model. The Gluteus Medius forces estimated by the HFE NMS

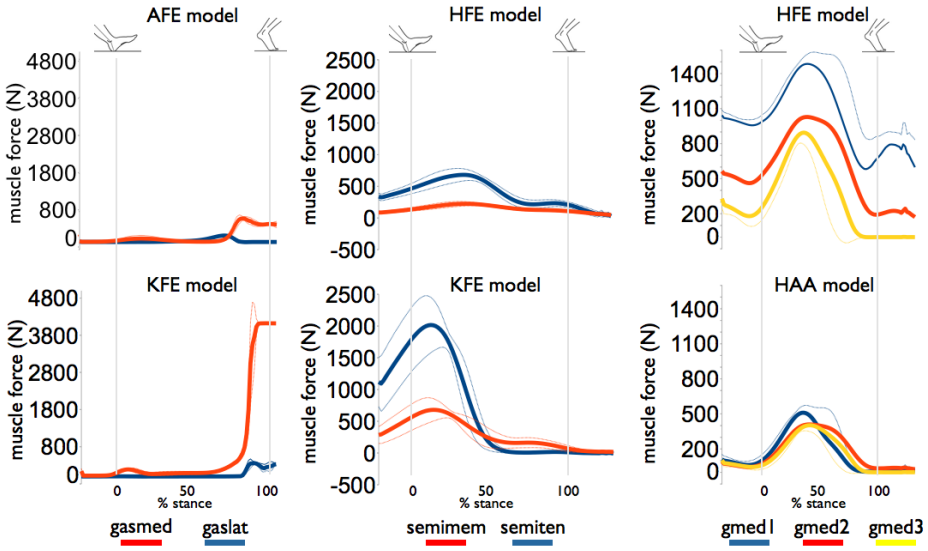

Figure 6.2: Comparison of muscle forces estimated by different single-DOF models. Gastrocnemius Medialis and Lateralis forces are estimated during fast walking trials. Semimembranosus and Semitendinosus forces are estimated during running trials. Gluteus Medius forces are estimated during side-stepping trials.

model were significantly higher than those estimated by the HAA NMS model. In general different single-DOF models produced different force estimates for the same muscle during the same specific movement. Similar results were obtained for all other muscles. This validates the hypothesis defined in Section 6.4. This test shows that although each single-DOF NMS model was driven by the same EMG signals, a high discrepancy in the behavior of different models was still produced. This is because the NMS model is not only EMG-driven but it is also Optimization-driven. That is, the calibration process that is performed prior to the model execution strongly influences the way muscles convert EMG into force *post-calibration*. Therefore, the same EMG signal for the same muscle can be converted in an extremely different muscle force if different single-DOF models are used. Indeed, the parameter sets associated to different single-DOF models are highly diverse.

Results from the second test are shown in Fig. 6.3. The multi-DOF NMS model achieved better performances in the prediction of the AFE moments in all 4 motor tasks. The multi-DOF NMS model behaved very similarly to the

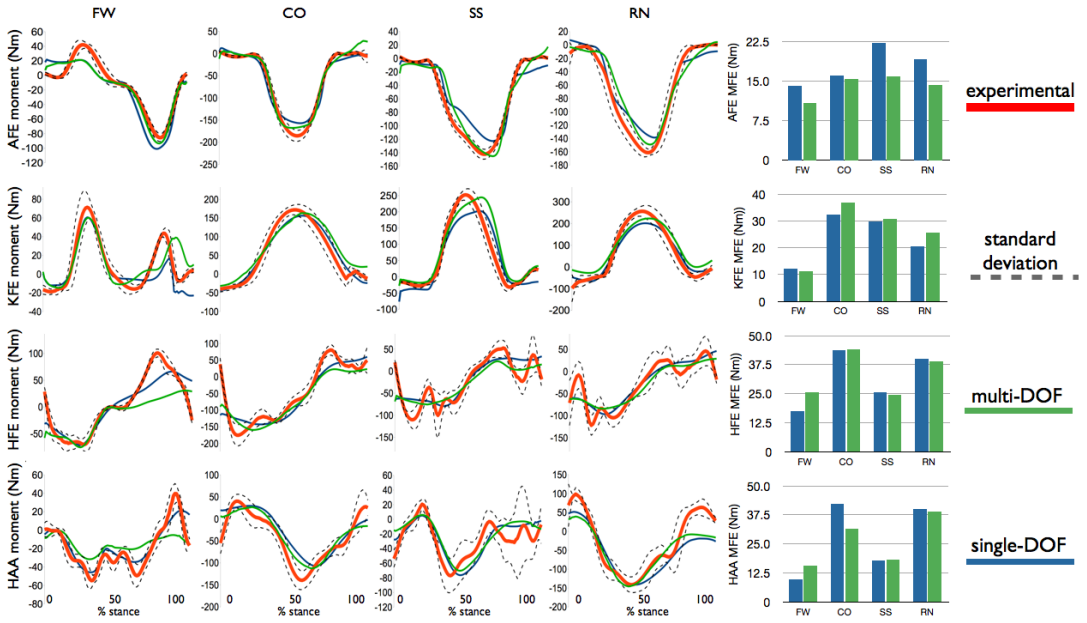

Figure 6.3: The joint moment prediction accuracy of the multi-DOF model was compared to that of the 4 single-DOF models during fast walking (FW), cross-over (CO), side-stepping (SS) and running (RN). The mean fitting error (MFE) was also used as measure of accuracy.

single-DOF KFE NMS model in the prediction of KFE moments in the FW ad SS motor tasks. Slightly better results were produced by the single-DOF model in the CO and RN tasks. Multi-DOF and single-DOF HFE NMS models produced very similar results in the estimation of HFE moments during CO, SS and RN tasks. Slightly better results during the FW task were produced by the single-DOF model. Finally, the multi-DOF NMS model produced slightly worse estimates of HAA moment during the FW task but significantly more accurate estimates during the CO task and very similar results to the single-DOF HAA NMS model during SS and RN tasks. This test suggests the proposed multi-DOF NMS model was able to concurrently predict the joint moments preserving the accuracy of the single-DOF models. The proposed multi-DOF calibration scheme (Section 6.3.5) was therefore able to constrain the operation of the 34 lower limb MTAs to satisfy the moments produced at multiple joints and DOFs simultaneously.

Results from the third test are shown in Fig. 6.4. Force estimates associated to the Hamstrings group (i.e. *bicfemsh*, *bicfemlh*, *semimem* and *semiten*) generated by the single-DOF KFE NMS model showed a predominant activity of the *semimem* MTA with smaller and similar contributions from the *bicfemlh* and *semiten* MTAs

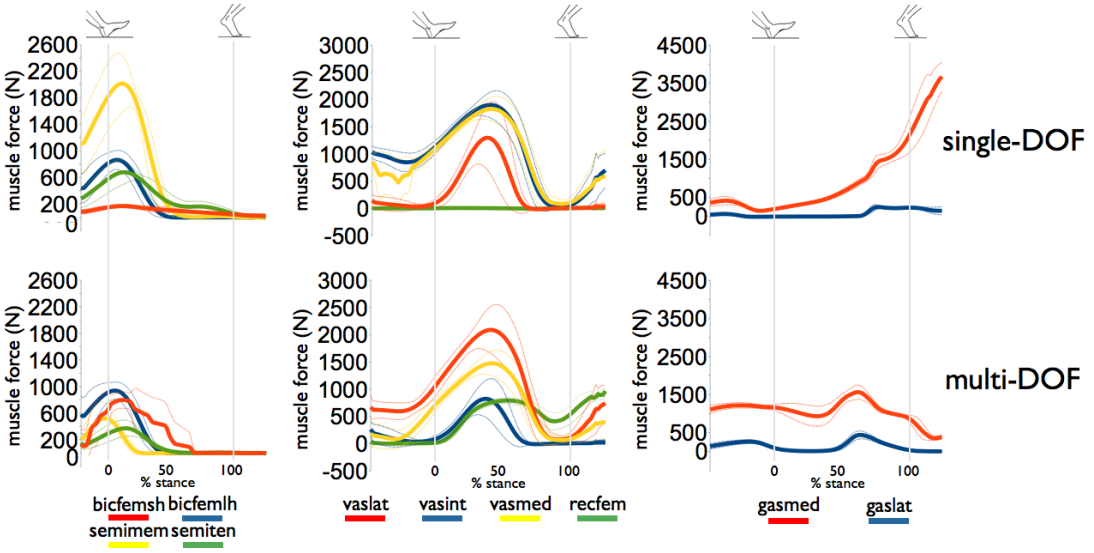

Figure 6.4: Muscle forces estimated during running tasks. The estimates of the multi-DOF model were compared to those of the single-DOF KFE model.

and very little force produced by the *bicfemsh* MTA. On the other hand, the force dynamics estimated by the multi-DOF model suggested these MTAs shared the load at the knee joint more equally. Indeed, the two MTAs comprising the Lateral Hamstrings *bicfemlh* and *bicfemsh* were estimated to generate similar curves. The same results were obtained for the *semimem* and *semiten* MTAs. Results produced by the multi-DOF model are in line with findings from the biomechanics community [24, 76].

Force estimates associated to the Quadriceps group (i.e. *vaslat*, *vasint*, *vasmed* and *recfem*) generated by the single-DOF KFE NMS model showed a predominant activity of the *vasmed* and *vasint* MTAs and a negligible production of force from the Rectus Femoris (*recfem*) MTA. On the other hand, the forces estimated by the multi-DOF model were more proportioned between the MTAs forming the Quadriceps group. More importantly the estimated behavior of the Rectus Femoris showed this MTA significantly produces force during running as also demonstrated in [76, 77]. The single-DOF KFE model could not predict this behavior because the *recfem* MTA is mostly active during running to support the hip flexion-extension movement. The proposed multi-DOF NMS model did not

fail to catch such important feature because it properly constrained its operation to satisfy not only KFE moments but also HFE and HAA moments.

Force estimates associated to the Gastrocnemius group (i.e. *gasmed* and *gaslat*) generated by the single-DOF KFE NMS model showed a drastically predominant activity of the *gasmed* MTA towards the end of the stance phase. On the other hand the dynamics estimated by the multi-DOF NMS model more equally apportioned the force to both MTAs.

6.6 Conclusions and Future Work

The research work presented in this Chapter, developed a novel EMG-driven neuromusculoskeletal model of the lower limb that uses EMG signals recorded from 16 muscles to derive the activity of 34 muscles and to estimate moments about hip, knee and ankle joints. Results showed that the force a muscle can generate during a specific movement can be predicted in extremely different ways when different single-DOF models are used. This fact introduces indeterminacy as it is not possible to know what single-DOF model is best to use. The proposed multi-DOF NMS model allows removing this indeterminacy by providing a single solution to the problem. The proposed model was able to predict joint moments with the same accuracy of the 4 individual single-DOF EMG-driven models thus proving each muscle was successfully constrained to satisfy moments about all associated joints and DOFs. As a result, the multi-DOF model was able to produce force dynamics estimates that were more in line with biomechanics findings. The single-DOF KFE model failed to estimate the force produced by the Rectus Femoris muscle during running because this is a muscle that is mostly active to support the hip flexion. The multi-DOF model correctly predicted this. Future version of the multi-DOF NMS model will feature a predictive algorithm for the estimation of the activation of muscles without EMG. This will allow estimating muscle forces generated by the Illiacus and Psoas muscles. Pattern recognition technology will be integrated in the NMS model and used to extrapolate more information out of the EMG signals as discussed in Chapter 8. A study on a larger population will be conducted to further validate the methodology.

This technology can offer great solutions for the implementation of more realistic virtual humans by providing a more accurate estimation of the human internal state [5]. This can also be applied to the design of more intuitive assistive devices control systems for the simultaneous actuation of multiple joints and the support of an even wider range of movements.

Chapter 7

Scaling Tendons Preserving the Consistency of the EMG-to-Activation Relationship

Neuromusculoskeletal modeling is a powerful tool for understanding how the nervous system controls muscles to generate movements. Experiments conducted in this thesis and the results that were obtained demonstrated that to properly *scale* NMS models to different subjects, physiological parameters that characterize individual muscle properties must be integrated in the NMS model design and properly calibrated. However, most of them cannot be measured directly unless invasive or expensive approaches are adopted. This is the case for the tendon slack length (l_s^t). This is a key-parameter because it directly defines how muscle develop force as a function of their fibre length.

There is very little information in the literature in regards to tendon slack lengths of lower limb musculature mostly because of the difficulty in measuring these values and the ill-defined junction between muscle and tendon. It was therefore decided to investigate a robust methodology for properly deriving physiologically relevant values for this important parameter.

This Chapter presents a method for scaling l_s^t for muscles crossing the knee joint. This method can be used alone or in addition to the standard calibration procedure (Section 2.3.4) to significantly refine the parameter initial guess.

7.1 Data Collection

Experiments were performed at the Gait Laboratory of the School of Sport Science Exercise and Health of the University of Western Australia. Data were collected from one male subject (age: 28, weight: 67, height: 183 cm) who gave informed consent. The subject performed knee flexion-extension (FE) maximal isometric trials using a Biodex dynamometer (Shirley, NY) at different knee joint angles: $-30°$, $-60°$, $-90°$, $-120°$, where $0°$ represents the leg totally extended and aligned with the thigh (Fig. 2.2). The hip joint was firmly held at $80°$ according to the convention depicted in Fig. 2.2. During each FE trial, EMG signals were recorded from the muscles crossing the knee as described in Section 3.5.2.

One walking trial was also performed and motion capture data were used to measure the knee FE moment generated following the procedure presented in Chapter 2.

7.2 Rationale

The aim of this study is to show that if l_s^t is not properly calibrated, the EMG-to-activation relationship (Fig. 2.16) is not consistent between different trials. That is, a different curve is generated when the knee joint is placed at different angles. The EMG-to-activation relationship becomes therefore a function of muscle fiber length if l_s^t is not properly calibrated. This should not happen because the EMG-to-activation relationship is independent of muscle fibre length for definition as described by equation (2.1).

In this study an initial guess of l_s^t is obtained by using the standard calibration procedure. This is used to also calibrate muscle strength coefficients, activation shape factor and optimal fibre length. Then, the scaling procedure presented in this Chapter is applied to further adjust the tendon slack length for every muscle in such a way that the computation of the muscle activation based on the EMG signal for a specific muscle is consistent for all joint angles.

7.3 Methods

One table per muscle (i) per trial (k) is created. The normalized EMG linear envelope u_i is linearly mapped to a specific entry of the table as follows:

$$h_{i,k} = \left\lfloor \frac{u_i}{S} \right\rfloor \tag{7.1}$$

where $h_{i,k}$ is the h^{th} entry of the table associated to the i^{th} muscle and corresponding to the k^{th} trial. S is the *entry width* which was chosen to be $0.0025mV$. At the end of this process every muscle owns K tables, where K is the number of trials. The data stored in the $h_{i,k}$ entry is shown below:

$u_{h_{k,i}}$	$\tilde{l}^m_{h_{k,i}}$	$F^m_{h_{k,i}}$	na

The table is sorted based by increasing values of $u_{h_{k,i}}$ in the first column. The $\tilde{l}^m_{h_{k,i}}$ and $F^m_{h_{k,i}}$ terms, represent the normalized muscle fiber length and the muscle force generated during the k^{th} maximal isometric trial associated to the i^{th} muscle. These are calculated using the NMS model presented in this thesis (Chapter 3). Every table row is averaged with new values whenever the table entry is selected for storing new data. The na term represents the number of updates.

In isometric conditions, $F^m_{h_{k,i}}$ is not a function of the fibre contraction velocity and can be expressed as a function of muscle activation and muscle fibre length only:

$$F^m = ((f_A(\tilde{l}^m))a(u) + (f_P(\tilde{l}^m)))F^m_0 \tag{7.2}$$

where $f_A(\tilde{l}^m)$ and $f_P(\tilde{l}^m)$ are the active force length curve and the passive force length curve respectively as a function of the normalized muscle fiber length $\tilde{l}^m$. Finally, F^m_0 denotes the maximum muscle force at optimal fiber length, l^m_0.

It is possible now to rearrange (7.2) in the following way:

$$a(u) = \frac{\frac{F^m}{F^m_0} - f_P(\tilde{l}^m)}{f_A(\tilde{l}^m)} \tag{7.3}$$

which indirectly expresses $a(u)$ as a function of the tendon slack length. Indeed, $\tilde{l}^m$ is a function of l^t_s (Chapter 3).

We can now compute the standard deviation ($\sigma_{h,i}$) of (7.3) for the table entry h from all K tables associated to the i^{th} muscle:

$$\sigma_{h,i}(l_s^t) = \sqrt{\frac{1}{K}\sum_{k=1}^{K}(a_{h_{k,i}} - \overline{a}_{h,i})^2} \tag{7.4}$$

where $\overline{a}_{h,i}$ is the average of $a_{h_{k,i}}$ over all K trials. The notation used in (7.4) highlights the fact that the standard deviation is also a function of the tendon slack length, i.e. $\sigma_{h,i}(l_s^t)$.

It is now possible to optimize l_s^t so that it minimizes the average of $\sigma_{h,i}$ over all table rows:

$$min_{l_s^t}(\overline{\sigma}(l_s^t)) = min_{l_s^t}\left(\frac{1}{N_h}\sum_{h=1}^{N_h}(\sigma_h(l_s^t))\right) \tag{7.5}$$

where N_h is the number of entries in the tables. A simulated annealing algorithm (Section 2.3.4) was used to vary l_s^t within a 15% of its initial guess for each muscle.

7.4 Results

In Fig. 7.1 it is shown the effect of the geometry calibration on one extensor muscle (vastus lateralis) and one flexor muscle (biceps femoris). Same results were obtained for the other muscles. When l_s^t is not calibrated the muscle activation function assumes different values in the correspondence of the same level of normalized postprocessed EMG for different trials (Figs 7.1a and 7.1c). After the scaling procedure discussed in Section 7.3 is performed, the muscle activation has a more similar behavior over different trials.

Fig. 7.2 shows that using the proposed scaling procedure, the EMG-driven NMS model better is capable of better estimating knee joint FE moments as opposed to when the standard calibration alone is used. The results in Fig. 7.2 are obtained during one walking trial.

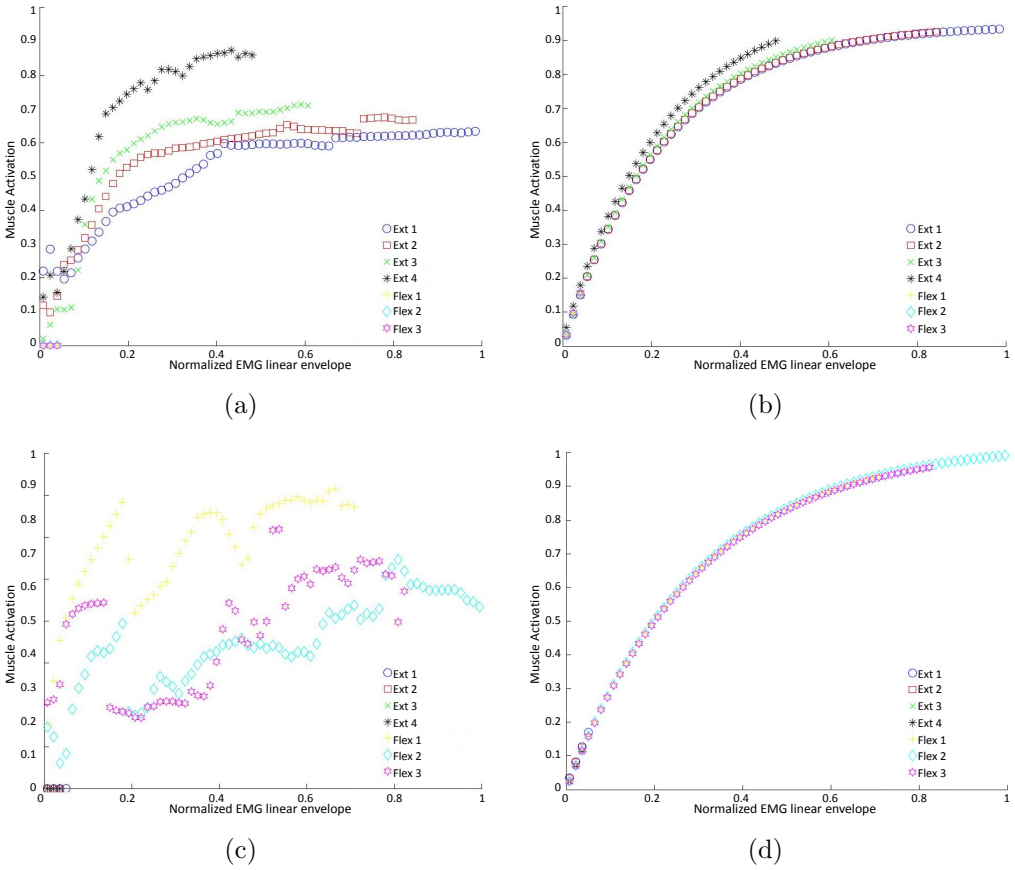

Figure 7.1: Muscle activation functions behave differently for the same level of postprocessed EMG over different trials when l_s^t is not calibrated. (a) Vastus lateralis (l_s^t not calibrated). (b) Vastus lateralis (l_s^t calibrated). (c) Biceps femoris (l_s^t not calibrated). (d) Biceps femoris (l_s^t calibrated).

7.5 Conclusions and Future Work

In this Chapter a method for scaling the tendon slack length (l_s^t) of muscles crossing the knee joint was presented. Results showed that the standard calibration procedure (Chapter 3) does not optimally scale the tendon slack length parameter. As a result, the EMG-to-activation relationship changes as a function of muscle fibre length. This is a dangerous inconsistency that the proposed scaling methodology allows eliminating. A similar methodology was used in [9] to scale l_s^t as well as F_0^m and the EMG-to-activation shape factor A. However, an objective function was used to solve the muscle redundancy problem. The joint flexion-extension moment was recorded using external force sensor during isometric trials. Then a specific

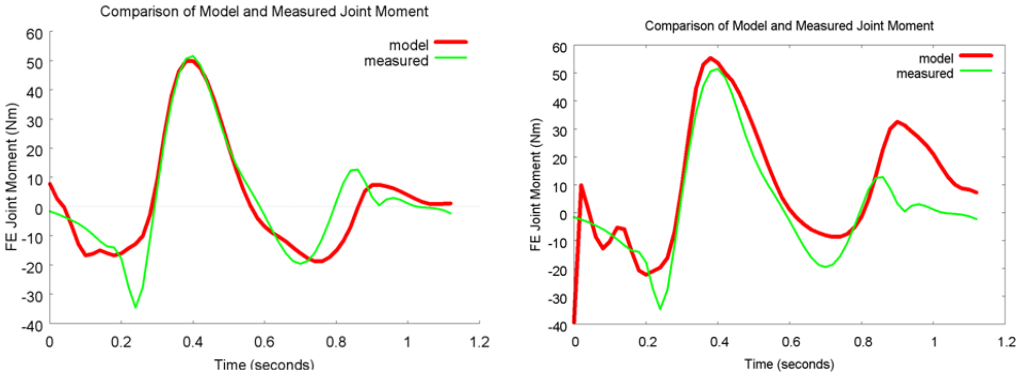

(a) (b)

Figure 7.2: (a) Prediction accuracy of the NMS model calibrated using standard calibration as well as the l_s^t adjustment described in this Chapter. (b) Prediction accuracy of the NMS model calibrated using standard calibration only.

objective function was used to derive the force generated by 4 thigh muscles from the experimental knee FE moment. However, no evidence of physiological accuracy was given. The approach proposed in this Chapter does not make any assumptions on the way muscles shares the load at the knee joint. In fact, the muscle redundancy is solved by the experimental EMG signals and the developed EMG-driven NMS model.

The presented methodology was not used in the studies presented in the previous chapters due to lack of time. However, preliminary results here shown are promising and future work will use ultra sound technology to experimentally measure l_s^t and further validate the proposed approach.

Chapter 8

Classification of Locomotion Modes

The previous Chapters of this thesis focused on the design and validation of the multi-DOF EMG-driven NMS model of the lower limb. This was presented as a means for establishing an EMG-based interface for the continuous extraction of somatosensory information from the human movement and provide an effective solution to actively control lower limb powered orthoses.

This Chapter, takes a different path. EMG signals are evaluated by a phase-dependent Support Vector Machine (SVM) classifiers for the identification of locomotion modes. This approach does not rely on biologically relevant models of the human musculoskeletal system and does not aim to realize continuous device control. The aim is to obtain *context knowledge* from the movement the user wants to perform, i.e. understanding whether the subject wants to walk rather than turning left or right and so forth. This study was conducted with the plan of combining the EMG-driven NMS model presented in the previous Chapters with the EMG-classifier to achieve a superior neuromuscular HMI that maximizes the information exchange between the human and the machine. More details about this integration will be provided in the following Sections.

8.1 Introduction

In the EMG-based pattern recognition venture, one of the main problems is that lower limb EMG signals are highly non-stationary. Therefore it is not easy to recognize patterns and subsequently classify the subject's motor intentions.

However, it has been recently shown that the difficulties in classifying different motor tasks could be partially overcome by reducing the duration of the time windows where task-characterizing features are captured [29, 78].

This Chapter investigates the suitability of Support Vector Machine (SVM) [79] to recognize locomotion modes when EMG features are computed in a $150ms$ time window. To date, the adoption of SVM methods for the classification of EMG signals is limited and was mostly applied to the upper limb [80]. Experimental results presented in this Chapter demonstrate the current implementation of the classifier allows predicting the different locomotion modes from EMG signals recorded from lower limb muscles with a high accuracy.

8.2 Methods

Experiments were performed at the Gait Laboratory of the Department of Information Engineering, University of Padova. Three healthy subjects were consecutively recruited for this study, 2 females and 1 male, with a mean age of 29±8.9 years and a mean body mass index (BMI) of 21.9±0.2 $\frac{kg}{m^2}$. The subjects were taken through the testing protocols and informed consent was obtained prior to data collection.

Each subject's right leg muscular activity was monitored through a sixteen channels surface electromyography (EMG) system (Pocket EMG, BTS Spa, frequency 1KHz). EMG signals were detected from the following muscles: *gluteus maximus (GLMA), gluteus medius (GLME), sartorius (SAR), rectus femoris (RF), vastus lateralis (VAL), vastus medialis (VAM), gracilis (GR), biceps femoris (BFCL), semitendinosus (ST), tibialis anterior (TA), peroneus longus (PEL), gastrocnemius lateralis (GAL), gastrocnemius medialis (GAM), soleus (SOL) and extensor digitorum brevis (EXD).* Three foot switches were attached under the

monitored foot in correspondence of the first and fifth metatarsal head, and the calcaneus. A 6-camera (150Hz) motion capture system (BTS SpA, Padova) was used to collect lower limb kinematics, synchronized with the EMG acquisition system. Each subject performed the motion tasks bare foot including: *level walking, stepping over an obstacle, turning right, ascending stairs, descending stairs, standing still*. Stepping over an obstacle was performed asking the subject to step over a wooden block of 14.5 cm hight, 40 cm width and 28.5 cm depth, while walking. In this context the non-tested side passed over the obstacle first, followed by the instrumented leg. A two-step staircase 16 cm high, 80 cm wide, and 28 cm deep was used for the stair ascending and descending test. The turning right was acquired asking the subject to perform a 90° turn while walking, pivoting on their own controlateral leg. Each subject performed the 6 motion modes randomly during each trial within the same experimental session. At least 12 complete *stride* cycles of each task were acquired.

8.2.1 Signal Analysis

The first and the last strides were excluded from each trial due to *noise* introduced by gait initiation and termination. Each subject's gait speed was measured by using the foot switch to verify whether it fell within the normal range. Indeed, muscle activation patterns are related to gait velocity [81]. Timings of *footContact* and *footOff* events were identified by means of basographic and motion analysis data. The *footContact* event is characterized by the activation of any of the three foot switch signals. The *footOff* event is recognized by the deactivation of all signals. Analysis windows within which data were processed and classified, were identified as occurring immediately before the *foot-contact* and after the *foot-off* events. Four phases were taken into consideration: *preContact*, *postContact*, *preOff* and *postOff* (Fig. 8.1). The window length was set to $150ms$ following recommendations in literature: EMG signals can be considered quasi-stationary within $200ms$ intervals, while they are not sufficiently informative when analysis windows shorter than $50ms$ are used [29]. Features were extracted from EMG linear envelopes (Section 2.1).

Features defined in the time-domain were used. These included: mean absolute

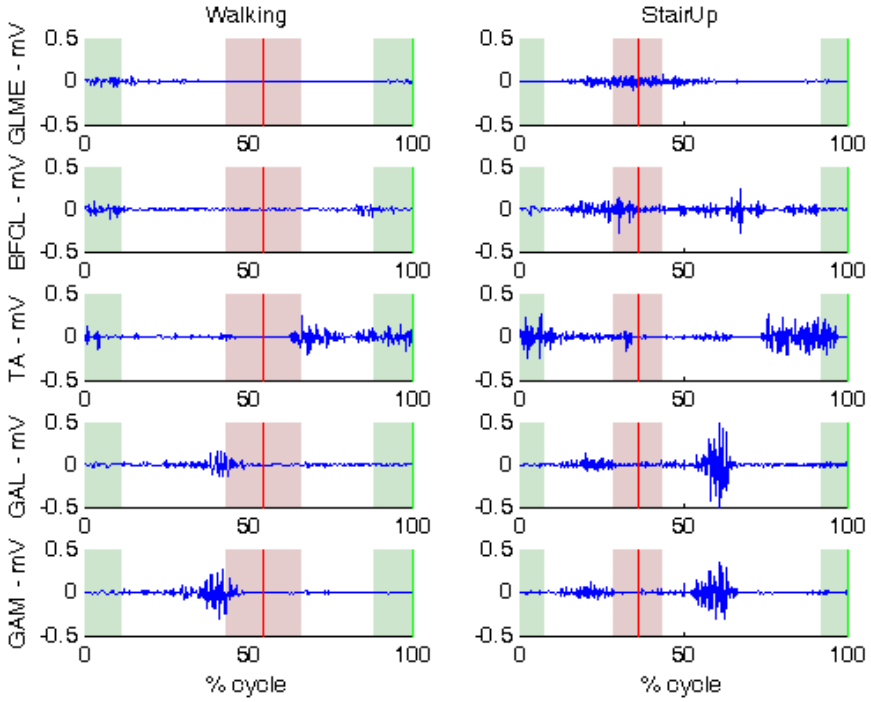

Figure 8.1: Example of filtered EMG signals for two types of locomotion modes (left: level ground walking; right: ascending stairs). A contact-to-contact cycle is reported. *footContact* and *footOff* events are shown (green and red vertical lines, respectively). Analysis windows that are taken into consideration are also highlighted: from left to right, the first green area corresponds to *postContact* phase, then *preOff* and *postOff* (red areas) occur respectively before and after *footOff*, finally *preContact* is shown as occurring before the following *footContact* event (last green area).

value (MAV), number of zero-crossings (ZC), waveform length (WFL), number of slope sign changes (SSC), root mean square (RMS) [78]. Furthermore, 3rd-order auto-regression coefficients (AR1, AR2, AR3) as defined in [29] were also considered.

8.2.2 Support Vector Machine

Support vector machine (SVM) is a well-established technique used to classify a novel set of data after a *training process* that is conducted on a collection of *pre-classified events*. In this study, the pre-classified events are feature vectors associated to the same phase but generated during different locomotion modes. During the training process, the pre-classified event vectors are prescribed to SVM together with the information associated to the respective locomotion mode.

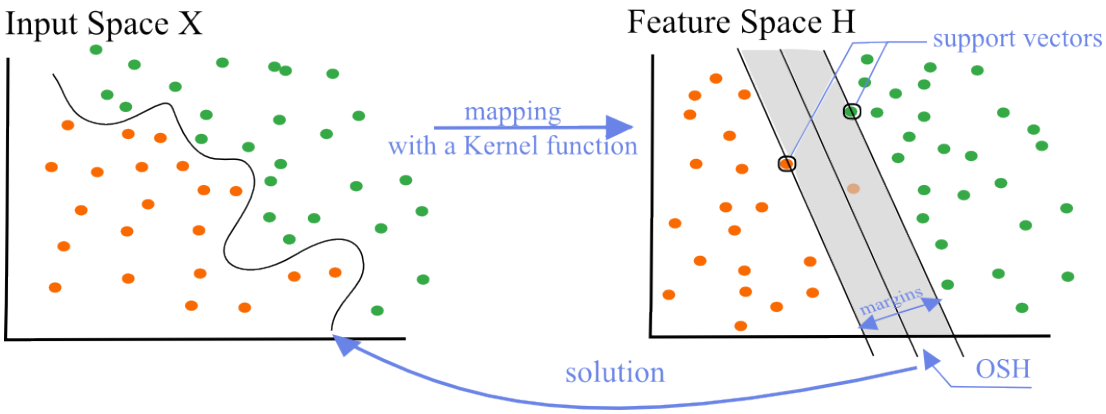

Figure 8.2: Two classes are not linearly separable in the input space X. A kernel function is used to map X in a feature space H where the two classes become linearly separable. The hyperplane built by SVM algorithm in H corresponds to a non-linear solution in the input space X.

A detailed description of the theoretical foundations and applications associated to SVM can be found in [79, 82]. This Section briefly describes the ideas and motivations behind SVM, explaining its four basic concepts: 1) the separating hyperplane, 2) the kernel function, 3) the optimal separating hyperplane, and 4) the soft margin. An introduction on the extension to multi-class classification will be also given.

The main objective of a SVM algorithm is to identify a line, or *hyperplane* in a n-dimensional space H (Fig. 8.2), *separating* a set of input points, each one known to belong to either one of two different classes. If the algorithm is successful in finding an hyperplane that reduces the probability of misclassifying future data, the new sample is easily classified based on what side of the hyperplane it lies on.

However, it is often not possible to linearly separate the data represented in the original space X. The idea is that, by mapping the input data into a higher dimensional space H, a linear separation my be achievable. The mapping is done by using the *kernel function*. The objective is to find the kernel function that allows the data to be linearly separated while keeping the final dimension of the H space *reasonable*.

In the higher dimensional space H, it is usually possible to identify several linear classifiers that separate the data. The *optimal separating hyperplane* (OSH) allows maximizing the margin that separates the distance between the hyperplane and the nearest data points of each class. The points closest to OSH are called

support vectors.

Data can often contain errors. To deal with the noise in the training data, the standard OSH algorithm would usually *overfit* the data. That is, the solution is found, but the price you pay is a useless increment in the dimension of the feature space H. To tolerate training errors, the SVM algorithm was modified introducing the concept of *soft margin*. This allows accepting a few outliers on the wrong side of the hyperplane. The definition of the proper number of outliers and the size of the margin, requires a process of parameter tuning for the specific problem.

The generalization to *multiclass SVM* classification can be achieved with different methods. Two common strategies include: 1) *one-against-all* and 2) *one-against-one*. In the one-against-all approach, SVM compares one pre-classified class to the samples of all the other classes. This is done for each class. The one-against-one approach is often a more robust solution because it allows minimizing the amount of misclassifications [83]. This approach is based on binary classifiers which compare one given class to another one. Given m classes, $m(m-1)$ binary classifiers are generated and trained to recognize the *right* class from a given pair. A bottom-up binary tree is created to perform the pair-classification on the whole data set. The given m classes are first arranged in $m/2$ pairs. At the binary tree lowest level, $m/2$ classes are selected by $m/2$ classifiers from the initial $m/2$ pairs. Each classifier is trained with data taken from a different pair. The $m/2$ selected classes as regarded as *winner-classes*. These access the next upper-level. Here, $m/4$ classifiers, which are trained on the pairs associated to the winner classes, select the next $m/4$ *winner-classes* that are allowed to access the next step. The class that reaches the root of the binary tree, is the class predicted by the multiclass SVM.

8.3 Validation Procedure

To quantify the classification accuracy of our methodology, the *leave-one-out cross-validation* (LOOCV) approach was used. This is used in situations in which a limited set of samples is available for validation. Every sample in the dataset is used to test the multiclass SVM trained on the rest of the samples. Performances

can therefore be quantified in terms of overall classification error, i.e. the ratio between the number of samples that are not classified correctly and the size of the whole dataset. LOOCV ratios are summarized in a *confusion matrix*. This is a square matrix of size m, where m is the number of the classes. The c_{ij} element represents the percentage of samples belonging to class j that are misclassified as belonging to class i. If no errors occur, the confusion matrix is an identity matrix with non-zero elements only on the main diagonal. The confusion matrix allows identifying the pairs of classes that are not properly separated by the OSH.

The proposed multiclass SVM classifier was implemented in a custom C++ using the Open-Source library *libSVM* [84]. This provides standard implementations of different SVM algorithms as well as a set of tools to automatically optimize SVM parameters. A RBF kernel function was used in this study as previous research demonstrated it achieves good performances in the classification of upper limb motions [80].

Validation comprised three tests. For each phase, results were averaged over all subjects and locomotion modes. The first test assessed what combination of EMG features gives the best classification performances on different phases. The second test assessed whether the classification accuracy of the proposed multiclass SVM method varies depending on the phase that is used to extract the features from. The third test assessed how classification accuracy was influenced by reducing the number of muscles to extract the EMG features from. This was done to obtain the optimal minimum set of muscles that allows minimizing the the amount of input data and sensors needed. In the context of the design of wearable devices this plays an important role. The muscles selected for this study were chosen based on the physiology governing their recruitment during the analyzed motion modes. Furthermore, their activation timing was also considered. The GLMA, GLME, and BFCL muscles regulate hip extension, which is particularly important during *preContact* and *postContact* phases. The GLMA and BFCL muscles, together with GR, are also hip adductors and are activated in *preOff* and *postOff* phases. The GLME muscles acts as hip abductor during the *footContact* phase. Hip flexion is mainly regulated by RF, GR and SAR during *postContact*, *preOff* and *postOff* phases. As for knee motion, it is mainly regulated by quadriceps' VAL, VAM,

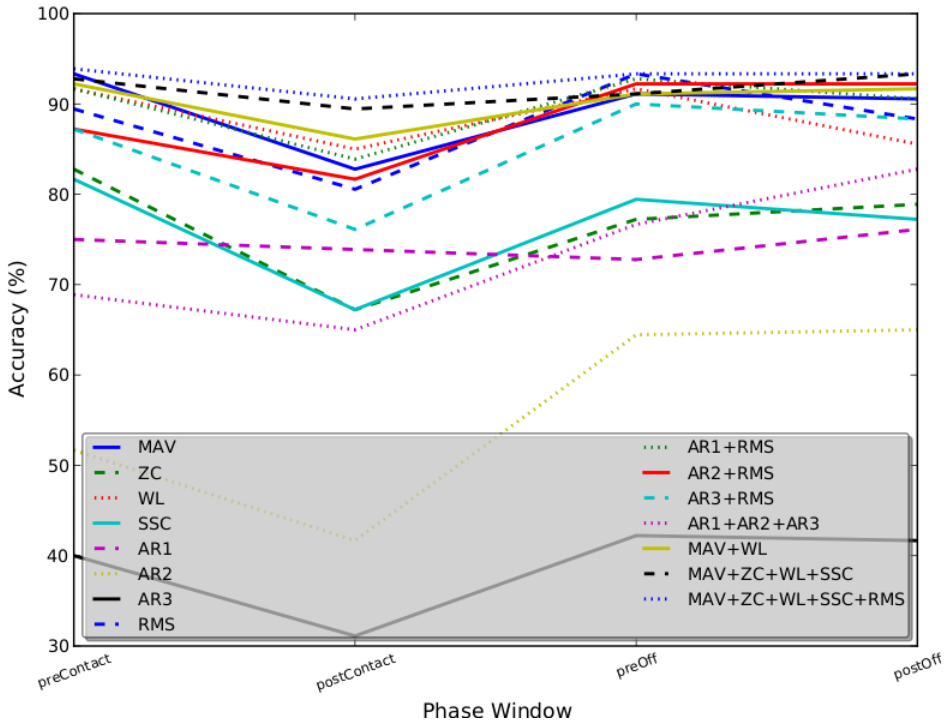

Figure 8.3: Classification accuracy for different sets of feature combinations.

RF and by GLMA (extension, *pre* and *postContact*), and by GAL, GAM, SAR, BFCL, GR (flexion, *postContact*, *pre* and *postOff*). Finally, the ankle joint motion can be described efficiently by means of its dorsal (TA, EXD) and plantarflexors (GAL, GAM, SOL, PEL). The latter are generally active during *postContact*, while activity of the formers can be registered during all four phases, as they often participate in the control of plantarflexion velocity reduction during contact [81, 85]. Some muscles are therefore responsible for the motion of more than one joint, while others regulate a specific joint function completely overlapping the action of other muscles. The influence of single muscles' EMG signal on the classifier was verified by testing its performance while excluding one muscle at the time. A full set of muscles was finally excluded: GLME, VAL, GR, GAL, SOL. These are the muscles who are not entirely responsible of the actuation of a specific joint and their action can be *replaced* by the other muscles in the model. This may be considered as a good trade-off between reduced instrumental set up and classification performance.

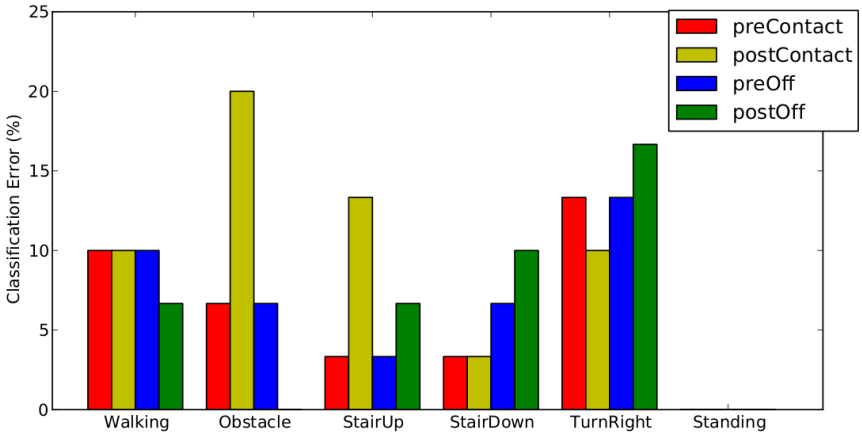

Figure 8.4: Average classification errors for each locomotion mode in the four phases.

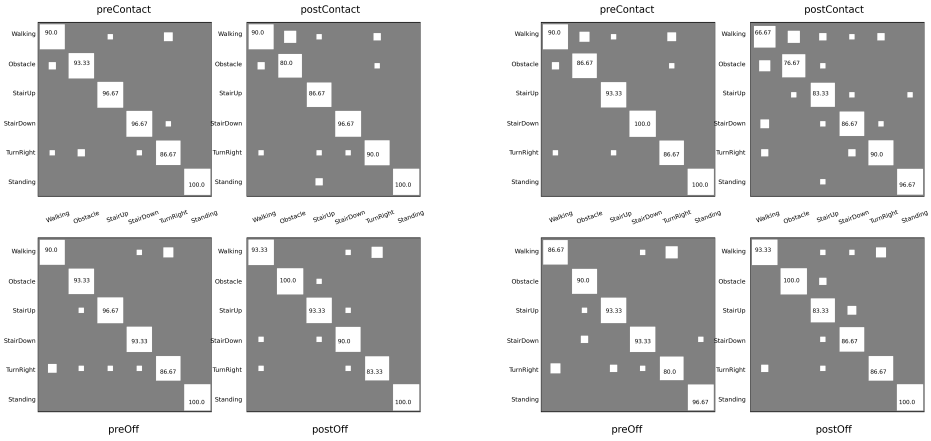

(a) (b)

Figure 8.5: (a) Hinton diagram of the average confusion matrix. This represents classification accuracy on the optimal set of features extracted from all muscles. The size of the squares is proportional to matrix values. Full size corresponds to 100% accuracy. Classification errors mainly occur for *turn right* class. (b) Average confusion matrix obtained using the minimal set of muscles (GLME, SAR, RF, BFCL, ST, TA PEL, GAM, EXD).

8.4 Results

Results from the first test are shown in Fig. 8.3. Time-domain features outperformed autoregressive coefficients as previously demonstrated in [29]. The best classification performances were obtained by combining together all time-domain features: MAV, ZC, WL, SSC and RMS. Accuracy ranged from 90% in the correspondence of the *postContact* phase, to 95%, in the correspondence of the *postOff*

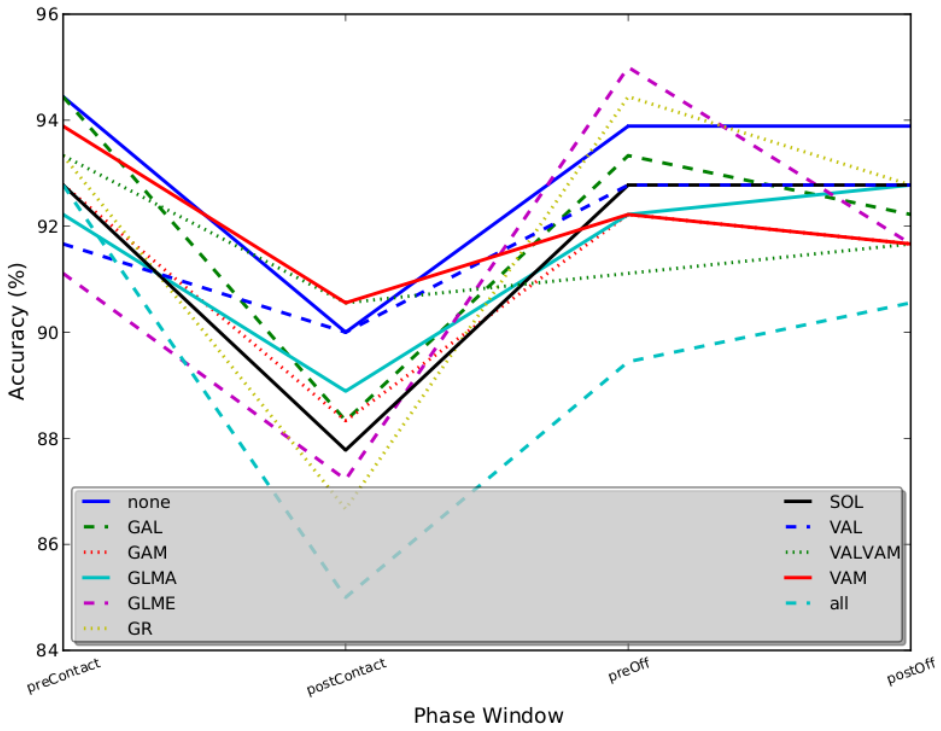

Figure 8.6: SVM classification accuracy for reduced sets of muscles, and optimal set of feature types. Muscles have been removed one at a time from the set; the legend shows the corresponding acronym. Accuracy for the proposed minimal set (GLME, SAR, RF, BFCL, ST, TA, PEL, GAM, EXD) is also shown.

phase.

Results from the second test are shown in Figs 8.4 and 8.5a. Results showed the multiclass SVM classification accuracy significantly depended on the phase used to extract the EMG features from. As an example, the *postContact* phase provided good accuracy for the classification of the *descending stair* movement. On the other hand, it provided poor classification performances in the classification of the *stepping over an obstacle* movement. Total consistency between all phases was achieved during the *standing* movement which was never misclassified. The confusion matrix depicted in Fig 8.5a gives a broader overview of classification performances associated to different phases.

Results from the third test are shown in Figs 8.5 and 8.6. Better performances were achieved using the complete set of muscles (Fig. 8.5a). However, the use of the reduced set of muscles produced comparable performances and produced extremely similar confusion matrices. This demonstrate the potential to successfully classify

locomotion modes using a reduced set of lower limb muscles.

In general, the misclassification errors were associated to tasks that were quite similar and the corresponding EMG features naturally assumed similar *trends*. Misclassification is mainly associated to walking, stepping over an obstacle and turning. In this study the obstacles that were used were particularly narrow and low. Furthermore, turning were not abrupt. There were therefore classified as ground-level walking.

8.5 Combining the EMG-driven NMS Model to the SVM Classifier

The study presented in this Chapter aims to be directly integrated with the EMG-driven NMS model presented in the previous Chapters. This integration can be implemented in two ways.

The first way is to use the EMG-driven NMS model to provide more stationary and more descriptive input data for the classifier. In this context the NMS model is used to convert EMG signals into muscle force. This is a more stable signal which better describes the action of single muscles and better differentiate locomotion modes. The hypothesis is that classifying muscle forces instead of EMG signals will provide a straightforward solution to improve classification performances. This will also allow using wider time windows to extract the force features from. This application can help improve the control of robotics prostheses.

The second way is to use the *context knowledge* on the locomotion mode provided by the classifier to improve the operation of the EMG-driven NMS model. This will help improving the force prediction for those muscles whose EMG activity cannot be recorded experimentally such as the Psoas and Illiacus muscles. Indeed, by knowing what kind of movement the subject wants to perform it is possible to use task-specific objective functions in optimization problems to share the residual joint moments to those two muscles. This approach is superior to the approach currently used in literature in which one single objective function is used to solve an optimization problem for all movements.

8.6 Conclusions and Future Work

This paper presented a classifier based on support vector machine. Experimental results showed that SVM provides good accuracy when a time dependent multi-feature set is used. Misclassification errors were mostly on pair of tasks with high similarity, such as walking and stepping over an obstacle. Results on the selection of important muscles demonstrated that it is possible to reduce the number of EMG signals without significantly affecting the classifier accuracy. This allows to reduce the number of electrodes to place on the leg, thus improving the usability of powered orthoses. Future studies will integrate the SVM classifier and the EMG-driven NMS model presented in the previous Chapters within a common framework. This will allow reducing the limitation that both methods inherently have.

Chapter 9

Conclusions

This work presented the design and development of a novel EMG-driven Neuro-MusculoSkeletal (NMS) model of the human lower limb. The theoretical results that were obtained provided solutions to better understand the mechanisms of human muscle actuation. Understanding these mechanisms is the key to realize effective human interaction with wearable assistive devices. This work did not realize real-time synchronization with powered orthoses. Neither did it improve disabled people's mobility using robotics assistive devices.

This work provided the technology needed to achieve this, i.e. to establish an EMG-driven human-machine interface (HMI) for the simultaneous actuation of multiple joints in a lower limb powered orthosis. The software developed in this thesis will be made available to researchers who wish to use this technology.

Neuromusculoskeletal modeling technology not only can offer great solutions for exoskeletons control and humanoids actuation, but can also boost research that aims to realize more realistic virtual humans by providing a more accurate estimation of the human internal state.

9.1 Summary

Chapter 1 defined the research problem investigated within this thesis. It gave an overview of the research conducted in the field of EMG-driven musculoskeletal modeling, it highlighted the novelty and the significance of the proposed research

as well as the research questions to be addressed and the boundaries within which this research work investigates.

Chapter 2 presented the general *workflow* used in this study. It described how the the human movement can be recorded utilizing motion capture technology and digitized to create realistic motion simulations. The OpenSim Application Programming Interface (API) was used in a custom C++ program to develop advanced methods for the simulation of the human movement and provide the most accurate input for the NMS model. A new knee joint model was developed in which functional axes could be defined and scaled to the subject's characteristics. Also, a foot-ground contact model was created using an elastic foundation model and used in conjunction with Residual Reduction Analysis (RRA) to derive even more accurate estimates of joint loading during movement. The use of the OpenSim API allowed for a direct integration of OpenSim's optimization algorithms into the NMS model framework. This provided full access to a number of powerful software tools including: Functional Scaling, Inverse Kinematics, and Residual Reduction Analysis.

Chapters 3 and 4 presented a novel muscle dynamics model and a novel musculotendon kinematics model respectively. These are used by the EMG-driven NMS model to achieve fast operation and high muscle force and joint moment predictive accuracy. The muscle dynamics model was designed under the assumption that tendons are infinitely-stiff. This allowed eliminating the need for solving an ordinary differential equation at each time step for the computation of muscle fibre length and the subsequent musculotendon force. The infinitely stiffness assumption allowed obtaining a closed-form expression that could be computed inexpensively. Results showed the stiff-tendon model could be executed 250 times faster than the elastic-tendon model with no loss of accuracy in the prediction of joint moments. The musculotendon kinematics model was design to allow fast and accurate estimation of musculotendon length (l^{mt}) and muscle moment arms (r). These values are used by the muscle dynamics model to compute musculotendon force. The musculotendon kinematics model uses a single multidimensional cubic spline per muscle to generate estimates for both l^{mt} and r from nominal values of musculotendon length only, corresponding to discrete combinations of generalized

coordinates. This method provided fast and accurate estimation of musculotendon kinematics and superior results in terms of fitting accuracy with respect to the approach currently used in literature that is based on polynomial regression. Chapter 3 also illustrated how the proposed NMS model can be used to control a powered orthosis for the knee joint support. Furthermore, it demonstrates the proposed EMG-driven NMS model is fast enough to meet the real-time deadline associated to this specific application. Chapter 3 suggested how the NMS model can be used to actuate humanoid robots equipped with artificial muscles.

In Chapter 5 a novel method is developed to achieve faster calibration of EMG-driven models based on elastic tendons. Indeed, some applications may require accurate estimates of the instantaneous tendon and muscle fibre lengths. The idea was that of using the stiff-tendon muscle model to quickly solve a global optimization problem and obtain a sub-optimal parameter set for the elastic-tendon model. A refinement step is then performed to further refine the initial sub-optimal solution. Results showed the proposed methodology allowed calibrating the elastic-tendon model achieving the same calibration accuracy of the procedures currently used in literature but in significantly less time.

Chapter 6 extended the results obtained in the previous Chapter to realize a novel *multi-DOF* EMG-driven NMS model. It was shown it is possible to use EMG signals recorded from 16 muscles to estimate the activity of 34 musculotendon actuators (MTAs) in the lower limb. A novel calibration algorithm was designed to constrain the operation of each MTA in the model to satisfy the moments simultaneously produced at the hip, knee and ankle joints about 4 degrees of freedom including: hip adduction-abduction, hip flexion-extension, knee flexion-extension and ankle dorsi-plantar flexion. To date, only single-DOF EMG-driven NMS models were proposed. That is, EMG signals were used to estimate muscle forces that satisfy moments about a single DOF of a single joint only. Results showed that the force that a muscle can generate during a specific movement can be predicted in extremely different ways when different single-DOF models are used. This fact introduces indeterminacy as it is not possible to know what single-DOF model is best to use. The proposed multi-DOF NMS model allows removing this indeterminacy by providing a single solution to the problem. As

a result, the multi-DOF model was able to produce muscle force estimates that were more in line with biomechanics findings. The multi-DOF EMG-driven model significantly improved the estimation of the force produced by biarticular muscles. Results obtained using the single-DOF knee flexion-extension model showed it could not properly predict the activity of the Rectus Femoris muscle. This is a muscle crossing both the hip and knee joint and it is mostly active during running to support the hip flexion-extension movement. The proposed multi-DOF NMS model did not fail to catch such important feature because it properly constrained its operation to satisfy not only the knee flexion-extension moments but also the hip flexion-extension moments.

Chapter 7 presented a new technique to scale the tendon slack length of each individual musculotendon unit in the model. Experiments proved that a good rationale to scale tendons is to preserve the consistency of the EMG-to-activation relationship across the whole joint operating range of motion. Results proved this new scaling technique allows deriving physiologically appropriate estimates of the tendon length and significantly contributes to improve the prediction accuracy of the NMS model.

In Chapter 8, EMG signals were evaluated by a phase-dependent Support Vector Machine (SVM) classifier for the identification of locomotion modes. This approach did not rely on biologically relevant models of the human musculoskeletal system and did not aim to realize continuous device control. The aim was to obtain *context knowledge* of the movement the user wants to perform, i.e. understanding whether the subject wants to walk rather than turning left or right and so forth. This study was conducted with the plan of combining the EMG-driven NMS model presented in this thesis with the EMG-classifier to achieve a superior neuromuscular HMI that maximizes the information exchange between the human and the machine.

9.2 Future Work

This research work was conducted on healthy subjects only. Future work will therefore test the behavior of the model on disabled people.

In this work, the EMG-driven NMS model was used to predict muscle force and joint moments using data *previously* collected during the subject's movement. This work represented the first step towards the creation of a neuromuscular HMI for assistive device control. Therefore, the study was focused on the pure validation of the model operation and not on its synchronization with real-time data acquisition systems. Future studies will integrate the proposed EMG-driven NMS model into real-time systems. This will allow executing the NMS model *in parallel* to the subject's movement and obtaining real-time estimates of muscle force and joint moments. This work designed and developed the technology for achieving this. The next step will then be that of utilizing the real-time NMS model to control a real powered orthosis.

This research work combined for the first time advanced motion simulation techniques (Chapter 2) to EMG-driven NMS modeling (Chapters 3 and 6). This process integrated anatomical and dynamic consistency into NMS model. Future work will validate whether providing input data that better represent the dynamics of the human movement, improves the ability of the EMG-driven NMS model to *learn* the prescribed muscle dynamics.

Fast operation in calibration will be further exploited in future research to develop more advanced algorithms for the continuous calibration of the model biomechanical parameters. As the NMS model executes, the *on-line calibration* algorithm will keep refining those parameters that vary with muscle fatigue such as: optimal fiber length, maximum isometric force, maximum EMG. This will allow designing more advanced powered orthosis control systems that will be able to adapt to the user's conditions on the fly. Fast operation in execution will be exploited in future research to further extend the multi-DOF EMG-driven NMS model (Chapter 6) to whole-body level. This study will assess whether the proposed approach can be scaled up to simulate all muscles in the human body maintaining fast execution and calibration.

The use of the proposed spline method in Chapter 4 is not limited to fitting l^{mt} data from musculoskeletal geometry software packages such as OpenSim [46]. Alternatively, l^{mt} could be determined from the centriods of three dimensional muscles based on MRI data or from three dimensional geometric modeling of

musculoskeletal systems. In this context the spline approach can be used to create a multivariate function that can reliably replicate the behavior of complex systems at low computational cost.

The multi-DOF NMS model presented in Chapter 6 will be extended to include predictive algorithms for the estimation of the activation of muscles without EMG. This will be achieved by using the *context knowledge* from the locomotion mode provided by the SVM classifier presented in Chapter 8. Indeed, by knowing what kind of movement the subject wants to perform it is possible to use task-specific objective functions in optimization problems to share the residual joint moments to muscles for which EMG signals are not available. This approach is superior to the approach currently used in literature in which one single objective function is used to solve an optimization problem for all movements.

The multi-DOF NMS model (Chapter 6) will be also used to actuate humanoid robots that have a musculoskeletal architecture and artificial muscles by following the approach illustrated in Section 3.8. Experiments will be done in simulation.

The approach proposed in Chapter 7 to scale tendon slack length will be further validated using ultra sound technology to experimentally measure the tendon length and compare experimental values to the predicted estimates.

The EMG-driven NMS model will be used in future studies to provide more stationary and more descriptive input data for the SVM classifier (Chapter 8). Precisely, the NMS model will convert EMG signals into muscle force. Experiments will then assess whether classification performance will benefit from this.

Bibliography

[1] F. E. Zajac, "Muscle and tendon: properties, models, scaling, and application to biomechanics and motor control," *Crit. Rev. Biomed. Eng.*, vol. 17, no. 4, pp. 359–411, 1989.

[2] T. Buchanan, D. G. Lloyd, K. Manal, and T. Besier, "Neuromusculoskeletal modeling: Estimation of muscle forces and joint moments and movements from measurements from neural command," *J. of Applied Biomechanics*, vol. 20, no. 4, pp. 367–395, 2004.

[3] D. G. Lloyd and T. F. Besier, "An EMG-driven musculoskeletal model to estimate muscle forces and knee joint moments in vivo," *J. of Biomech.*, vol. 36, no. 6, pp. 765–776, 2003.

[4] D. Lloyd, T. Besier, C. Winby, and T. Buchanan, "Neuromusculoskeletal modelling and simulation of tissue load in the lower extremities," in *Routledge handbook of Biomechanics and Human Movement Science*, Y. Hong and R. Barlett, Eds., 2008, pp. 3–17.

[5] M. Viceconti, G. Clampworthy, and S. Jan, "The virtual human: A european initiative for in silico human modeling," *J. Physiol Sci.*, vol. 58, no. 7, pp. 441–446, 2008.

[6] Y. Nakamura, K. Yamane, Y. Fujita, and S. I., "Somatosensory computation for man-machine interface from motion-capture data and musculoskeletal human model," *IEEE Trans. Robot.*, vol. 21, no. 1, pp. 58–66, 2005.

[7] J. Pons, Ed., *Wearable Robots. Biomechatronic Exoskeletons.* Wiley, 2008.

[8] A. Dollar and H. Herr, "Lower extremity exoskeletons and active orthoses: Challenges and state-of-the-art," *IEEE Trans. Biomed. Eng.*, vol. 24, no. 1, pp. 144–158, 2008.

[9] C. Fleischer and G. Hommel, "A human-exoskeleton interface utilizing electromyography," *IEEE Trans. Robot.*, vol. 24, no. 4, pp. 872–882, 2008.

[10] E. Cavallaro, J. Rosen, J. Perry, and S. Burns, "Real-time myoprocessors for a neural controlled powered exoskeleton arm," *IEEE Trans. Biomed. Eng.*, vol. 53, no. 11, pp. 2387–2396, 2006.

[11] S. Delp, F. Anderson, A. Arnold, P. Loan, A. Habib, C. John, E. Guendelman, and D. Thelen, "Opensim: Open-source software to create and analyze dynamic simulations of movement," *IEEE Trans. Biomed. Eng.*, vol. 54, no. 11, pp. 1940–1950, Nov. 2007.

[12] K. Narioka and K. Hosoda, "Designing synergistic walking of a whole-body humanoid driven by pneumatic artificial muscles: An empirical study," *Advanced Robotics*, vol. 22, no. 10, pp. 1107–1123, 2008.

[13] T. Yoshikai, I. Mizuuchi, D. Sato, S. Yoshida, M. Inaba, and H. Inoue, "Behavior system design and implementation in spined musle-tendon humanoid kenta," *J. of Robotics and Mechatronics*, vol. 15, no. 2, pp. 143–152, 2003.

[14] M. Vukobratovic, D. Hristic, and Z. Stojiljkovic, "Development of active anthropomorphic exoskeletons," *Med. Biol. Eng.*, vol. 12, no. 1, pp. 66–80, 1974.

[15] D. P. Ferris, K. E. Gordon, G. S. Sawicki, and A. Peethambaran, "An improved powered ankle-foot orthosis using proportional myoelectric control," *Gait Posture*, vol. 23, no. 4, pp. 425–428, 2006.

[16] K. Yamamoto, M. Ishii, K. Hyodo, T. Yoshimitsu, and T. Matsuo, "Development of power assisting suit (miniaturization of supply system to realize wearable suit)," *JSME Intl. Journal Series C*, vol. 46, no. 3, pp. 923–930, 2003.

[17] H. Kawamoto and Y. Sankai, "Power assist system hal-3 for gait disorder person," in *Intl. Conf. Computers Helping People with Special Needs (ICCHP), Lecture Notes on Computer Science (LNCS).* Berlin, Germany: Springer Verlag, 2002.

[18] H. Herr, "Exoskeletons and orthoses: classification, design challenges and future directions," *J. NeuroEngineering and Rehabilitation*, vol. 6, no. 1, p. 21, 2009.

[19] A. Zoss, H. Kazerooni, and A. Chu, "Biomechanical design of the berkeley lower extremity exoskeleton (bleex)," *IEEE/ASME Trans. Mechatronics*, vol. 11, no. 2, pp. 128 –138, 2006.

[20] J. Pratt, S. H. Collins, B. Krupp, and K. Morse, "The roboknee: An exoskeleton for enhancing strength and endurance during walking," in *IEEE Intl. Conf. Robotics and Automation*, 2004.

[21] J. M. Carmena, M. A. Lebedev, R. E. Crist, J. E. O'Doherty, D. M. Santucci, D. F. Dimitrov, P. G. Patil, C. S. Henriquez, and M. A. L. Nicolelis, "Learning to control a brainmachine interface for reaching and grasping by primates," *PLoS Biol*, vol. 1, no. 2, pp. 192–208, 2003.

[22] G. Santhanam, S. Ryu, B. You, A. Afshar, and K. Shenoy, "A high-performance braincomputer interface," *Nature*, vol. 442, no. 2, pp. 195–198, 2006.

[23] L. Qin, L. Ding, and B. He, "Motor imagery classification by means of source analysis for brain computer interface applications," *J. of Neural Engineering*, vol. 4, no. 2, pp. 65–72, 2005.

[24] A. d'Avella, P. Saltiel, and E. Bizzi, "Combinations of muscle synergies in the construction of a natural motor behavior," *Nature Neuroscience*, vol. 6, no. 3, pp. 300–308, 2003.

[25] K. Pearson, O. Ekeberg, and A. Bushges, "Assessing sensory function in locomotor systems using neuro-mechanical simulations," *Trend in Neurosciences*, vol. 29, no. 11, pp. 625–631, 2006.

[26] R. Merletti, *Electromyography: Physiology, Engineering, and Non-Invasive Applications*, P. Parker, Ed. IEEE Pres., 2004.

[27] A. Nordez, T. Gallot, S. Catheline, A. Guvel, C. Cornu, and F. Hug, "Electromechanical delay revisited using very high frame rate ultrasound," *J. of Applied Physiology*, vol. 106, no. 6, pp. 1970–1975, 2009.

[28] G. Li, A. Schultz, and T. Kuiken, "Quantifying pattern recognition-based myoelectric control of multifunctional transradial prostheses," *IEEE Trans. Neural Syst. Rehabil. Eng.*, vol. 18, no. 2, pp. 185 –192, 2010.

[29] H. Huang, T. Kuiken, and R. Lipschutz, "A strategy for identifying locomotion modes using surface electromyography," *IEEE Trans. Biomed. Eng.*, vol. 56, no. 1, pp. 65 –73, 2009.

[30] C. Pattichis, C. Schizas, and L. Middelton, "Neural network models in emg diagnosis," *IEEE Trans. Biomed. Eng.*, vol. 42, no. 5, pp. 486–496, 1995.

[31] R. Norman, "A barrier to understanding human motion mechanisms: a commentary," in *Future directions in exercise and sport science research*, C. L. D. Skinner, J.S. Corbin, Ed., 1989, pp. 151–161.

[32] J. Soechting and F. M., "Evaluating an integrated musculoskeletal model of the human arm." *J. of Biomechanical Engineering*, vol. 119, no. 1, pp. 93–102, 1997.

[33] M. Nussbaum and D. Chaffin, "Lumbar muscle force estimation using a subject-invariant 5-parameter emg-based model," *J. of Biomechanics*, vol. 31, no. 7, pp. 667 – 672, 1998.

[34] B. Laursen, B. Jensen, G. Nmeth, and G. Sjgaard, "A model predicting individual shoulder muscle forces based on relationship between electromyographic and 3d external forces in static position," *J. of Biomechanics*, vol. 31, no. 8, pp. 731 – 739, 1998.

[35] C. Winby, D. Lloyd, and T. Kirk, "Evaluation of different analytical methods for subject-specific scaling of musculotendon parameters," *J. of Biomech.*, vol. 41, no. 8, pp. 1682–1688, 2008.

[36] L. Schutte, "Using musculoskeletal models to explore strategies for improving performance in electrical stimulation-inducted leg cycle ergonometry." Ph.D. dissertation, Stanford University, 1992.

[37] D. G. Lloyd and T. S. Buchanan, "A model of load sharing between muscles and soft tissues at the human knee during static tasks," *J. of Biomechanical Engineering*, vol. 118, no. 3, pp. 367–376, 1996.

[38] H. Kawamoto and Y. Sankai, "Comfortable power assist control method for walking aid by hal-3," in *IEEE Intl. Conf. Systems, Man and Cybernetics*, 2002.

[39] J. Challis and K. D.G., "An analytical examination of muscle force estimations using optimization techniques." *Proc Inst Mech Eng H.*, vol. 207, no. 3, pp. 139–148, 1993.

[40] J. Challis, "Producing physiologically realistic individual muscle force estimations by imposing constraints when using optimization techniques," *Medical Engineering & Physics*, vol. 19, no. 3, pp. 253 – 261, 1997.

[41] T. Buchanan and D. Shreeve, "An evaluation of optimization techniques for the prediction of muscle activation patterns during isometric tasks." *J. of Biomechanical Engineering*, vol. 114, no. 4, pp. 565–74, 1996.

[42] J. Cholewicki, , and S. McGill, "Emg assisted optimization: A hybrid approach for estimating muscle forces in an indeterminate biomechanical model," *J. of Biomechanics*, vol. 27, no. 10, pp. 1287 – 1289, 1994.

[43] C. Winby, D. Lloyd, T. Besier, and T. Kirk, "Muscle and external load contribution to knee joint contact loads during normal gait." *J. of biomechanics*, vol. 42, no. 14, pp. 2294–2300, 2009.

[44] S. Delp, J. Loan, M. Hoy, F. Zajac, E. Topp, and J. Rosen, "An interactive graphics-based model of the lower extremity to study orthopaedic surgical procedures," *IEEE Trans. Biomed. Eng.*, vol. 37, no. 8, pp. 757–767, 1990.

[45] "Simm software suite," Available at: http://www.musculographics.com.

[46] "Opensim project overview," Available at: https://simtk.org/home/opensim.

[47] T. Besier, D. Sturnieks, J. Anderson, and D. Lloyd, "Repeatability of gait data using a functional hip joint centre and a mean helical knee axis," *J. of Biomechanics*, vol. 36, no. 8, pp. 1159–1168, 2003.

[48] C. Spoor and F. Veldpaus, "Rigid body motion calculated from spatial co-ordinates of markers," *J. of Biomechanics*, vol. 13, no. 4, pp. 391–393, 1980.

[49] C. Reinschmidt and T. van den Bogert, "Kinemat: a matlab toolbox for three-dimensional kinematic analyses," 1997.

[50] M. Stokdijk, C. G. M. Meskers, H. E. J. Veeger, Y. A. de Boer, and P. M. Rozing, "Determination of the optimal elbow axis for evaluation of placement of prostheses," *Clinical Biomechanics*, vol. 14, no. 3, pp. 177 – 184, 1999.

[51] J. Kalker, "Three-dimensional elastic bodies in rolling contact," in *Solid Mechanics and Its Application*, K. A. Publishers, Ed., 1990.

[52] P. Huijing, "Important experimental factors for skeletal muscle modelling: nonlinear changes of muscle length force characteristics as a function of degree of activity," *European Journal of Morphology*, vol. 34, no. 1, pp. 47–54, 1996.

[53] A. V. Hill, "The Heat of Shortening and the Dynamic Constants of Muscle," *Proc. of the Royal Society of London. Series B, Biological Sciences*, vol. 126, no. 843, pp. 136–195, 1938.

[54] A. Guimaraes, W. Herzog, Y. Zhang, and S. Day, "Effects of muscle length on the emg-force relationship of the cat soleus muscle studied using non periodic stimulation of ventral root filaments." *J. of Experimental Biology*, vol. 193, no. 1, pp. 49–64, 1994.

[55] J. Loan, *Dymanics Pipeline*. Evanston, IL: Musculographics Inc., 1992.

[56] K. Genovese, L. Lamberti, and C. Pappalettere, "Improved global-local simulated annealing formulation for solving non-smooth engineering optimization problems." *Intl. J. of Solids and Structures*, vol. 42, no. 1, pp. 203 – 237, 2005.

[57] J. Potvin, R. Norman, and S. McGill, "Mechanically corrected emg for the continuous estimation of erector spinae muscle loading during repetitive lifting," *European Journal of Applied Physiology & Occupational Physiology,*, vol. 74, no. 1, pp. 119 – 132, 1996.

[58] A. Frigon and S. Rossignol, "Experiments and models of sensorimotor interactions during locomotion," *Biological Cybernetics*, vol. 95, no. 6, pp. 607–627, 2006.

[59] "Musculoskeletal robotics and mechanical testing core," Available at: http://www.lerner.ccf.org/orc/cores/mrmtc/.

[60] I. Mizuuchi, Y. Nakanishi, Y. Sodeyama, Y. Namiki, T. Nishino, N. Muramatsu, J. Urata, K. Hongo, T. Yoshikai, and M. Inaba, "An advanced musculoskeletal humanoid kojiro," in *IEEE-RAS Intl. Conf. Humanoids*, 2007, pp. 294 – 299.

[61] I. Mizuuchi, T. Yoshikai, Y. Sodeyama, Y. Nakanishi, A. Miyadera, T. Yamamoto, T. Niemela, M. Hayashi, J. Urata, Y. Namiki, T. Nishino, and M. Inaba, "A musculoskeletal flexible-spine humanoid kotaro aiming at year 2020," in *36th Intl. Symp. Robotics*, 2005.

[62] K. Hosoda, T. Takuma, A. Nakamoto, and S. Hayashi, "Biped robot design powered by antagonistic pneumatic actuators for multi-modal locomotion," *Robotics and Autonomous Systems*, vol. 56, no. 1, pp. 46–53, 2008.

[63] "The anybody modeling system," Available at: http://www.anybodytech.com/.

[64] K. Artemiadis and K. Kyriakopoulos, "Emg-based position and force estimates in coupled human-robot systems: Towards emg-controlled exoskeletons," *Experimental Robotics*, vol. 54, pp. 241–250, 2009.

[65] M. Sartori, M. Reggiani, C. Mezzato, and E. Pagello, "A lower limb emg-driven biomechanical model for applications in rehabilitation robotics," in *IEEE Intl. Conf. Advanced Robotics*, 2009, pp. 144–158.

[66] M. Sartori, D. Lloyd, M. Reggiani, and E. Pagello, "A stiff tendon neuromusculoskeletal model of the knee," in *IEEE Workshop Advanced Robotics and its Social Impacts*, 2009, pp. 132–138.

[67] ——, "Fast operation of anatomical and stiff tendon neuromuscular models in emg-driven modeling," in *IEEE Intl. Conf. Robotics and Automation*, 2010, pp. 2228–2234.

[68] C. Habermann and F. Kindermann, "Multidimensional spline interpolation: Theory and applications," *Comput. Econ.*, vol. 30, no. 8, pp. 153–166, 2007.

[69] L. Menegaldo, D. Fleury, and H. Weber, "Moment arms and musculotendon lengths estimation for a three-dimensional lower-limb model," *J. of Biomechanics*, vol. 37, no. 9, pp. 1447–14 453, 2004.

[70] A. Arnold, S. Salinas, D. Asakawa, and S. Delp, "Accuracy of muscle moment arms estimated from mri-based musculoskeletal models of the lower extremity." *Computer Aided Surgery*, vol. 5, no. 2, pp. 108 –119, 2000.

[71] S. Blemker, D. Asakawa, G. Gold, and S. Delp, "Image-based musculoskeletal modeling: applications, advances, and future opportunities." *J. Magnetic Resonance Imaging*, vol. 25, no. 2, pp. 441 –451, 2007.

[72] J. Fernandez, P. Mithraratne, S. Thrupp, M. Tawhai, and P. Hunter, "Anatomically based geometric modelling of the musculo-skeletal system and other organs," *Biomechanics and Modeling in Mechanobiology*, vol. 2, no. 3, pp. 139–155, 2004.

[73] J. Fernandez and P. Hunter, "An anatomically based patient-specific finite element model of patella articulation: towards a diagnostic tool," *Biomechanics and Modeling in Mechanobiology*, vol. 4, no. 1, pp. 20–38, 2005.

[74] K. Oberhofer, N. Scott, K. Mithraratne, and I. Anderson, "Subject-specific modelling of lower limb muscles in children with cerebral palsy." *Clinical biomechanics*, vol. 25, no. 1, pp. 88–94, 2010.

[75] K. McKinnon, "Convergence of the nelder–mead simplex method to a nonstationary point," *SIAM J. on Optimization*, vol. 9, no. 1, pp. 148–158, 1998.

[76] T. F. Besier, D. Lloyd, and T. Ackland, "Muscle activation strategies at the knee during running and cutting maneuvers," *Medicine & Science in Sports & Exercise*, vol. 35, no. 1, pp. 119–127, 2003.

[77] S. Hamner, A. Seth, and S. Delp, "Muscle contributions to propulsion and support during running," *J. of Biomechanics*, vol. 43, no. 14, pp. 2709–2716, 2010.

[78] B. Hudgins, P. Parker, and R. Scott, "A new strategy for multifunction myoelectric control," *IEEE Trans. Biomed. Eng.*, vol. 40, no. 1, pp. 82–94, 1993.

[79] T. Hormann, B. Scholkopf, and A. J. Smola, "Kernel methods in machine learning," *The Annals of Statistics*, vol. 36, no. 3, pp. 1171–1220, 2008.

[80] M. A. Oskoei and H. Hu, "Support vector machine-based classification scheme for myoelectric control applied to upper limb," *IEEE Trans. Biomed. Eng.*, vol. 55, no. 8, pp. 1956–1965, 2008.

[81] J. Perry, *Gait Analysis, Normal and Pathological Function.* New York: McGraw-Hill, 1992.

[82] O. Bousquet, S. Boucheron, and G. Lugosi, "Theory of classification: a survey of recent advances," *ESAIM Probab. Statist.*, vol. 9, pp. 323–375, 2005.

[83] C. W. Hsu and C. J. Lin, "A comparison of methods for multiclass support vector machines," *IEEE Trans. Neural Netw.*, vol. 13, no. 2, pp. 415–425, 2002.

[84] C.-C. Chang and C.-J. Lin, *LIBSVM: a library for support vector machines*, 2001, software available at http://www.csie.ntu.edu.tw/~cjlin/libsvm.

[85] D. Winder, "Biomechanics of normal and pathological gait: implications for understanding human locomotor control," *J. Mot. Behav.*, vol. 21, no. 4, pp. 337–355, dec 1989.